LAMINAR MIXED CONVECTION IN VERTICAL CHANNELS

BY

SHAIK SAMIVULLAH

A Thesis Presented to the

DEANSHIP OF GRADUATE STUDIES

KING FAHD UNIVERSITY OF PETROLEUM & MINERALS

DHAHRAN, SAUDI ARABIA

In Partial Fulfillment of the
Requirements for the Degree of

MASTER OF SCIENCE

In

MECHANICAL ENGINEERING

MAY, 2005

KING FAHD UNIVERSITY OF PETROLEUM AND MINERALS
DHAHRAN 31261, SAUDI ARABIA

DEANSHIP OF GRADUATE STUDIES

This thesis, written by **SHAIK SAMIVULLAH** under the direction of his Thesis Advisor and approved by his Thesis Committee, has been presented to and accepted by the Dean of Graduate Studies, in partial fulfillment of the requirements for the degree of **MASTER OF SCIENCE IN MECHANICAL ENGINEERING.**

Thesis Committee

15/11/05
Dr. Esmail M. A. Mokheimer (Advisor)

15/11/2005
Dr. Habib Abu Al-Hamayel (Member)

Nov. 15, 2005
Dr. Syed M. Zubair (Member)

Dr. Faleh Al-Sulaiman
Department Chairman

Dr. Mohammad A. Al-Ohali
Dean of Graduate Studies

١٤٢٦/١٠/١٧

Date 19-11-2005

عمادة الدراسات العليا
DEANSHIP OF GRADUATE STUDIES

Dedicated to My Parents, My Brothers, My Sisters and My Aunty & Uncle

Acknowledgements

All praise and thanks are due to ALLAH (SWT), the most Compassionate, the most Merciful, and the most Benevolent. Peace and blessings be upon prophet Muhammad (PBUH), his family and companions. I thank Almighty ALLAH (SWT) for giving me this opportunity and patience to complete this work.

I would like to express my profound gratitude and appreciation to my advisor Dr. Esmail M. A. Mokheimer, for his consistent help, guidance and attention that he devoted throughout the course of this work. He was always kind, understanding and sympathetic to me. His valuable experience, suggestions and constructive discussions made this work interesting to me. Thanks are also due to my thesis committee members Dr. Habib Abu Al-Hamayel and Dr. S. M. Zubair for their interest, cooperation and valuable suggestions.

I am grateful to chairman of Mechanical Engineering Department Dr. Faleh Al-Sulaiman for his strong support and cooperation. I am also thankful to all faculty and staff members including department secretaries Mr. Lateef, Mr. Jameel and Mr. Thomas for their kind support and continuous assistance. I would like to acknowledge with deep gratitude and appreciation, the support and facilities provided by King Fahd University of Petroleum and Minerals during the course of this work.

My heartfelt appreciations and gratefulness are dedicated to my parents, my brothers, my sisters and all my relatives. My deep gratitude is towards my parents, aunty and uncle for their incessant prayers, moral support, guidance, encouragement and patience during

the course of my studies. They are the source of power, inspiration and confidence in me.

Finally, I would like to thank my seniors Mujtaba, Ghulam Arshad, Jameel Ahmed, Syed Nazim, Farrukh Saghir, Bilal, Hasan, Iftekhar and all the ME graduates for their concern and help. Thanks are also due to my friends Humayun Baig, Yousuf, Haseeb, Basha, Gayazullah, Rizwan baba, Hafeez, Qaiyyum, Saad, Abbas, Rihan Ahmed, Atif, Shafeeq, Shujath, Razwan, Faheem Patel, Zahed, Omer, Khaliq, Khaleel Ahmed, Mir Riyaz Ali, Anees, Irfan Ahmed (room-mate), Azher and Feroz for their friendship and the memorable days shared together. Special thanks are due to Jalaluddin Shah, Arifussalam and Irfan Hussaini for their moral support and good wishes. I also acknowledge entire Indian Community at KFUPM for providing a friendly environment.

TABLE OF CONTENTS

List of Tables

List of Figures

Nomenclature

A, B, D & E	Constants given in the Table 4.2
b	Gap width between the parallel plates
C^* & C^{**}	Constants given in page 29 for equations (3. 27) and (3. 29)
C_1, C_2 & C_3	Constants defined and used in the analytical solutions
C_p	Specific heat of the fluid
D_h	Hydraulic or equivalent diameter of the vertical channel;
	b (parallel plates), r_o (circular tube and concentric annulus)
	$2(r_o - r_i)$ (eccentric annulus)
dp/dz	Pressure gradient
dP/dZ	Dimensionless pressure gradient
$(dP/dZ)_{fd,mxd}$	Dimensionless fully developed pressure gradient for mixed convection
$(dP/dZ)_{fd,forced}$	Dimensionless fully developed pressure gradient for forced convection
e	Eccentricity
E	Dimensionless eccentricity, $e/(r_o - r_i)$
g	Gravitational body force per unit mass (acceleration)
Gr	Grashof number, $\frac{g\beta(T_w - T_o)D_h^3}{\upsilon^2}$ (for isothermal BC's)
	$\frac{g\beta q'' D_h^4}{\upsilon^2 k}$ (for isoflux thermal BC's)

h	Coordinate transformation scale factor, $a/(\cosh\eta-\cos\xi)$
H	Dimensionless geometric scale factor, $\frac{h}{D_h}=\frac{0.5\sinh(\eta_o)}{(1-N)(\cosh(\eta)-\cos(\xi))}$
k	Thermal conductivity of fluid
m	No. of segments in ξ-direction
n	No. of segments in η-direction
N	Radius ratio, $\frac{r_i}{r_o}$
Nu_h	Nusselt number on the heated side of the vertical channel
Nu_c	Nusselt number on the cold side of the vertical channel
p	Local pressure at any cross section of the vertical channel
p_o	Hydrostatic pressure, $\rho_o gz$ at channel entrance
P	Dimensionless pressure inside the channel at any cross section, $\frac{p-p_o}{\rho u_o^2}$
Pr	Prandtl number, $\frac{\mu C_p}{k}$
q"	Constant heat flux
r	Radial coordinate
r_i	Radius of inner cylinder of the vertical concentric and vertical eccentric channel
r_o	Radius of outer cylinder of the vertical concentric and vertical eccentric channel
R	Dimensionless radial coordinate

Re	Reynolds number, $\frac{\rho u_o D_h}{\mu}$
T	Dimensional temperature at any point in the channel
T_o	Ambient or fluid inlet temperature
T_w	Isothermal temperature of circular heated wall
T_1, T_2	Isothermal temperatures of plate 1 and plate 2 of parallel plates
T_{iw}, T_{ow}	Temperatures of inner and outer walls of concentric & eccentric annuli
u	Axial velocity component
$\overline{u}$	Average axial velocity
u_o	Uniform entrance axial velocity
U	Dimensionless axial velocity at any point, $\frac{u}{u_o}$
$U_{fd,mxd}$	Fully developed dimensionless axial velocity for mixed convection
$U_{fd,forced}$	Fully developed dimensionless axial velocity for forced convection
v	Transverse velocity component
V	Dimensionless transverse velocity, $\frac{v}{u_o}$ (parallel plates), $\frac{\mathrm{Re}\, v}{u_o}$ (circular tube), $\frac{vD_h}{\upsilon}$ (concentric annulus & eccentric annulus)
w	Tangential component in ξ-direction for vertical eccentric annulus
W	Dimensionless tangential component, $\frac{wD_h}{\upsilon}$
y	Transverse coordinate of the vertical channel between parallel plates

Y	Dimensionless transverse coordinate, $\frac{y}{D_h}$
z	Axial coordinate (measured from the channel entrance)
Z	Dimensionless axial coordinate in cartesian, cylindrical and bipolar coordinate systems, $\frac{z}{D_h \,\mathrm{Re}}$ (parallel plates, circular tube & eccentric annulus) and $\frac{2(1-N)z}{D_n \,\mathrm{Re}}$ (concentric annulus)
Z_I	Distance from the channel entrance to the location of zero pressure gradient
Z_{II}	Distance from the channel entrance to the location of zero pressure
Z_{in}	Distance from the channel entrance to the location of numerical instability
Z_{fr}	Distance from the channel entrance to the location of onset of flow reversal
Z_{fd}	Distance from the channel entrance to the location of hydrodynamic fully development length

Greek Letters

η	Transverse direction of bipolar coordinate system
ξ	Tangential direction of bipolar coordinate system
η_i	Value of η on the inner surface of the eccentric annulus

$$\log_e\left[\frac{N\left(1+E^2\right)+\left(1-E^2\right)}{2NE}+\sqrt{\left(\frac{N\left(1+E^2\right)+\left(1-E^2\right)}{2NE}\right)^2-1}\right]=Cosh^{-1}\left[\frac{N\left(1+E^2\right)+\left(1-E^2\right)}{2NE}\right]$$

η_o Value of η on the outer surface of the eccentric annulus

$$\log_e\left[\frac{N\left(1-E^2\right)+\left(1+E^2\right)}{2E}+\sqrt{\left(\frac{N\left(1-E^2\right)+\left(1+E^2\right)}{2E}\right)^2-1}\right]=Cosh^{-1}\left[\frac{N\left(1-E^2\right)+\left(1+E^2\right)}{2E}\right]$$

$\Delta\eta$ Numerical grid mesh size in η-direction, $\left(\eta_i-\eta_o\right)/n$

$\Delta\xi$ Numerical grid mesh size in ξ-direction, π/m

θ Dimensionless temperature, $\left(T-T_o\right)/\left(T_w-T_o\right)$ (for isothermal case)

$\left(T-T_o\right)/q"D_h/k$ (for isoflux case)

θ_m Mean bulk temperature

θ_T Wall temperature difference ratio

$\left(\frac{T_2-T_o}{T_1-T_o}\right)$ for parallel plate

$\left(\frac{T_{ow}-T_o}{T_{iw}-T_o}\right)$ for both concentric and eccentric annuli, Case 1.I

$\left(\frac{T_{iw}-T_o}{T_{ow}-T_o}\right)$ for both concentric and eccentric annuli, Case 1.O

ρ Density of the fluid

ρ_o Density of the fluid at the channel entrance

μ Dynamic viscosity of the fluid

υ Kinematic viscosity of the fluid, μ/ρ

β Volumetric coefficient of thermal expansion

Miscellaneous

Gr/Re Buoyancy parameter

$(Gr/Re)_{crt}$ Critical value of buoyancy parameter

Abstract (English)

Name: **SHAIK SAMIVULLAH**

Title: **LAMINAR MIXED CONVECTION IN VERTICAL CHANNELS**

Degree: **MASTER OF SCIENCE**

Major Field: **MECHANICAL ENGINEERING (THERMO FLUIDS)**

Date of Degree: **MAY 2005**

The present work aims at the study of laminar mixed convection in vertical channels of different geometries. The geometries considered are namely, vertical channels between parallel plates, vertical circular tubes, vertical concentric circular annulus and vertical eccentric annulus. Emphasis is devoted to analyze the hydrodynamic behavior of mixed convection flow in such vertical channels under isothermal boundary conditions. In this regard the pressure and pressure gradient variation along the channel (from the entrance till the fully developed region) is obtained numerically. The effect of Prandtl number on the developing pressure and pressure gradient along the channel is investigated between parallel plates as an example. Moreover, critical values of the buoyancy parameter Gr/Re beyond, which, the mixed convection results in, build up of the pressure (or in other words, leads to a positive pressure gradient), are determined. These critical values are obtained analytically and numerically. Moreover, other hydrodynamic and heat transfer parameters of relevant importance are also presented for all cases under consideration.

Master of Science Degree

King Fahd University of Petroleum & Minerals

Dhahran, Saudi Arabia

May 2005

Abstract (Arabic)

الاســــــــــم: شيخ سميع الله

عنوان الرسالة: أنتقال الحراره بالحمل الطبائقى المختلط فى قنوات رأسيه

التخصـــــص: الهندسة الميكانيكيه

تاريخ التخـرج: مايو 2005 م

يهدف هذا البحث الى دراسه انتقال الحراره بالحمل الطبائقى المختلط فى قنوات رأسيه ذات اشكال هندسيه مختلفه وهى بالاسم القنوات بين الالواح الرأسيه المتوازيه, الانابيب الحلقيه الدائريه المركزيه و اللا مركزية . ولقد تم التركيز فى هذا البحث على ديناميكا سريان المائع داخل هذه القنوات الرأسيه تحت ظروف انتقال الحراره بالحمل الطبقى المختلط.

وفى هذا الصدد تم الحصول على تغير الضغط ومعدل تغير الضغط داخل هذه القنوات بأستخدام الطرق العدديه مع دراسه تاثير نوع المائع متمثلا بقيمه رقم براندل (Pr) على هذه التغيرات فى حاله الالواح المتوازيه كمثال. كما تم الحصول على القيم الحرجه لمعامل الطفو Gr/Re والذى يؤدى زيادته الى زياده الضغط فى اتجاه السريان بعد مسافه معينه من المدخل نتيجه تأثير الحمل المختلط ولقد تم الحصول على هذه القيم الحرجه بالطرق التحليليه كما تم عرض قيم المتغيرات ذات الصله بموضوع البحث.

درجة الماجستير

جامعة الملك فهد للبترول والمعادن

الظهران- المملكة العربية السعودية

مايو 2005 م

Chapter 1

INTRODUCTION

Combined forced and free convection flows (or mixed convection flows) inside vertical channels, such as parallel-plate channels, circular tubes, concentric and eccentric annular ducts, are encountered in many industrial applications, engineering devices. Investigations have shown considerable changes in heat transfer and friction coefficient due to mixed convection effects. This may provide the potential for optimizing some designs of heat transfer devices such as cooling systems for electronic components and reactors, cooling passages in turbine blades, combustion chambers, and many other heat exchanging surfaces. Mixed convection takes place when the presence of a temperature difference in a forced-flow field gives rise to density differences and thus to a buoyancy force. The buoyancy force may be expected to influence the transport phenomena of heat and momentum when the buoyancy force is considerably greater than those accompanying the forced flow. Depending upon whether the buoyancy force is acting to aid or to oppose the forced flow, the flow is referred to as aiding or opposing flow. In other words, flow is called buoyancy-aided flow if the buoyancy forces act in the flow direction while it is called buoyancy-opposed flow if the buoyancy forces oppose the flow direction. Buoyancy influences internal forced-convection heat transfer in ways that depend on whether the flow is laminar or turbulent, up-flow or down-flow and on duct geometry.

This makes it difficult to make a priori assumptions concerning buoyancy effects in internal flow. Design information for mixed convection should reflect the interacting effects of free and forced convection. It is important to realize that heat transfer and pressure drop in mixed convection can significantly differ from its value in both pure free and pure forced convection. Detailed information and a care classification of the flow and heat transfer (i.e., buoyancy-aided or buoyancy-opposed flow) as indicated are very crucial in the analysis of mixed convection in internal flows.

Even though most equipment are designed for operation in the turbulent flow regime, laminar flow has to be considered for partial load operation or during natural-circulation cooling, during the shut-off periods due to a sudden pump failure in a nuclear reactor. Due to its important applications, the literature pertinent to laminar mixed convection in vertical channels will be presented in the following Chapter 2.

The problem formulation of the given problem followed by objectives is discussed in Chapter 3. Analytical solutions for fully developed laminar mixed convection in vertical channels under different isothermal boundary conditions were obtained and presented in Chapter 4. Numerical technique and method of solution for the governing equations for the developing laminar mixed convection is outlined in Chapter 5. Validation of the present computer code by comparisons with the obtained analytical and available numerical results is presented in Chapter 6. Chapters 7, 8 and 9 present the results of hydrodynamic and thermal parameters and discuss the buoyancy effects on these parameters for different vertical channels under different isothermal boundary conditions. Finally, conclusions and recommendations are presented in Chapter 10.

Chapter 2

LITERATURE REVIEW

This chapter briefly presents the previous research that has been conducted in the area of combined free and forced convection flows in vertical channels of different geometries in fully developed and developing conditions under different thermal boundary conditions. Aung [1] presented a detailed literature review for the work reported on mixed convection in internal flows for the period (1942-1986). The following literature is classified according to the type of geometry.

2.1 Laminar Mixed Convection between Vertical Parallel Plates

With the technological demand on heat transfer enhancement, most markedly related to compact heat exchangers, solar energy collection, as in the conventional flat plate collector and cooling of electronic equipment analysis, the parallel-plate channel geometry gained further attention from thermal engineering researchers.

Understanding the flow development is essential in the analysis of the flow of heat as well as the development of temperature and other heat transfer parameters. The research related to flow and heat transfer through parallel plate channels has been well cited by Inagaki and Komori [2]. The literature pertinent to mixed convection in vertical channels between vertical parallel plates is reviewed hereunder and is divided according to the flow status (i.e., fully developed or developing).

2.1.1 Hydrodynamically and Thermally Fully Developed Flow between Vertical Parallel Plates

For laminar flow, in the fully developed region, i.e. in the region far from the channel entrance, the fluid velocity does not undergo appreciable changes in the stream-wise direction. Under these conditions, mixed convection between vertical parallel plates has been of interest in research for many years. Early work includes studies by Cebeci et al. [3] and by Aung and Worku [4]. The work by these investigators has shown that mixed convection between parallel plates exhibits both similarities and contrasts with flow in a vertical tube.

Using dimensionless parameters, Aung and Worku [4] solved the problem of mixed convection between parallel plates and obtained closed form analytical solution. From the closed-form solution for U, the criterion for the existence of reversed flow has been deduced under thermal boundary conditions of uniform heating on one wall while the other wall was thermally insulated. The relations between the Nusselt number and the Rayleigh number, and between the friction factor times the Reynolds number and the Rayleigh number were presented. For assisted flow, the Nusselt number increases with the Rayleigh number, while the opposite is true for opposed flow. The behavior of the product of friction factor and Reynolds number is similar to that of the Nusselt number. In general, these behaviors are similar to those for laminar flow in a uniformly heated vertical tube. Recently, Boulama and Galanis [5] presented exact solutions for fully developed, steady state laminar mixed convection between parallel plates with heat and mass transfer under the thermal boundary conditions of UWT and UHF. The results

revealed that buoyancy effects significantly improve heat and momentum transfer rates near heated walls of the channel. They [5] also analyzed the conditions for flow reversal.

To analyze the behavior of the flow with opposing buoyancy forces, Hamadah and Wirtz [6] studied the laminar mixed convection under three different thermal boundary conditions (i.e. both walls isothermal, both walls at constant heat flux and one wall at constant heat flux and other is maintained at constant temperature). They obtained closed form solutions to the fully developed governing equations and found that the heat transfer rates are dependent on Gr/Re and the ratio of wall thermal boundary. In their analysis, they obtained values of Gr/Re beyond which flow reversal takes place.

The vertical parallel plate configuration is applicable in the design of cooling systems for electronic equipment and of finned cold plates in general. In such systems, where the height of the channel is small, developing flow mode should be applicable.

2.1.2 Hydrodynamically and Thermally Developing Flow between Vertical Parallel Plates

An analysis of the mixed convection in a channel provides information on the flow structure in the developing region and reveals the different length scales accompanying the different convective mechanisms operative in the developing flow region. Yao [7] studied mixed convection in a channel with symmetric uniform temperature and symmetric uniform flux heating. He presented no quantitative information; he conjectured that fully developed flow might consist of periodic reversed flow. Quantitative information on the temperature and velocity fields has been provided in a numerical study reported by Aung and Worku [8]. These authors noted that buoyancy effects dramatically increase the hydrodynamic development distance. With asymmetric

heating, the bulk temperature is a function of Gr/Re and θ_T, and decreases as θ_T is reduced. Buoyancy effects are noticeable through a large segment of the channel, but not near the channel entrance or far downstream from it.

Wirtz and McKinley [9] conducted laboratory experiments on downward mixed convection between parallel plates where one plate heated the fluid (i.e., buoyancy-opposed flow situation). A laminar developing flow was observed in the absence of heating. The initial application of a plate heat flux resulted in a shifting of the mass flux profile away from the heated wall, a reduction in mass flow rate between the plates, and a corresponding decrease in plate heat transfer coefficient. A large application of plate heat flux resulted in a continuous decrease in mass flow rate with an increase in plate heat transfer coefficient. Turbulence intensity measurements suggested that the heating destabilizes the flow adjacent to the wall, giving rise to an increase in convective transport, which ultimately offsets the effect of the reduction in flow rate. These results suggest that a computational model of mixed convection applied to this flow geometry will require a turbulence model which includes buoyancy force effects, even at flow rates normally associated with laminar convection. Ingham et al. [10] presented a numerical investigation for the steady laminar combined convection flows in vertical parallel plate ducts with asymmetric constant wall temperature boundary conditions. Reversed flow has been recorded in the vicinity of the cold wall for some combinations of the ratio (Gr/Re) and the difference in the temperature between the walls. It was concluded that for a fixed value of θ_T (value of the dimensionless temperature at the wall) heat transfer is most efficient for Gr/Re large and negative (i.e. opposed flow) and that for a fixed value of Gr/Re heat transfer is most efficient when the entry temperature of the fluid is equal to

the temperature of the cold wall. Zouhair Ait Hammou [11] in 2004, studied laminar mixed convection of humid air in a vertical channel with evaporation or condensation at the wall. The results showed that the effect of buoyancy forces on the latent Nusselt number is small. However the axial velocity, the friction factor, the sensible Nusselt number and the Sherwood number are significantly influenced by buoyancy forces.

2.2 Laminar Mixed Convection in Circular Tubes

This section of the literature review is related to combined forced and free convection in circular tubes. The cited material is organized according to the flow whether it is fully developed or developing.

2.2.1 Hydrodynamically and Thermally Fully Developed Laminar Flow in Vertical Circular Tubes

Barletta et al. [12] analytically studied the fully developed laminar mixed convection in vertical circular duct under non-axisymmetric boundary conditions such that the fluid temperature does not vary along the axial direction. They studied two special cases. A duct subjected to a sinusoidal wall temperature distribution and a duct subjected to external convection with two environments having different references temperatures. Their results showed that for arbitrary thermal boundary conditions, which do not yield a net fluid heating, buoyancy forces do not affect the dimensionless temperature distribution, the dimensionless pressure drop parameter and the Fanning friction factor while the inverse of Nusselt number is a linear function of Gr/Re. In both cases, the dimensionless velocity profile depends on Gr/Re.

Behazdmehr et al. [13] have numerically studied upward mixed convection of air in a long vertical tube with UHF conditions. They conducted the study for Re = 1000 and 1500 and Gr $\leq 10^8$ using a low Reynolds number k-ε model. Their results for the fully developed region identify two Grashof numbers for each Reynolds number, which correspond to laminar-turbulent transition and relaminarization of the flow. The value of Grashof for transition from laminar to turbulent is approximately 8×10^6 for Re = 10^3 and 2×10^6 for Re = 1500. It is worth noting here that these values are close to those early reported by Metais and Eckert chart [14]. For the highest Grashof number, Gr = 7×10^7, the fully developed flow field is turbulent for Re = 1500 and laminar for Re = 1000. This second transition from laminar to turbulent is due to the laminarization effect of buoyancy-induced acceleration. Behazdmehr et al. [13] found that the value of Gr for relaminrization of turbulent flow is 5×10^7 for Re = 1000 and 10^8 for Re = 1500. Moreover, they presented a correlation that expresses the fully developed Nusselt number in terms of Grashof and Reynolds numbers. These authors [13] also showed Re-Gr combinations that result in a pressure decrease over the tube length from those resulting in a pressure increase. They reported the values of Gr above which a pressure increase, rather than a pressure decrease, will take place over the tube length in the flow direction due to the buoyancy effects as Gr = 4×10^5 for Re = 1000 and Gr = 3×10^5 for Re = 1500.

2.2.2 Thermally Developing Laminar Flow in Vertical Circular Tubes

When the flow enters the heated section under hydrodynamically fully developed conditions, the problem is called a thermally developing flow problem and it is also known as Graetz problem. In some cases, analytical solutions may be obtained for such

problem. However, numerical solution techniques are usually employed to solve developing problems. Marching scheme may be used for either UWT or the UHF case. A parabolic axial velocity profile i.e. $U = 2(1 - R^2)$ is given at the entrance of the heat transfer section. The buoyancy effects distort this profile as the fluid moves through the tube. Specifically, in buoyancy-aided flows, the centerline velocity decreases while the velocity near the wall, where the buoyancy force is dominant, increases. After a minimum is reached, the centerline velocity increases until, for constant property fluids, the velocity profile resumes its original fully developed parabolic shape at large distances from the entrance. Experimental results provided by Hallman [15] have shown that the thermal entrance length first decreases with the buoyancy effects (expressed in terms of Rayleigh number) then increases at large Rayleigh numbers.

At high heating rates, property variations are significant, and terms dealing with viscous dissipation and pressure work must be added to the energy equation. A number of approaches may be used to represent the property variations with temperature. Brauer et. al. [16] applied numerical methods to study both cases of heating and cooling of mixed convection in vertical tubes under the conditions of temperature-dependent fluid density, constant wall temperature and parabolic profile of axial velocity at the tube entrance. Barletta and di Schio [17] analyzed the effect of viscous dissipation and buoyancy on laminar and parallel (hydrodynamically fully developed) flow of a Newtonian fluid in a vertical circular-cross section duct under UHF conditions. Their results showed that the effect of viscous dissipation, for positive fixed values of the parameter Gr^*/Re, reduces the value of the Nusselt number and increases the value of the Fanning friction factor. It was also shown that for buoyancy aided flow, $Gr/Re > 0$, the dimensionless velocity

close to the wall increases with the increase of viscous dissipation effect in terms of Brinkman number (Br).

2.2.3 Hydrodynamically and Thermally Developing Laminar Flow in Vertical Circular Tubes

The situations in which the velocity profile is assumed to be flat at the entrance to the heat transfer section are described as hydrodynamically and thermally developing flows. For this type of problems, the pressure drop parameter is usually defined as the difference between the buoyancy pressure and the friction terms. This buoyancy pressure is the difference between the static pressure prevailing with the fluid heated and the static pressure that would exist if the fluid in the tube remains at the temperature at the tube entrance. The measurement of pressure drop in vertical, mixed convection flow is very difficult because the actual pressure differences are quite small and due to complex temperature field which depends on both radial and axial distances. Hence, Joye [18] developed a prediction equation for pressure drop in vertical, internal, aiding flow situations with UWT and is given as:

$$\Delta P / \Delta P_{lam} = 1 + 1565\, Gr_L^{3/4}\, \mathrm{Pr}^{1/2} / (0.952 + \mathrm{Pr})^{3/4}\, \mathrm{Re}^2 \times (L/D)^2 \Big|_b$$

where all fluid properties are evaluated at the bulk average temperature. This work was an extension of a previous work by Saylor and Joye [19] in which they presented a hydrostatic correction and pressure drop measurement in mixed convection heat transfer in a vertical tube with UWT or constant wall temperature (CWT).

The correlation for the pressure drop show that the pressure drop monotonically increases with the buoyancy effect represented by the Grashof number for all values of Reynolds number. This represents a contradiction with the results of Behazdmehr et al.

[13]. However, in one of the very deeply thoughtful articles, Han [20] proved that in aiding flow situations with UHF, there is a certain point at which, dP/dZ will become positive, i.e. the pressure will build up in the axial direction of the vertical heated pipe if the pipe is tall (long) enough. This was also proved by Mokheimer and El-Sharawi [21] who showed the presence of critical values of Gr/Re beyond which pressure build up takes place due to mixed convection in vertical ducts. They conducted the investigation of the critical values of Gr/Re for laminar mixed convection of air in vertical eccentric annuli under isothermal/adiabatic boundary conditions. It is also worth noting here that works of Behazdmehr et al. [13], Han [20] and Mokheimer and El-Shaarawi [21] were for air (Pr = 0.7) while the work of Joye [18] was for water (Pr = 4.53). The use of different fluids (different Prandtl number) might justify the contradicted findings of [13] and [18] about the pressure variation along a vertical tube due to mixed convection.

The variable-property effects in laminar aiding and opposing mixed convection of air in vertical tubes has been numerically investigated by Nesreddine et al. [22] in order to determine these effects on the flow pattern and heat transfer performance. Various Grashof numbers were investigated with a fixed entrance Reynolds number of 500 using both the Boussinesq approximation (constant-property model) and a variable-property model. In the latter model, the fluid viscosity and thermal conductivity of the fluid were allowed to vary with absolute temperature according to simple power laws; the density was varied linearly with the temperature, while the heat capacity was assumed constant. The comparison between the constant- and variable-property models showed a substantial difference in the temperature and velocity fields when Grashof number Gr is increased. The results also revealed that the friction factor is underestimated by the Boussinesq

approximation for the aiding flow and it is overestimated for the opposing flow. However, the effects on the heat transfer performance remains negligible except for cases with flow reversal. They concluded that the variable-property model predicts flow reversal at lower values of Gr, especially for cases with opposing buoyancy forces.

2.3 Laminar Mixed Convection in Concentric Annuli

Mixed convection in cylindrical cavities is of particular interest to industry in the design of various types of machinery, which involve heating and/or cooling. Some examples of machinery are coolant channels for power transformers, electric motors and generators, nuclear reactors, components of turbo machinery, double-pipe heat exchangers, and specific types of catalytic devices. In order to improve the design of such equipment and hence minimize possible failures, a better knowledge of heat transfer and hydrodynamics and flow patterns inside the device is necessary. Due to its importance, the literature pertinent to the laminar mixed convection in concentric circular annuli will be reviewed in this section. The literature will be limited to vertical annuli and will be divided according to the flow status (i.e., fully developed or developing).

2.3.1 Hydrodynamically and Thermally Fully Developed Laminar Mixed Convection in Vertical Circular Concentric Annuli

The early experimental and theoretical work, prior to 1987, pertinent to this problem was relatively limited and was thoroughly reviewed by Aung [1]. As reported by Aung [1], these investigations showed that in aided, hydrodynamically and thermally fully developed flow, buoyancy effects are negligible for $Ra < 10^3$. A step increase in Nu_i is evident beyond this value for all radius ratios, and the variation may be represented

approximately as $Nu_i \propto Ra^{1/4}$. The effects of viscous dissipation on velocity and temperature field are negligible for fully developed flow. However, the Nusselt number decreases as viscous dissipation increases. For upward flow, Kim [23] investigated the problem of fully developed laminar combined natural and forced convection in vertical circular tube annulus. Using arbitrary combination of uniform heat fluxes prescribed on the inner and on the outer surfaces of the annulus, Kim [23] obtained complete closed form analytical solutions for velocity and temperature. Nusselt number was determined from these solutions. It has been shown that the problem was characterized by the diameter ratio, the Grashof-to-Reynolds number ratio, and the heat flux ratio. Fundamental solutions that are independent on the heat flux were obtained, from which the general solutions for any heat flux ratio can be easily obtained, simply by using the superposition principle. This is possible for the fully developed conditions for flow of fluids with constant properties where nonlinearity is absent. Results showed that heat transfer enhances significantly with the increase of Gr/Re. On the other hand, Zaki et al. [24] collected and correlated heat transfer data for fully developed natural laminar flow and combined natural and forced laminar flow of water in a vertical annulus for $140 < Re < 1200$ and Ra up to 1.7×10^6. For $Ra < 5 \times 10^5$, Nu was independent of Ra; beyond that the variation of Nu was correlated as $Nu_i \propto Ra$. They also collected and correlated data for buoyancy aiding and opposing laminar and transition flows for $140 < Re < 10\ 000$. For $1000 < Re < 4000$, the values of Nu for buoyancy opposing flow were about 25 % lower than those for buoyancy aiding flow. For laminar flow ($Re < 500$), Nu values were consistent for both natural and forced circulation.

Investigating the fully developed laminar mixed convection in a vertical annular duct Barletta [25] obtained an analytical solution to the governing equations for the power law fluid. The conditions of flow reversal for fixed values of power-law index and of the ratio between the ducts inner and outer radii were determined.

2.3.2 Thermally Developing Laminar Mixed Convection in Vertical Circular Concentric Annuli

In such situation, the velocity profile is fully developed at the entrance of the heated section. The literature pertinent to this situation is also limited. Aung [1] reviewed the related literature prior to 1987. In 1989, El-Genk and Rao [26] presented intensive experiments and correlations for low Reynolds-number hydrodynamically developed but thermally developing buoyancy-aided and –opposed flows of water in vertical annuli. They proposed a correlation for the Nusselt number as: $Nu_L = (Nu_{F,L}^3 + Nu_{N,L}^3)^{1/3}$, where $Nu_{F,L}$ and $Nu_{N,L}$ are the Nusselt numbers for laminar forced and natural convection, respectively.

2.3.3 Hydrodynamically and Thermally Developing Mixed Convection in Vertical Circular Concentric Annuli

Developing mixed convection for laminar boundary-layer flow in a vertical annulus with a rotating inner cylinder was investigated by El-Shaarawi and Sarhan [27]. They considered both aiding and opposing flow for a fluid of Pr = 0.7 in annulus of a given radius ratio. The vanishing of the velocity gradient normal to the wall was considered an indication of the onset of flow reversal. The hydrodynamic development length as well as the distance from the entrance to the location of flow reversal onset depends on the

heating condition and whether the buoyancy is aiding or opposing the forced flow in addition to the rotational speed of the inner cylinder. Thus for thermal boundary conditions of the third kind (the inner rotating wall is isothermal and the outer stationary wall is adiabatic), with buoyancy-aided flow, the increase of the inner cylinder rotational speed moves the location of flow reversal onset in the direction to decrease the hydrodynamic development length. At a fixed Gr/Re, the inner-cylinder rotation causes an increase in the local heat transfer coefficient and bulk fluid temperature if the inner-cylinder wall is heated and vice versa if the outer-cylinder wall is heated. Simulating the geometry of the gaps at the ends of the rotor of a small, air cooled, vertically mounted electric motor, Hessami et al. [28] numerically investigate the laminar flow patterns and heat transfer for air contained in the enclosure formed between two vertical, concentric circular cylinders and two horizontal planes. The inner cylinder and one of the horizontal planes are heated and rotated about the vertical axis while the other horizontal plane and the outer cylinder are cooled and kept stationary. The results facilitate the thermal design of such a motor. In this regard, they developed a single correlation to calculate the heat transfer for design purposes. Ho and Tu [29] evaluated the perturbing effect of forced convection due to axial rotation of the inner cylinder on natural convection heat transfer of cold water with density inversion effects in a vertical cylindrical annulus. The mixed convection heat and fluid flow structures in the annulus were found to be strongly affected by the density inversion effects. The centrifugally forced convection can result in significant enhancement of the buoyant convection heat transfer of cold water with the density inversion parameter being equal to 0.4 or 0.5. Thus the slow axial rotation of the

inner cylinder can be a viable means of heat transfer augmentation of cold water natural in a vertical annulus.

2.4 Laminar Mixed Convection in Vertical Eccentric Annuli

The study of combined convection in vertical eccentric annuli constitutes a problem of particular interest due to its relevance in a variety of industrial applications. Such applications are encountered in the drilling and completion procedures in an oil well, electrical, nuclear, petroleum, solar and thermal storage fields. Therefore, the study in eccentric annuli has proved to be a useful model.

Sathymurthy et al. [30] presented a numerical study for laminar fully developed mixed convection in vertical eccentric annular ducts. They solved the equations governing the velocity and temperature on a body conforming grid by using a finite-volume technique. Patel and Ingham [31] solved the problem of fully developed mixed (combined forced and free) convection for a Newtonian fluid in an eccentric annulus for non-Newtonian fluids. Recently, Ingham and Patel [32], [33] extended their previous work [31] to solve the developing combined convection in an eccentric annulus for both Newtonian and non-Newtonian fluids. In their solution, they used a six- equation model solving for the five unknowns U, V, W, P and T in addition to the vertical (axial) pressure gradient as the sixth variable. The numerical technique used was based on the finite-element method at each plane, which eliminates the need for coordinate transformation, and the use of finite difference for marching the solution in the axial direction. In these two papers, Ingham and Patel presented results for an annulus having radius ratio of 0.5 and eccentricity 0 and 0.5. In these results the controlling parameters were the buoyancy

term Gr/Re = 100 & 250, Pr =1, 10 & 25 in addition to the flow behavior index n = 0.8 & 1.2 for the case of non-Newtonian fluids.

2.5 Summary

The in-depth literature cited above has revealed that, in spite of the huge amount of knowledge accumulated over the last few decades into the subject of laminar mixed convection in vertical channels, the mixed convection in such geometry is still not fully understood, especially the hydrodynamics of it. For instance, the term “aiding flow” is generally used in the literature as synonym for “upflow in a heated vertical channel or downflow for a cooled vertical channel” and vice versa for the term “opposing flow”. The general findings in the literature are that buoyancy effects enhance the pressure drop in buoyancy-aided flow (upward flow in a vertical heated channel), i.e., there is a monotonic pressure decrease of pressure in the axial direction of upward flow in a vertical heated channel. However, Han [20] and Mokheimer and El-Sharawi [21] proved that in aiding flow situations the pressure build up in the axial direction of the vertical channel. In these two articles it was shown that above certain values of the buoyancy parameter (Gr/Re), the vertical channel can act as a diffuser. However, flow reversal was shown for higher buoyancy effect, which was also pointed out by Han [20] who showed that for more buoyancy effects, the aiding flow is converted to opposed flow. Based on these findings, Han [20] introduced a more precise definition for the terms aiding and opposing flows such that the term aiding flow is used when the external pressure forces and the buoyancy forces works together in the same direction and vice versa for opposing flow.

This vagueness about the hydrodynamics of the developing mixed convection in vertical channels and insufficient information reported in the literature motivated the present work. The main objectives of the present work are outlined in the next chapter.

Chapter 3

OBJECTIVES OF THE PRESENT STUDY AND PROBLEM FORMULATION

3.1 Objectives

The objectives of the present study are as follows:

1. To analytically demonstrate the existence of a critical value of the buoyancy-parameter Gr/Re at which the buoyancy forces balance out the viscous forces and the pressure gradient becomes zero in the fully developed region for buoyancy-aided flow situations.
2. To quantify analytically and/or numerically the critical values of $(Gr/Re)_{crt}$ at which pressure gradient $(dP/dZ)_{fd,\ mxd} = 0$, and beyond which the pressure gradient (dP/dZ) starts to become positive and the pressure build up takes place for all the investigated cases.
3. To closely investigate the developing mixed convection in vertical channels of different geometries in order to study the mixed convection effects on the hydrodynamic and thermal parameters.
4. To study the effect of Prandtl number on the hydrodynamic parameters such as pressure gradient and local pressure in vertical channel between parallel plates for developing laminar mixed convection as an example.

3.2 Mathematical model/Problem Formulation

The general governing equations of any flow and heat transfer problem are the conservation equations of mass, momentum (Navier-Stokes equations) and energy. Assuming constant physical properties, one can write the full conservation equations in a vectorial form as follows.

Continuity Equation

$$\nabla . V = 0 \tag{3. 1}$$

Momentum Equation

$$\rho \frac{DV}{Dt} = F - \nabla P + \mu \nabla^2 V \tag{3. 2}$$

Energy Equation

$$\rho C_p \frac{DT}{Dt} = k \nabla^2 T + Q''' + \mu \Phi \tag{3. 3}$$

It is worth mentioning that the left-hand side of equation (3. 2) represents the inertia forces; the terms on the right-hand side denote the body force (buoyancy), the pressure gradient and viscous friction forces respectively.

The first step in any analytical or numerical solution of fluid and heat flow problems is to choose an orthogonal coordinate system such that its coordinate surfaces coincide with the boundary surfaces of the region under consideration. For example the rectangular coordinate system is useful for rectangular regions the cylindrical coordinate systems are used for regions having boundaries with cylindrical shapes, while the spherical coordinate system is used for bodies having spherical boundaries and so on.

Thus cartesian coordinates will be used to write the governing equations for flow and heat transfer between parallel plates, cylindrical coordinates will be used for circular tubes and circular concentric cylinders while the bipolar coordinates will be used for eccentric annular geometry.

3.2.1 Parallel plates

Figs. 3.1(a & b) depict two-dimensional channel between two vertical parallel plates. The distance between the plates is 'b' i.e., the channel width. The Cartesian coordinate system is chosen such that the z-axis is in the vertical direction that is parallel to the flow direction and the gravitational force 'g' always acting downwards independent of flow direction. The y-axis is orthogonal to the channel walls, and the origin of the axes is such that the positions of the channel walls are y = 0 and y = b. The classic Boussinesq approximation is invoked to model the buoyancy effect.

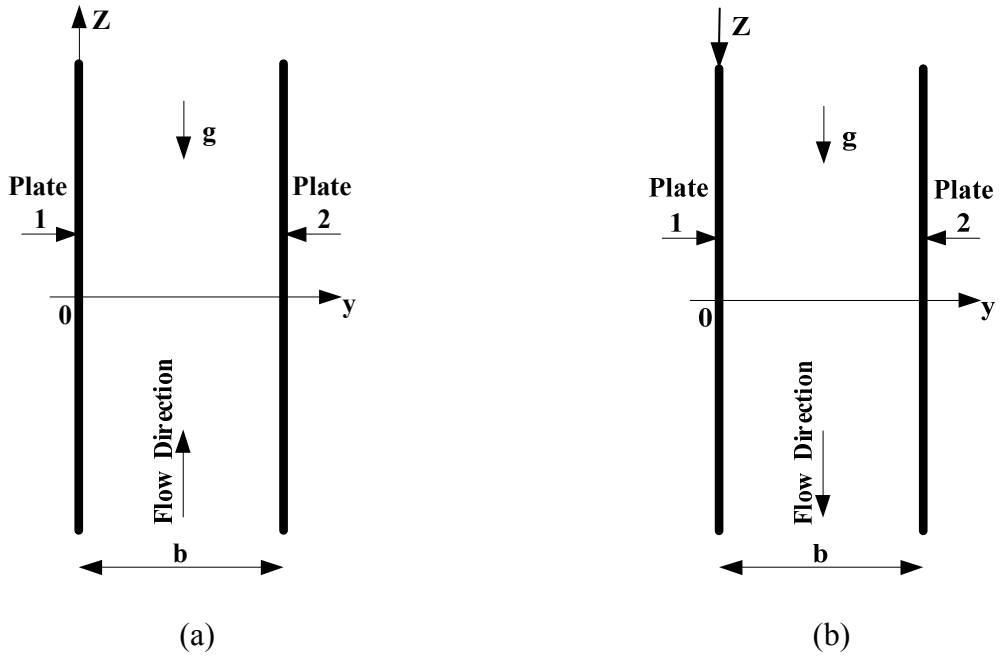

Figure. 3.1 Schematic view of the system and coordinate axes corresponding to (a) Upflow (b) Downflow

3.2.1.1 Dimensional form of the governing equations

The dimensional form of the governing equations for the combined forced and free convection between vertical parallel plates after performing order of magnitude analysis and applying boundary layer approximation can be written as:

Continuity Equation

$$\frac{\partial u}{\partial z}+\frac{\partial v}{\partial y}=0 \tag{3. 4}$$

z-Momentum Equation

$$\rho\left[u\frac{\partial u}{\partial z}+v\frac{\partial u}{\partial y}\right]=-\frac{\partial p}{\partial z}\mp\rho g+\mu\left(\frac{\partial^2 u}{\partial y^2}\right) \tag{3. 5}$$

It is worth repeating here that the positive direction (z) of the Cartesian coordinate is taken in the direction of flow. So, the gravitational body force $\left(\rho g\right)$ that always acts vertically downwards would have the negative sign for upward flow and positive sign for downward flow.

In the absence of forced convection heat transfer, there exists a hydrostatic pressure p_o at the tube entrance where the temperature T_o is uniform everywhere. Hence, for this special case the pressure gradient due to the hydrostatic pressure is given as:

$$-\frac{dp_o}{dz}\mp\rho_o g=0 \tag{3. 6}$$

where subscript '*o*' indicates conditions at the tube entrance

Subtracting equation (3. 6) from equation (3. 5), we have:

$$\rho\left[u\frac{\partial u}{\partial z}+v\frac{\partial u}{\partial y}\right]=-\frac{\partial p}{\partial z}-\left(-\frac{\partial p_o}{\partial z}\mp\rho_o g\right)\mp\rho g+\mu\left(\frac{\partial^2 u}{\partial y^2}\right) \tag{3. 7}$$

Applying the Boussinesq approximation $\rho = \rho_o\left(1 \mp \beta\left|T - T_o\right|\right)$ one can write the equation (3. 7) as:

$$\rho\left[u\frac{\partial u}{\partial z} + v\frac{\partial u}{\partial y}\right] = -\frac{\partial p}{\partial z} - \left(-\frac{\partial p_o}{\partial z} \mp \rho_o g\right) \mp \rho_o g\left(1 \mp \beta\left|T - T_o\right|\right) + \mu\left(\frac{\partial^2 u}{\partial y^2}\right) \qquad (3.\ 8)$$

where **plus** and **minus** in the Boussinesq approximation indicate the conditions for **cooling** and **heating** respectively.

It is possible to have two cases; whether the flow is either **upflow** or **downflow**. Each case can be further divided into two cases; **heating** or **cooling**. Thus we might have four possible cases, which are namely upflow with heating or upflow with cooling, downflow with heating or downflow with cooling. In situations of upflow with heating and downflow with cooling, the buoyancy forces works in the flow direction, so they are referred to as buoyancy aided flow. On the other hand, upflow with cooling and downflow with heating are referred to as buoyancy-opposed flow or more generally, when the buoyancy forces act in the direction opposite to the flow.

Upflow situations

The equation of motion in the z-direction for the upflow conditions when the body force acts vertically downwards would have the negative sign, thus equation (3. 8) can be written as:

$$\rho\left[u\frac{\partial u}{\partial z} + v\frac{\partial u}{\partial y}\right] = -\frac{\partial p}{\partial z} - \left(-\frac{\partial p_o}{\partial z} - \rho_o g\right) - \rho_o g\left(1 \mp \beta\left|T - T_o\right|\right) + \mu\left(\frac{\partial^2 u}{\partial y^2}\right)$$

$$\rho\left[u\frac{\partial u}{\partial z} + v\frac{\partial u}{\partial y}\right] = -\frac{\partial\left(p - p_o\right)}{\partial z} + \rho_o g - \rho_o g\left(1 \mp \beta\left|T - T_o\right|\right) + \mu\left(\frac{\partial^2 u}{\partial y^2}\right)$$

where **minus** and **plus** signs in the volumetric expansion term are for **heating** and **cooling,** respectively.

$$\rho\left[u\frac{\partial u}{\partial z}+v\frac{\partial u}{\partial y}\right]=-\frac{\partial(p-p_o)}{\partial z}+\cancel{\rho_o g}-\cancel{\rho_o g}\pm\rho_o g\beta|T-T_o|+\mu\left(\frac{\partial^2 u}{\partial y^2}\right)$$

Therefore, the final form of equation of motion for this flow condition is given as:

$$\rho\left[u\frac{\partial u}{\partial z}+v\frac{\partial u}{\partial y}\right]=-\frac{\partial(p-p_o)}{\partial z}\pm\rho_o g\beta|T-T_o|+\mu\left(\frac{\partial^2 u}{\partial y^2}\right) \quad (3.\ 9)$$

where **plus** and **minus** signs in the above equation are for **heating** and **cooling** respectively.

Downflow situations

The downflow heating and cooling equation of motion in the z-direction when the body force acts vertically downwards in the flow direction would have positive sign, thus equation (3. 8) can be written as:

$$\rho\left[u\frac{\partial u}{\partial z}+v\frac{\partial u}{\partial y}\right]=-\frac{\partial p}{\partial z}-\left(-\frac{\partial p_o}{\partial z}+\rho_o g\right)+\rho_o g\left(1\mp\beta|T-T_o|\right)+\mu\left(\frac{\partial^2 u}{\partial y^2}\right)$$

$$\rho\left[u\frac{\partial u}{\partial z}+v\frac{\partial u}{\partial y}\right]=-\frac{\partial(p-p_o)}{\partial z}-\rho_o g+\rho_o g\left(1\mp\beta|T-T_o|\right)+\mu\left(\frac{\partial^2 u}{\partial y^2}\right)$$

$$\rho\left[u\frac{\partial u}{\partial z}+v\frac{\partial u}{\partial y}\right]=-\frac{\partial(p-p_o)}{\partial z}-\cancel{\rho_o g}+\cancel{\rho_o g}\mp\rho_o g\beta|T-T_o|+\mu\left(\frac{\partial^2 u}{\partial y^2}\right)$$

Therefore, the final form of equation of motion for this flow condition is given as:

$$\rho\left[u\frac{\partial u}{\partial z}+v\frac{\partial u}{\partial y}\right]=-\frac{\partial(p-p_o)}{\partial z}\mp\rho_o g\beta|T-T_o|+\mu\left(\frac{\partial^2 u}{\partial y^2}\right) \quad (3.\ 10)$$

where **positive** sign for **cooling** and **negative** sign for **heating**

The two momentum equations for upflow and downflow can be written as one equation:

$$\rho\left[u\frac{\partial u}{\partial z}+v\frac{\partial u}{\partial y}\right]=-\frac{\partial(p-p_o)}{\partial z}\pm\rho_o g\beta|T-T_o|+\mu\left(\frac{\partial^2 u}{\partial y^2}\right) \quad (3.\ 11)$$

where **plus** and **minus** signs indicate **buoyancy aiding flow** and **buoyancy opposing flow** respectively.

Energy Equation

$$u\frac{\partial T}{\partial z}+v\frac{\partial T}{\partial y}=\frac{k}{\rho C_p}\left(\frac{\partial^2 T}{\partial y^2}\right) \tag{3. 12}$$

Integral form of Continuity Equation

$$\bar{u}=\frac{1}{b}\int_0^b u\,dy \tag{3. 13}$$

3.2.1.2 Dimensional form of boundary conditions

Entrance conditions

$$\text{At } z=0,\ 0\le y\le b:\ u=u_o,\ v=0,\ p=p_o,\ T=T_o \tag{3. 14}$$

No slip conditions

$$\begin{aligned}&\text{At } z>0,\ y=0:\ u=v=0\\&\text{At } z>0,\ y=b:\ u=v=0\end{aligned} \tag{3. 15}$$

For the flow between parallel plates, there exist four kinds of fundamental thermal boundary. These four fundamental thermal boundary conditions are combinations of having either of the walls subjected to isoflux or isothermal while the other is kept isothermal or adiabatic. The present study is devoted to only thermal boundary conditions in which at least one of the walls is kept isothermal.

Thermal boundary conditions

Table 3.1(a) Fundamental thermal boundary conditions for parallel plates

Kind	Wall 1	Wall 2
1	$T=T_1$	$T=T_2$
3	$T=T_o$	$\left(\frac{\partial T}{\partial y}\right)_{y=b}=0$
4	$q''=\mp k\left(\frac{\partial T}{\partial y}\right)_{y=0}$	$T=T_o$

3.2.1.3 Non-dimensional form of the governing equations

Using the pertinent dimensionless parameters given in the nomenclature the above governing equations can be written in dimensionless form as:

Continuity Equation

$$\frac{\partial U}{\partial Z}+\frac{\partial V}{\partial Y}=0 \tag{3. 16}$$

Z-Momentum Equation

$$\left[U\frac{\partial U}{\partial Z}+V\frac{\partial U}{\partial Y}\right]=-\frac{dP}{dZ}\pm\frac{Gr}{\mathrm{Re}}\theta+\left(\frac{\partial^2 U}{\partial Y^2}\right) \tag{3. 17}$$

Energy Equation

$$U\frac{\partial \theta}{\partial Z}+V\frac{\partial \theta}{\partial Y}=\frac{1}{\mathrm{Pr}}\left(\frac{\partial^2 \theta}{\partial Y^2}\right) \tag{3. 18}$$

The form of Continuity Equation can be written in integral form as

$$\int_0^1 U\,dY\ =1 \tag{3. 19}$$

3.2.1.4 Non-dimensional form of the boundary conditions

Entrance conditions

$$\text{At } Z=0,\ 0<Y<1:\ U=1, V=P=\theta=0 \tag{3. 20}$$

No slip conditions

$$\begin{aligned}&\text{At } Z>0,\ Y=0:\ U=V=0\\&\text{At } Z>0,\ Y=1:\ U=V=0\end{aligned} \tag{3. 21}$$

Thermal boundary conditions

Table 3.1(b) Dimensionless forms of fundamental thermal boundary conditions for parallel plates

Kind	Wall 1	Wall 2
1	$\theta = 1$	$\theta = \theta_T$
3	$\theta = 1$	$\left(\frac{\partial \theta}{\partial Y}\right)_{Y=1} = 0$
4	$\left(\frac{\partial \theta}{\partial Y}\right)_{Y=0} = -1$	$\theta = 0$

3.2.2 Circular Tubes and Concentric Annulus

Consider a steady laminar Newtonian fluid inside vertical cylindrical channels as shown in Fig.3.2. Let the fluid enter with a uniform velocity over the flow cross section.

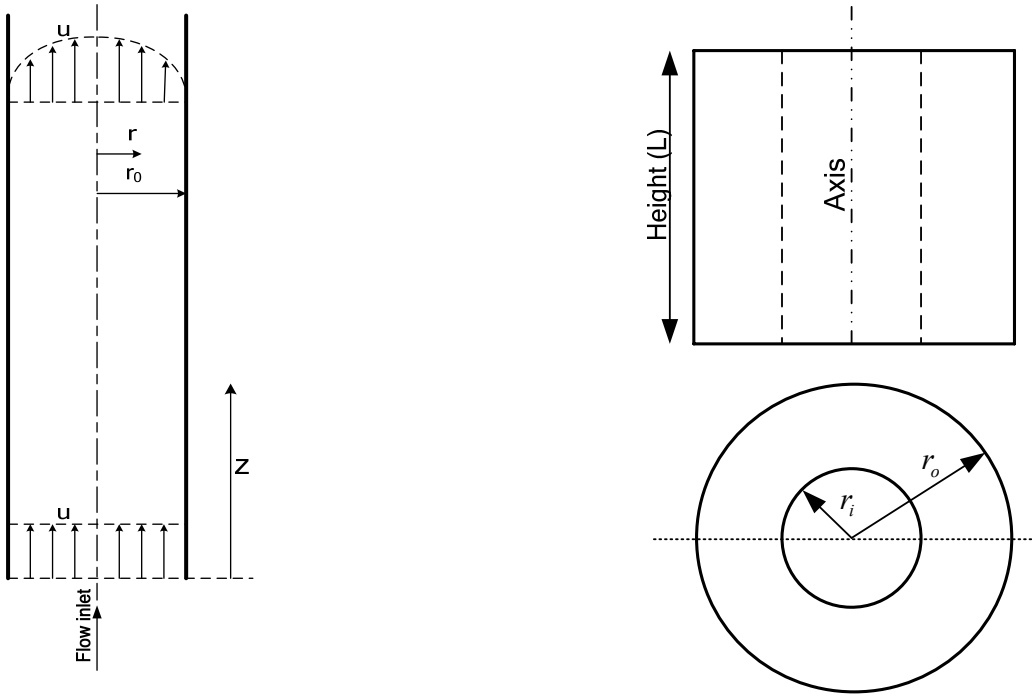

(a) (b)

Figure.3.2 (a) Flow in a circular tube (b) Schematic view of concentric annulus

3.2.2.1 Dimensional form of the governing equations

For the flow and heat transfer analysis in circular tubes and circular concentric annuli, the cylindrical coordinate system is the best coordinates to adopt so as to simplify the form of the governing equations and easily impose the boundary conditions.

Assuming that the flow and heat transfer are steady, pressure change only in the stream-wise direction, no axial diffusion of heat and momentum and axially symmetric flow and heat transfer, the boundary layer governing equations in cylindrical coordinates expressing the conservation equations of mass, momentum and energy for mixed convection in vertical circular and concentric ducts respectively are:

Continuity Equation

$$\frac{1}{r}\frac{\partial}{\partial r}(\rho r v) + \frac{\partial}{\partial z}(\rho u) = 0 \tag{3. 22}$$

z-Momentum Equation

$$\rho\left(v\frac{\partial u}{\partial r} + u\frac{\partial u}{\partial z}\right) = -\frac{d(p-p_o)}{dz} \pm \rho_o g\beta(T-T_o) + \frac{1}{r}\frac{\partial}{\partial r}\left(r\mu\frac{\partial u}{\partial r}\right) \tag{3. 23}$$

Energy Equation

$$\rho C_p\left[v\frac{\partial T}{\partial r} + u\frac{\partial T}{\partial z}\right] = \frac{1}{r}\frac{\partial}{\partial r}\left(rk\frac{\partial T}{\partial r}\right) \tag{3. 24}$$

Integral form of the Continuity Equation

For circular tube

$$\bar{u} = \frac{1}{\pi r_o^{\,2}}\int_0^{r_o} 2\pi u r\, dr$$

For concentric annulus

$$\bar{u} = \frac{1}{\pi\left(r_o^{\,2} - r_i^{\,2}\right)}\int_{r_i}^{r_o} 2\pi u r\, dr \tag{3. 25}$$

3.2.2.2 Non-dimensional form of the governing equations

Using the pertinent dimensionless parameters given in the nomenclature, the governing equations in cylindrical coordinates can be written as:

Continuity Equation

$$\frac{\partial V}{\partial R}+\frac{V}{R}+\frac{\partial U}{\partial Z}=0 \tag{3. 26}$$

Z-Momentum Equation

$$\left(V\frac{\partial U}{\partial R}+U\frac{\partial U}{\partial Z}\right)=-\frac{dP}{dZ}\pm C^{*}\frac{Gr}{\mathrm{Re}}\theta+\left(\frac{\partial^{2}U}{\partial R^{2}}+\frac{1}{R}\frac{\partial U}{\partial R}\right) \tag{3. 27}$$

Energy Equation

$$\left[V\frac{\partial \theta}{\partial R}+U\frac{\partial \theta}{\partial Z}\right]=\frac{1}{\mathrm{Pr}}\frac{1}{R}\frac{\partial}{\partial R}\left(R\frac{\partial \theta}{\partial R}\right) \tag{3. 28}$$

The form of Continuity Equation can be written in integral form as:

$$2\int_{0}^{1}U\,R\,dR=C^{**} \tag{3. 29}$$

where C^{*} and C^{**} in equations (3. 27) and (3. 29) are equal to:

$$C^{*}=\begin{cases}1 & \text{for circular tube}\\ \dfrac{1}{4\left(1-N\right)^{2}} & \text{for concentric annulus}\end{cases}$$

$$C^{**}=\begin{cases}1 & \text{for circular tube}\\ \left(1-N^{2}\right) & \text{for concentric annulus}\end{cases}$$

where $N=\dfrac{r_i}{r_o}$ represents the radius ratio

3.2.2.3 Non-dimensional form of the boundary conditions

1. For Circular Tube

Entrance conditions

$$\text{At } Z=0,\ 0<R<1:\ U=1, V=P=\theta=0 \tag{3. 30}$$

No Slip conditions

$$\text{At } Z>0,\ R=1:\ U=V=0 \tag{3. 31}$$

Symmetry conditions

$$\text{At } Z>0,\ R=0:\ \frac{\partial U}{\partial R}=\frac{\partial V}{\partial R}=0 \tag{3. 32}$$

Dimensionless form of the thermal boundary conditions

$$\begin{aligned}&\text{At } R=0:\ \frac{\partial \theta}{\partial R}=0\\ &\text{At } R=1:\ \ \theta=1\end{aligned} \tag{3. 33}$$

2. For Concentric Annulus

Entrance conditions

$$\text{At } Z=0,\ N<R<1:\ U=1, V=P=\theta=0 \tag{3. 34}$$

No slip conditions

$$\begin{aligned}&\text{At } Z>0,\ R=N:\ U=V=0\\ &\text{At } Z>0,\ R=1:\ U=V=0\end{aligned} \tag{3. 35}$$

Thermal boundary conditions

Table 3.2 Dimensionless forms of fundamental thermal boundary conditions for concentric annulus

Case	**Inner wall I (R = N)**	**Outer wall O (R = 1)**
1.I	$\theta = 1$	$\theta = \theta_T$
1.O	$\theta = \theta_T$	$\theta = 1$
3.I	$\theta = 1$	$\left(\frac{\partial \theta}{\partial R}\right)_{R=1} = 0$
3.O	$\left(\frac{\partial \theta}{\partial R}\right)_{R=N} = 0$	$\theta = 1$
4.I	$\left(\frac{\partial \theta}{\partial R}\right)_{R=N} = \pm \frac{1}{1-N}$	$\theta = 0$
4.O	$\theta = 0$	$\left(\frac{\partial \theta}{\partial R}\right)_{R=1} = \mp \frac{1}{1-N}$

It is worth mentioning here that in the case of uniform heat flux boundary conditions on the heat transfer wall (Case 4.I), the plus and minus signs in the conditions on R = N are applicable for heating and cooling respectively. However, for Case 4.O, the minus and plus signs in the boundary conditions on R = 1 stand for heating and cooling respectively. In the present investigation only cooling the heat transfer boundary will be considered during the analysis of the two cases 4.I and 4.O.

3.2.3 Eccentric Annulus

As shown in the Figure 3.3 (a), a two-dimensional cross-sectional channel of infinite length comprises of vertical eccentric annulus open at both ends. An incompressible fluid with constant properties enters the channel assuming it to be Newtonian. The flow is assumed steady with negligible viscous dissipation, no internal heat generation and no radiation heat transfer. The transformation of governing equations from Cartesian to general orthogonal curvilinear system is very tedious. However, the details of transformation into a general orthogonal curvilinear system were reported earlier [35].

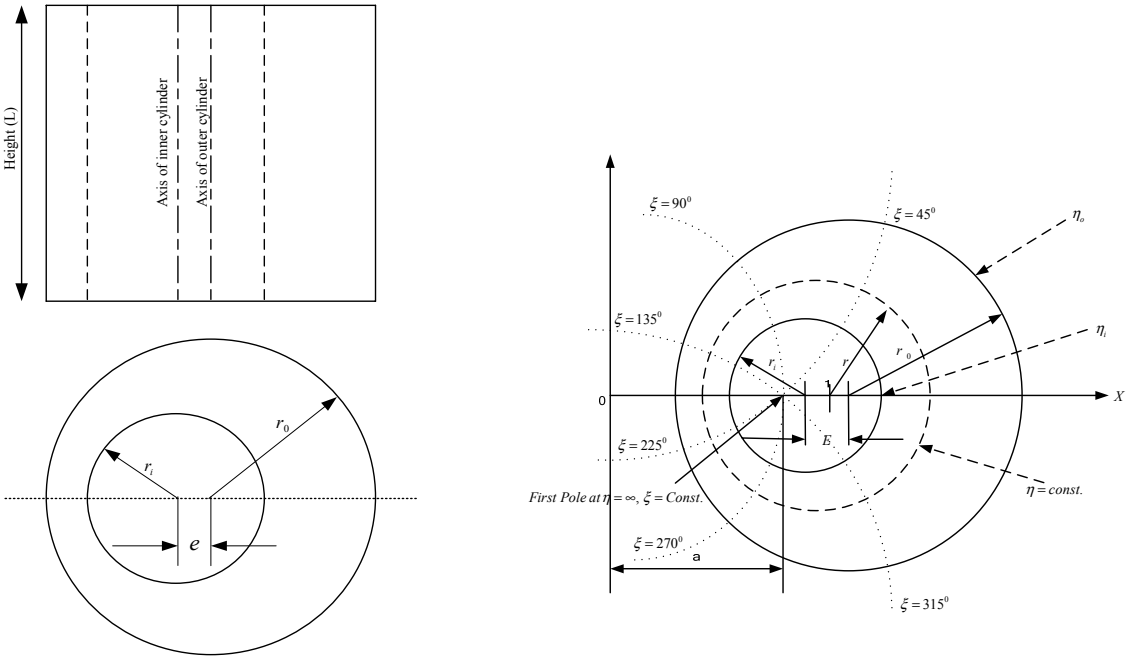

(a) (b)

Figure.3.3 (a) Schematic view of the eccentric annulus with channel height L (b) Bipolar Coordinate System

3.2.3.1 Dimensional form of the governing equations

Due to the absence of symmetry in the geometry under consideration the three velocity components exist. The governing equations for an incompressible fluid with constant properties in the bi-polar coordinate system based on the assumptions made are as follows:

Continuity Equation

$$\frac{\partial(hw)}{\partial\xi}+\frac{\partial(hv)}{\partial\eta}+\frac{\partial\left(h^2u\right)}{\partial z}=0 \tag{3. 36}$$

ξ - ***Momentum Equation***

$$\rho\left[\frac{w}{h}\frac{\partial w}{\partial\xi}+\frac{v}{h^2}\frac{\partial(hw)}{\partial\eta}+u\frac{\partial w}{\partial z}-\frac{v^2}{h^2}\frac{\partial h}{\partial\xi}\right]=-\frac{1}{h}\frac{\partial p}{\partial\xi}+\frac{\mu}{h}\left[\begin{array}{l}\frac{1}{h^2}\frac{\partial^2(hw)}{\partial\xi^2}+\frac{1}{h^2}\frac{\partial^2(hw)}{\partial\eta^2}+\frac{2}{h^2}\frac{\partial h}{\partial\xi}\frac{\partial(hu)}{\partial z}\\ +\frac{2}{h^3}\frac{\partial h}{\partial\eta}\left(\frac{\partial(hv)}{\partial\xi}-\frac{\partial(hw)}{\partial\eta}\right)\end{array}\right] \tag{3. 37}$$

z- Momentum Equation

$$\rho\left[\frac{w}{h}\frac{\partial u}{\partial\xi}+\frac{v}{h}\frac{\partial u}{\partial\eta}+u\frac{\partial w}{\partial z}\right]=-\frac{d\left(p-p_O\right)}{dz}\pm\rho_O g\beta\left(T-T_O\right)+\frac{\mu}{h^2}\left[\frac{\partial^2u}{\partial\xi^2}+\frac{\partial^2u}{\partial\eta^2}\right] \tag{3. 38}$$

Energy Equation

$$\left[\frac{w}{h}\frac{\partial T}{\partial\xi}+\frac{v}{h}\frac{\partial T}{\partial\eta}+u\frac{\partial T}{\partial z}\right]=\frac{\alpha}{h^2}\left[\frac{\partial^2T}{\partial\xi^2}+\frac{\partial^2T}{\partial\eta^2}\right] \tag{3. 39}$$

Integral form of the Continuity Equation

$$\pi\left(r_o{}^2-r_i^2\right)\overline{u}=2\int_0^{\pi}\int_{\eta_o}^{\eta_i}u\,h^2d\eta\,d\xi \tag{3. 40}$$

3.2.3.2 Non-dimensional form of the governing equations

Continuity Equation

$$\frac{\partial(HW)}{\partial\xi}+\frac{\partial(HV)}{\partial\eta}+K_1\frac{\partial\left(H^2U\right)}{\partial Z}=0 \tag{3. 41}$$

ξ -Momentum Equation

$$\left[\frac{W}{H}\frac{\partial W}{\partial\xi}+\frac{V}{H^2}\frac{\partial(HW)}{\partial\eta}+K_1U\frac{\partial W}{\partial Z}-\frac{V^2}{H^2}\frac{\partial H}{\partial\xi}\right]=K_4\frac{1}{H^3}\left[\frac{\partial^2(HW)}{\partial\xi^2}+\frac{\partial^2(HW)}{\partial\eta^2}\right]+K_5\frac{2}{H^3}\frac{\partial H}{\partial\xi}\frac{\partial(HU)}{\partial Z}+K_4\frac{2}{H^4}\frac{\partial H}{\partial\eta}\left(\frac{\partial(HV)}{\partial\xi}-\frac{\partial(HW)}{\partial\eta}\right) \tag{3. 42}$$

Z- Momentum Equation

$$\left[\frac{W}{H}\frac{\partial U}{\partial\xi}+\frac{V}{H}\frac{\partial U}{\partial\eta}+K_1U\frac{\partial U}{\partial Z}\right]=-K_2\frac{dP}{dZ}\pm K_3\theta+K_4\frac{1}{H^2}\left[\frac{\partial^2U}{\partial\xi^2}+\frac{\partial^2U}{\partial\eta^2}\right] \tag{3. 43}$$

Energy Equation

$$\left[\frac{W}{H}\frac{\partial\theta}{\partial\xi}+\frac{V}{H}\frac{\partial\theta}{\partial\eta}+K_1U\frac{\partial\theta}{\partial Z}\right]=K_6\frac{1}{H^2}\left[\frac{\partial^2\theta}{\partial\xi^2}+\frac{\partial^2\theta}{\partial\eta^2}\right] \tag{3. 44}$$

Integral Form of Continuity Equation

$$\overline{U}=\frac{8(1-N)}{\pi(1+N)}\int_0^{\pi}\int_{\eta_i}^{\eta_o}U\,H^2\,d\eta\,d\xi \tag{3. 45}$$

Parameters	K_1	K_2	K_3	K_4	K_5	K_6
Mixed Convection	1	1	$\frac{Gr}{\mathrm{Re}}$	1	1	$\frac{1}{\mathrm{Pr}}$

3.2.3.3 Non-dimensional form of the boundary conditions

Entrance conditions

$$\text{At } Z=0,\ \eta_i \le \eta \le \eta_o:\ U=1, V=W=P=\theta=0 \tag{3. 46}$$

No slip conditions

$$\begin{aligned} &\text{At } Z>0,\ \eta=\eta_i:\ U=V=W=0 \\ &\text{At } Z>0,\ \eta=\eta_o:\ U=V=W=0 \end{aligned} \tag{3. 47}$$

Symmetry conditions

$$\text{At } Z>0,\ \xi=0 \text{ and } \pi:\ \frac{\partial U}{\partial \xi}=\frac{\partial V}{\partial \xi}=\frac{\partial W}{\partial \xi}=\frac{\partial \theta}{\partial \xi}=0 \tag{3. 48}$$

Thermal boundary conditions

Table 3.3 Dimensionless form of fundamental thermal boundary conditions for eccentric annulus

Case	**Inner wall I** $\eta=\eta_i$	**Outer wall O** $\eta=\eta_o$
1.I	$\theta=1$	$\theta=0$
1.O	$\theta=0$	$\theta=1$

Chapter 4

ANALYTICAL SOLUTIONS FOR FULLY DEVELOPED LAMINAR MIXED CONVECTION IN VERTICAL CHANNELS

In this chapter, closed form analytical solutions for energy equation subjected to isothermal boundary conditions are obtained. These analytical solutions for temperature θ for different channels are substituted in the momentum equations, which are then solved analytically or numerically (for eccentric annuli).

The analytical solutions for the fully developed region (i.e. in the region far downstream of the channel entrance, the fluid velocity remains invariant) are readily available in the literature. However, these analytical solutions are derived here in order to demonstrate the presence of critical values of the buoyancy parameter Gr/Re above which pressure will build up in the flow in the vertical channels due to the buoyancy effects. Moreover, the obtained analytical solutions will be utilized to obtain these critical values of Gr/Re. For this problem the fluid is assumed to be Newtonian and the flow is assumed to be steady with negligible viscous dissipation and no heat generation. The assumption of a fully developed mixed convection flow implies here that the flow is both hydrodynamically and thermally fully developed. Under such conditions, $\partial\theta/\partial Z$ becomes zero for isothermal boundary conditions of first, third and fourth kind and hence for these boundary conditions, the governing equations reduce as mentioned in the following sections for the type of geometry considered.

4.1 Parallel plates

The problem of fully developed laminar mixed convection between vertical parallel plates is generally analyzed for both buoyancy aiding and opposing flows. After applying the above assumptions, the governing equations (3. 16)-(3. 18) reduce to:

Axial Momentum Equation

$$-\frac{dP}{dZ}\pm\frac{Gr}{\mathrm{Re}}\theta+\left(\frac{d^2U}{dY^2}\right)=0 \qquad (4.\ 1)$$

where plus and minus signs indicate buoyancy-aiding and buoyancy-opposing flows.

Energy Equation

$$\frac{d^2\theta}{dY^2}=0 \qquad (4.\ 2)$$

Complete-closed form solutions for the above equations are obtained for both buoyancy aiding and buoyancy opposing flows under the 1st, 3rd and 4th kind fundamental thermal boundary conditions that were discussed earlier. The no slip boundary conditions associated with equation (4. 1) are applicable (U=0) at both walls (i.e. at Y=0 and Y=1).

4.1.1 Fundamental solutions for the thermal boundary condition of first kind

Analytical solutions for fully developed energy and axial momentum equations are obtained for this kind of boundary condition. Energy equation for the fully developed laminar mixed convection flow represents pure conduction and it is completely independent of axial momentum equation. Hence, it is solved for temperature by applying the first kind thermal boundary condition, which is given as:

$$\theta=(\theta_T-1)Y+1 \qquad (4.\ 3)$$

where θ_T is the ratio of the two walls dimensionless temperature

The analytical temperature distribution obtained above is then substituted into the fully developed momentum equation given by equation (4. 1). After integrating twice and applying the no slip boundary conditions at the walls the fully developed axial velocity distribution is expressed as:

$$U_{fd,mxd} = -\left(\left(\frac{dP}{dZ}\right)_{fd,mxd} - \left(\pm\frac{Gr}{\mathrm{Re}}\right)\right)\frac{Y(1-Y)}{2} - \left(\pm\frac{Gr}{\mathrm{Re}}\right)(1-\theta_T)\frac{Y(1-Y^2)}{6} \tag{4. 4}$$

For forced convection (Gr/Re = 0)

$$U_{fd,forced} = -\left(\left(\frac{dP}{dZ}\right)_{fd,forced}\right)\frac{Y(1-Y)}{2} \tag{4. 5}$$

Calculation of Critical Value of Gr/Re

According to the definition of the dimensionless axial velocity for forced and mixed convection as u/u_o where u_o is the uniform inlet velocity, the average axial velocity at any section of the channel will be the same for both forced and mixed convection and both are equal to 1. Thus, one can write:

$$\bar{U}_{fd,forced} = \bar{U}_{fd,mxd} = 1$$

Therefore, the integral form of continuity equation for both forced convection and mixed convection can be written as:

$$\int_0^1 U_{fd,forced}\, dY = \int_0^1 U_{fd,mxd}\, dY$$

For vertical channel between parallel plates under thermal boundary conditions of first kind, the fully developed velocity profile is given as:

$$U_{fd,mxd} = C_1\frac{Y(1-Y)}{2} - C_2\frac{Y(1-Y^2)}{6}$$

and for forced convection, the fully developed velocity is:

$$U_{fd,\,forced} = C_3 \frac{Y(1-Y)}{2}$$

where

$$C_1 = -\left[\left(\frac{dP}{dZ}\right)_{fd,mxd} - \left(\pm\frac{Gr}{\mathrm{Re}}\right)\right],\; C_2 = \pm\frac{Gr}{\mathrm{Re}}(1-\theta_T),\; C_3 = -\left(\frac{dP}{dZ}\right)_{fd,forced}$$

$$\int_0^1 C_3 \frac{Y(1-Y)}{2}\,dY = \int_0^1 \left[C_1 \frac{Y(1-Y)}{2} - C_2 \frac{Y(1-Y^2)}{6}\right] dY$$

$$\frac{C_3}{2}\int_0^1 Y(1-Y)\,dY = \frac{C_1}{2}\int_0^1 Y(1-Y)\,dY \;-\; \frac{C_2}{6}\int_0^1 Y(1-Y^2)\,dY$$

After integrating, one gets:

$$C_3 = C_1 - \frac{1}{2}C_2$$

$$-\left(\frac{dP}{dZ}\right)_{fd,forced} = -\left[\left(\frac{dP}{dZ}\right)_{fd,mxd} - \left(\pm\frac{Gr}{\mathrm{Re}}\right)\right] - \frac{1}{2}\left(\pm\frac{Gr}{\mathrm{Re}}\right)(1-\theta_T)$$

and rearranging the terms as follows:

$$\left(\frac{dP}{dZ}\right)_{fd,mxd} = \left(\frac{dP}{dZ}\right)_{fd,forced} \pm \left(\frac{Gr}{\mathrm{Re}}\right)\frac{(1+\theta_T)}{2} \qquad (4.\,6)$$

with **plus** sign for **buoyancy aided flow** and **minus** sign for **buoyancy opposed flow**.

It is known that the pressure gradient for fully developed forced flow in any channel $(dP/dZ)_{fd,\,forced}$ is a constant negative value that depends on the channel geometry. So, it is clear from equation (4. 6), that the buoyancy effect will increase the negativity of the pressure gradient for buoyancy opposed flow. On the other hand, the buoyancy effect will reduce the negativity of the pressure gradient for buoyancy aided flow. Thus, for buoyancy aided flows, there exists a value of the buoyancy parameter (Gr/Re) that would

make the pressure gradient for mixed convection flow vanishes. The value can be obtained by equating the pressure gradient $\left(dP/dZ\right)_{fd,mxd}$ given by equation (4. 6) to zero and is given as:

$$\left(\frac{Gr}{\mathrm{Re}}\right)_{crt}=\frac{2\left(-\frac{dP}{dZ}\right)_{fd,forced}}{\left(1+\theta_T\right)} \tag{4. 7}$$

Equation (4. 7) represents the criterion for zero pressure gradient above which pressure build up will take place due to buoyancy effects. This value is a function of θ_T.

Some special cases

Knowing that $\left(-dP/dZ\right)_{fd,forced}=12$, the critical values of Gr/Re under thermal boundary condition of first kind can be calculated for different values of θ_T as given in the following table.

Table 4.1 Critical values of Gr/Re for different θ_T of parallel plates under the thermal boundary condition of first kind

θ_T ⟶	0	0.25	0.5	0.75	1.0
$(Gr/Re)_{crt}$ ⟶	24	19.2	16	13.7	12

Fully developed velocity profile

Substitution of equation (4. 6) into equation (4. 4) by taking $\left(dP/dZ\right)_{fd,forced}=-12$ leads to the following final form for the fully developed axial velocity profile:

$$U_{fd,mxd}=-6Y\left(Y-1\right)+\frac{1}{12}\left(\pm\frac{Gr}{\mathrm{Re}}\right)\left(1-\theta_T\right)\left(2Y^3-3Y^2+Y\right) \tag{4. 8}$$

This closed form solution of the velocity profile will be used to check the adequacy of the numerical model and solution of the developing flow in the entrance of the channel.

4.1.2 Fundamental solutions for the thermal boundary condition of third kind

The fully developed temperature and velocity profiles are obtained by solving the energy and axial momentum equations. This can be done by integrating equation (4. 2) twice and applying the dimensionless thermal boundary conditions as mentioned in the Table 3.1(b). Therefore, the final form of the fully developed temperature profile is given as:

$$\theta = 1 \tag{4. 9}$$

The form of velocity profile after substituting equation (4. 9) into equation (4. 1) and integrating twice with the application of no slip boundary conditions is expressed as:

$$U_{fd,mxd} = -\left(\left(\frac{dP}{dZ}\right)_{fd,mxd} - \left(\pm\frac{Gr}{\mathrm{Re}}\right)\right)\frac{Y(1-Y)}{2} \tag{4. 10}$$

Calculation of Critical Value of Gr/Re

According to the definition, the average axial velocity at any section of the channel will be the same for both forced and mixed convection and both are equal to 1. Thus, one can write:

$$\bar{U}_{fd,forced} = \bar{U}_{fd,mxd} = 1$$

The average velocity for both mixed and forced convection can be represented in an integral form of continuity equation as:

$$\int_0^1 U_{fd,forced}\, dY = \int_0^1 U_{fd,mxd}\, dY$$

$$U_{fd,mxd} = C_{mxd}\frac{Y(1-Y)}{2}$$

and for forced convection:

$$U_{fd,\,forced} = C_{forced}\frac{Y(1-Y)}{2}$$

This clearly shows that $C_{forced} = C_{mxd}$ where:

$$C_{mxd} = -\left[\left(\frac{dP}{dZ}\right)_{fd,\,mxd} - \left(\pm\frac{Gr}{\mathrm{Re}}\right)\right],\ C_{forced} = -\left(\frac{dP}{dZ}\right)_{fd,\,forced}$$

$$\left(\frac{dP}{dZ}\right)_{fd,\,mxd} = \left(\frac{dP}{dZ}\right)_{fd,\,forced} \pm \frac{Gr}{\mathrm{Re}} \qquad (4.\ 11)$$

where plus and minus signs indicate the buoyancy aided and buoyancy opposed flows respectively.

As mentioned earlier the value of Gr/Re, at which the pressure gradient becomes zero, is termed as critical value $(Gr/Re)_{crt}$. For buoyancy-aided flow, it can be obtained by equating the equation (4. 11) to zero and is given as follows:

$$\left(\frac{Gr}{\mathrm{Re}}\right)_{crt} = \left(-\frac{dP}{dZ}\right)_{fd,\,forced} = 12 \qquad (4.\ 12)$$

It is worth noting here that 12 in equation (4. 12) is nothing but fully developed pressure gradient for forced convection $\left(-dP/dZ\right)_{fd,\,forced} = 12$.

Fully developed velocity profile

The solution for fully developed velocity profile after substituting the equation (4. 11) into equation (4. 10) results into:

$$U_{fd,\,mxd} = -6Y(Y-1) \qquad (4.\ 13)$$

The above expression represents a particular case of first kind thermal boundary under symmetrical isothermal boundary conditions (θ_T = 1.0). Moreover, it is independent of Gr/Re (i.e. the profile remains unchanged for any value of Gr/Re).

4.1.3 Fundamental solutions for the thermal boundary condition of fourth kind

The fully developed temperature profile for the fourth kind of thermal boundary condition can be obtained by integrating and applying the appropriate thermal boundary conditions to the equation (4. 2) and is given as:

$$\theta = 1 - Y \tag{4. 14}$$

After obtaining fully developed temperature profile, the velocity distribution can be obtained by substituting equation (4. 14) into the equation (4. 1). By integrating twice and applying the no slip boundary conditions, the fully developed velocity profile is:

$$U_{fd,mxd} = -\left(\left(\frac{dP}{dZ}\right)_{fd,mxd} - \left(\pm\frac{Gr}{\mathrm{Re}}\right)\right)\frac{Y(1-Y)}{2} - \left(\pm\frac{Gr}{\mathrm{Re}}\right)\frac{Y\left(1-Y^2\right)}{6} \tag{4. 15}$$

Calculation of Critical Value of Gr/Re

From the definition of dimensionless axial velocity U = u/u_o, the average axial velocity at any section of the channel is same for both forced and mixed convection and is equal to 1. Thus, the average velocity can be written as:

$$\bar{U}_{fd,forced} = \bar{U}_{fd,mxd} = 1$$

By utilizing the integral form of continuity equation the average velocity for both forced convection and mixed convection can be written as:

$$\int_0^1 U_{fd,forced}\ dY = \int_0^1 U_{fd,mxd}\ dY$$

For vertical channel between parallel plates under thermal boundary condition of fourth kind, the fully developed velocity profile for mixed convection is given as:

$$U_{fd,mxd} = C_1\frac{Y(1-Y)}{2} - C_2\frac{Y\left(1-Y^2\right)}{6}$$

and for forced convection, the fully developed velocity profile is:

$$U_{fd,forced} = C_3 \frac{Y(1-Y)}{2}$$

where

$$C_1 = -\left[\left(\frac{dP}{dZ}\right)_{fd,mxd} - \left(\pm\frac{Gr}{\mathrm{Re}}\right)\right],\ C_2 = \pm\frac{Gr}{\mathrm{Re}},\ C_3 = -\left(\frac{dP}{dZ}\right)_{fd,forced}$$

$$\int_0^1 C_3 \frac{Y(1-Y)}{2} dY = \int_0^1 \left[C_1 \frac{Y(1-Y)}{2} - C_2 \frac{Y(1-Y^2)}{6}\right] dY$$

After integrating, one gets:

$$C_3 = C_1 - \frac{1}{2} C_2$$

$$-\left(\frac{dP}{dZ}\right)_{fd,forced} = -\left[\left(\frac{dP}{dZ}\right)_{fd,mxd} - \left(\pm\frac{Gr}{\mathrm{Re}}\right)\right] - \frac{1}{2}\left(\pm\frac{Gr}{\mathrm{Re}}\right)$$

and rearranging the terms as follows:

$$\left(\frac{dP}{dZ}\right)_{fd,mxd} = \left(\frac{dP}{dZ}\right)_{fd,forced} + \frac{1}{2}\left(\pm\frac{Gr}{\mathrm{Re}}\right) \qquad (4.\ 16)$$

where **plus** and **minus** in the above equation indicate the conditions for **buoyancy aided** and **buoyancy opposed** flows respectively.

As mentioned earlier, the critical value of buoyancy parameter (Gr/Re) beyond which the pressure build up will takes place exist only for buoyancy-aided flow and can be calculated by equating the equation (4. 16) to zero. The value is:

$$\left(\frac{Gr}{\mathrm{Re}}\right)_{crt} = 2\left(-\frac{dP}{dZ}\right)_{fd,forced} \qquad (4.\ 17)$$

It is worth reporting here that the value of pressure gradient $\left(-dP/dZ\right)_{fd,forced}$ for forced convection obtained from the integral form of the continuity equation is equal to 12. Thus, the critical value of buoyancy parameter $(\mathrm{Gr/Re})_{crt}$ can be written as:

$$\left(\frac{Gr}{\mathrm{Re}}\right)_{crt} = 24 \qquad (4.\ 18)$$

Fully developed velocity profile

The fully developed velocity profile for this case can be obtained by substituting the equation (4. 16) into equation (4. 15). The result is:

$$U_{fd,mxd} = -6Y(Y-1) + \frac{1}{12}\left(\pm\frac{Gr}{\mathrm{Re}}\right)\left(2Y^3 - 3Y^2 + Y\right) \qquad (4.\ 19)$$

4.2 Circular Tubes

Consider a steady state fully developed laminar flow of an incompressible fluid through a stationary simple cylindrical circular tube. Assuming constant properties with negligible axial heat conduction and axial momentum diffusion under hydrodynamically and thermally fully developed conditions, the velocity and temperature profiles become invariant and have no changes in the flow (axial) direction. Thus all the derivatives in the flow (axial) direction vanish. Moreover, the velocity component in the radial direction also vanishes in the fully developed region. Thus, the governing equations of such situations become a simplified form of the main governing equations. Therefore, the equation of motion in the flow direction and the energy equation reduced to:

z-Momentum Equation

$$-\frac{dP}{dZ} \pm \frac{Gr}{\mathrm{Re}}\theta + \frac{1}{R}\frac{d}{dR}\left(R\frac{dU}{dR}\right) = 0 \qquad (4.\ 20)$$

Energy Equation

$$\frac{1}{R}\frac{d}{dR}\left(R\frac{d\theta}{dR}\right) = 0 \qquad (4.\ 21)$$

Closed form solutions are obtained for the above equations by applying the appropriate boundary conditions. Energy equation is solved for temperature because it is

uncoupled with momentum equation. The obtained temperature is then substituted into fully developed axial momentum equation to get the velocity distribution keeping the pressure gradient term constant.

4.2.1 Fundamental solution for UWT boundary condition

Integrating the energy equation (4. 21) twice and applying the UWT boundary conditions, the fully developed temperature profile can be written as:

$$\theta = 1 \tag{4. 22}$$

Substituting for ($\theta = 1$), the equation (4. 20) can be written as:

$$\frac{1}{R}\frac{d}{dR}\left(R\frac{dU}{dR}\right) = \left(\left(\frac{dP}{dZ}\right)_{fd,mxd} - \left(\pm\frac{Gr}{\mathrm{Re}}\right)\right) \tag{4. 23}$$

The above equation can be written in a general form as:

$$\frac{1}{R}\frac{d}{dR}\left(R\frac{dU}{dR}\right) = C_{mxd} \tag{4. 24}$$

where $C_{mxd} = \left(\frac{dP}{dZ}\right)_{fd,mxd} - \left(\pm\frac{Gr}{\mathrm{Re}}\right)$

For forced convection (Gr/Re = 0), $\therefore C_{forced} = \left(\frac{dP}{dZ}\right)_{fd,forced}$

Integrating equation (4. 24) twice and applying the hydrodynamic boundary conditions mentioned in section 3.2.2, we get the following form for velocity profile:

$$U_{fd,mxd} = -\frac{C_{mxd}}{4}\left(1 - R^2\right) \tag{4. 25}$$

Calculation of Critical Value of Gr/Re

The critical value of Gr/Re can be calculated by using the definition of dimensionless axial velocity u/u_o. The average velocity at any cross section of the vertical circular tube

for both mixed and forced convection is same and is equal to 1/2. Thus, one can write the average velocity for both mixed and forced convection as:

$$\bar{U}_{fd,forced} = \bar{U}_{fd,mxd} = 1/2$$

By recalling the integral form of continuity equation, the average velocity for both forced convection and mixed convection is written as:

$$\int_0^1 U_{fd,mxd}\ R\,dR = \int_0^1 U_{fd,forced}\ R\,dR$$

$$-C_{mxd}\int_0^1 \left(1-R^2\right) R\,dR = -C_{forced}\int_0^1 \left(1-R^2\right) R\ dR$$

It is clear from the above expression, that $C_{mxd} = C_{forced}$

$$\left(-\frac{dP}{dZ}\right)_{fd,mxd} = \left(-\frac{dP}{dZ}\right)_{fd,forced} - \left(\pm\frac{Gr}{\mathrm{Re}}\right) \tag{4. 26}$$

Critical value is the value of Gr/Re at which the pressure start to build up and for buoyancy aiding flow, the value can be calculated by equating the pressure gradient given in the equation (4. 26) to zero. The value is equal to:

$$\left(\frac{Gr}{\mathrm{Re}}\right)_{crt} = \left(-\frac{dP}{dZ}\right)_{fd,forced} \tag{4. 27}$$

It is worth reporting here that the value of pressure gradient for fully developed forced convection is equal to:

$$\left(-\frac{dP}{dZ}\right)_{fd,forced} = 8 \tag{4. 28}$$

Thus, the critical value of buoyancy parameter $(Gr/Re)_{crt}$ is given as:

$$\left(\frac{Gr}{\mathrm{Re}}\right)_{crt} = 8 \tag{4. 29}$$

Fully developed velocity profile

Knowing the value of C_{mxd} equal to -8, the fully developed velocity profile can be written as:

$$U_{fd,mxd} = 2\left(1 - R^2\right) \tag{4. 30}$$

4.3 Concentric Annulus

Consider a steady laminar fully developed mixed convection flow inside an open-ended vertical concentric annulus of infinite length the walls of which are to be maintained at different fundamental thermal boundary conditions. Due to fully developed flow assumptions, the fluid enters the part under consideration of the annular passage with an axial velocity profile that remains invariant in the entire channel.

Under the above-mentioned assumptions, the equations of continuity, motion and energy (3. 26)-(3. 28) reduce to the following two simultaneous non-dimensional ordinary differential equations:

Axial Momentum Equation

$$-\frac{dP}{dZ} + \left(\pm \frac{1}{4\left(1-N\right)^2} \frac{Gr}{\mathrm{Re}} \right) \theta + \frac{d^2U}{dR^2} + \frac{1}{R}\frac{dU}{dR} = 0 \tag{4. 31}$$

where plus and minus signs indicate the buoyancy-aiding and buoyancy-opposing flow conditions.

Energy Equation

$$\frac{1}{R}\frac{d}{dR}\left(R\frac{d\theta}{dR} \right) = 0 \tag{4. 32}$$

Four boundary conditions are therefore needed to obtain analytical solutions for the above two second-order differential equations. The two conditions related to U are the no slip boundary conditions. On the other hand, there are many possible thermal boundary conditions applicable to the annular configuration that are discussed in the section on circular tubes and are shown in the Table 3.2.

4.2.1 Fundamental solutions for the thermal boundary condition of first kind

The first kind of fundamental thermal boundary condition can be divided into two cases based on the heat transfer boundary surface (Case 1.I and Case 1.O).

Solution for Case 1.I:

The solution for this case is obtained by solving the fully developed energy and axial momentum equations. The Case 1.I represents a first case of first kind thermal boundary condition with inner wall being the heat transfer boundary surface. Hence, solving the ordinary energy differential equation and applying the appropriate boundary conditions shown in the Table 3.2, the fully developed temperature profile is given as:

$$\theta = (1-\theta_T)\frac{\ln R}{\ln N} + \theta_T \tag{4. 33}$$

By substituting equation (4. 33) into equation (4. 31), the fully developed axial momentum equation becomes:

$$\frac{1}{R}\frac{d}{dR}\left(R\frac{dU}{dR}\right) = \frac{dP}{dZ} - \frac{1}{4(1-N)^2}\left(\pm\frac{Gr}{\mathrm{Re}}\right)\left[(1-\theta_T)\frac{\ln R}{\ln N} + \theta_T\right] \tag{4. 34}$$

Integrating the above equation twice and applying the no slip boundary conditions, the solution for $U_{fd,mxd}$ is written as:

$$U_{fd,mxd} = -\left(\frac{C_1 + C_2}{4}\right)\left[1 - R^2 - \frac{1-N^2}{\ln N}\ln R\right] - \frac{C_2}{4}\ln R\left(R^2 - N^2\right) \qquad (4.35)$$

where $C_1 = \left(\frac{dP}{dZ}\right)_{fd,mxd} - \frac{1}{4(1-N)^2}\left(\pm\frac{Gr}{\mathrm{Re}}\right)\theta_T$, $C_2 = \frac{1}{4(1-N)^2}\left(\pm\frac{Gr}{\mathrm{Re}}\right)\frac{(1-\theta_T)}{\ln N}$

Calculation of Critical Value of Gr/Re

From the definition of dimensionless axial velocity u/u_o the average velocity for both mixed and forced convection at any section of the vertical annulus is same and is equal to $\left(1-N^2\right)/2$. Hence by utilizing the integral form of the continuity equation, the average velocity for both mixed and forced convection can be written as:

$$\int_N^1 U_{fd,mxd}\, R\, dR = \int_N^1 U_{fd,forced}\, R\, dR = \frac{\left(1-N^2\right)}{2}$$

$$\int_N^1\left[-\left(\frac{C_1+C_2}{4}\right)\left[1-R^2-\frac{1-N^2}{\ln N}\ln R\right]-\frac{C_2}{4}\ln R\left(R^2-N^2\right)\right]R\,dR$$

$$= \int_N^1 -\frac{C_3}{4}\left[1-R^2-\frac{1-N^2}{\ln N}\ln R\right]RdR$$

where C_3 represents the pressure gradient for forced convection given by $\left(-dP/dZ\right)_{fd,forced}$

After integrating and rearranging the terms, the above expression takes the following form:

$$-\frac{\left(C_1+C_2\right)}{4}\frac{1-N^2}{2}\left[\frac{1+N^2}{2}+\frac{1-N^2}{2\ln N}\right]-\frac{C_2}{4}\frac{1-N^2}{2}\left[\frac{N^4}{2\left(1-N^2\right)}\ln N+\frac{N^2}{2}-\frac{1+N^2}{8}\right]$$

$$= -\frac{C_3}{4}\frac{1-N^2}{2}\left[\frac{1+N^2}{2}+\frac{1-N^2}{2\ln N}\right]$$

After simplifying the above expression, the relation between the constants represented by C_1, C_2 and C_3 is given as:

$$-C_1 - C_2\left(\frac{A+B+D+E}{A+B}\right) = -C_3$$

$$-\left(\frac{dP}{dZ}\right)_{fd,mxd} + \frac{1}{4(1-N)^2}\left(\pm\frac{Gr}{\mathrm{Re}}\right)\theta_T - \frac{1}{4(1-N)^2}\left(\pm\frac{Gr}{\mathrm{Re}}\right)\left(\frac{1-\theta_T}{\ln N}\right)\left(\frac{A+B+D+E}{A+B}\right) = -\left(\frac{dP}{dZ}\right)_{fd,forced} \quad (4.\ 36)$$

It is worth mentioning here that the pressure gradient for the fully developed forced convection can be written as:

$$-\left(\frac{dP}{dZ}\right)_{fd,forced} = \left(\frac{4}{A+B}\right) \quad (4.\ 37)$$

Therefore, the pressure gradient equation after substituting equation (4. 37) into equation (4. 36) can be written as:

$$-\left(\frac{dP}{dZ}\right)_{fd,mxd} = \left(\frac{4}{A+B}\right) - \frac{1}{4(1-N)^2}\left(\pm\frac{Gr}{\mathrm{Re}}\right)\left[\theta_T - \left(\frac{1-\theta_T}{\ln N}\right)\left(\frac{A+B+D+E}{A+B}\right)\right] \quad (4.\ 38)$$

It is possible to deduce a criterion at which the negativity of pressure gradient vanishes and beyond which the pressure build up will take place. This criterion or critical value of buoyancy parameter (Gr/Re) can be obtained by equating the equation (4. 38) to zero and is given as:

$$\left(\frac{Gr}{\mathrm{Re}}\right)_{crt} = \frac{4(1-N)^2}{\left[\theta_T - \left(\frac{1-\theta_T}{\ln N}\right)\left(\frac{A+B+D+E}{A+B}\right)\right]}\left(\frac{4}{A+B}\right) \quad (4.\ 39)$$

It is to remind the reader that the above critical value of buoyancy parameter (Gr/Re) is valid only for buoyancy aided flows.

Table 4.2 Definition of various parameters involved in the calculations based on radius ratio N

Radius Ratio r_i/r_o	A	B	D	E
N	$\frac{1+N^2}{2}$	$\frac{1-N^2}{2\ln N}$	$\frac{N^4}{2\left(1-N^2\right)}\ln N$	$\frac{N^2}{2}-\frac{1+N^2}{8}$

Table 4.3 Critical values of Gr/Re for different θ_T for a given radius ratio N of vertical concentric annulus, Case 1.I

$(Gr/Re)_{crt}$					
N	**$\theta_T = 0$**	**$\theta_T = 0.25$**	**$\theta_T = 0.5$**	**$\theta_T = 0.75$**	**$\theta_T = 1.0$**
0.1	176.90	101.70	71.35	54.95	44.69
0.2	149.30	95.80	70.53	55.81	46.18
0.3	133.90	91.51	69.50	56.02	46.92
0.4	123.70	88.17	68.49	56.00	47.36
0.5	116.20	85.45	67.56	55.87	47.63
0.6	110.40	83.18	66.71	55.69	47.79
0.7	105.80	81.24	65.94	55.49	47.90
0.8	102.00	79.57	65.24	55.28	47.96
0.9	98.76	78.10	64.59	55.07	47.99

Fully developed velocity profile

The fully developed velocity profile after substituting equation (4. 38) into equation (4. 35) is given as:

$$U_{fd,mxd}=\left[\frac{1+\frac{C_2}{4}(D+E)}{A+B}\right]\left[1-R^2-\frac{1-N^2}{\ln N}\ln R\right]-\frac{C_2}{4}\ln R\left(R^2-N^2\right) \qquad (4.\ 40)$$

Solution for Case 1.O

This is a case where outer wall of the concentric annulus is being treated as the heat transfer boundary surface. Since for a thermally fully developed flow, temperature is a function of radius R only, it follows that the integration of equation (4. 32) and the application of thermal boundary conditions, leads to the following fully developed temperature profile:

$$\theta=(\theta_T-1)\frac{\ln R}{\ln N}+1 \tag{4. 41}$$

After obtaining fully developed temperature profile, the ordinary differential equation (4. 31) assuming that the pressure gradient remains constant, is solved for the fully developed axial velocity profile, which is a function of radius R only. By substituting the equation (4. 41) into the equation (4. 31), the differential equation becomes:

$$\frac{1}{R}\frac{d}{dR}\left(R\frac{dU}{dR}\right)=\frac{dP}{dZ}-\frac{1}{4(1-N)^2}\left(\pm\frac{Gr}{\mathrm{Re}}\right)\left[(\theta_T-1)\frac{\ln R}{\ln N}+1\right] \tag{4. 42}$$

After integrating the above equation twice and applying the no slip boundary conditions at the walls, the solution for $U_{fd,mxd}$ is given as:

$$U_{fd,mxd}=-\left(\frac{C_1-C_2}{4}\right)\left[1-R^2-\frac{1-N^2}{\ln N}\ln R\right]+\frac{C_2}{4}\ln R\left(R^2-N^2\right) \tag{4. 43}$$

where $C_1=\left(\frac{dP}{dZ}\right)_{fd,mxd}-\frac{1}{4(1-N)^2}\left(\pm\frac{Gr}{\mathrm{Re}}\right)$ and $C_2=\frac{1}{4(1-N)^2}\left(\pm\frac{Gr}{\mathrm{Re}}\right)\frac{(1-\theta_T)}{\ln N}$

Calculation of Critical Value of Gr/Re

The procedure followed in Case 1.I is also adopted here to calculate the critical value of buoyancy parameter $(Gr/Re)_{crt}$. The pressure gradient equation for the fully developed mixed convection can be written as:

$$-\left(\frac{dP}{dZ}\right)_{fd,mxd}=\left(\frac{4}{A+B}\right)-\frac{1}{4(1-N)^2}\left(\pm\frac{Gr}{\mathrm{Re}}\right)\left[1+\left(\frac{1-\theta_T}{\ln N}\right)\left(\frac{A+B+D+E}{A+B}\right)\right] \quad (4.\ 44)$$

It is to remind the reader that the critical value of buoyancy parameter Gr/Re exist only for buoyancy aided flow and can be calculated by equating the equation (4. 44) to zero which is given as:

$$\left(\frac{Gr}{\mathrm{Re}}\right)_{crt}=\frac{4(1-N)^2}{\left[1+\left(\frac{1-\theta_T}{\ln N}\right)\left(\frac{A+B+D+E}{A+B}\right)\right]}\left(\frac{4}{A+B}\right) \quad (4.\ 45)$$

Table 4.4 Critical values of Gr/Re for different θ_T for a given radius ratio N of vertical concentric annulus, Case 1.O

$(Gr/Re)_{crt}$					
N	**$\theta_T = 0$**	**$\theta_T = 0.25$**	**$\theta_T = 0.5$**	**$\theta_T = 0.75$**	**$\theta_T = 1.0$**
0.1	59.78	55.13	51.14	47.70	44.69
0.2	66.86	60.13	54.63	50.05	46.18
0.3	72.23	63.65	56.89	51.43	46.92
0.4	76.73	66.43	58.57	52.37	47.36
0.5	80.70	68.76	59.90	53.06	47.63
0.6	84.26	70.76	60.99	53.59	47.79
0.7	87.53	72.53	61.92	54.01	47.90
0.8	90.55	74.10	62.71	54.35	47.96
0.9	93.36	75.51	63.39	54.63	47.99

Fully developed velocity profile

The fully developed velocity profile is obtained by using the integral form of the continuity equation and is written as:

$$U_{fd,mxd}=\left[\frac{1-\frac{C_2}{4}(D+E)}{A+B}\right]\left[1-R^2-\frac{1-N^2}{\ln N}\ln R\right]+\frac{C_2}{4}\ln R\left(R^2-N^2\right) \quad (4.\ 46)$$

4.2.2 Fundamental solutions for the thermal boundary condition of third kind

Solution for Case 3.I and Case 3.O

For these cases that fall under the third kind fundamental thermal boundary condition the fully developed temperature profile is given as:

$$\theta = 1 \tag{4. 47}$$

The fully developed axial momentum given in equation (4. 31) is solved for velocity distribution by substituting the equation (4. 47) into equation (4. 31) and is represented by:

$$\begin{aligned} \frac{1}{R}\frac{d}{dR}\left(R\frac{dU}{dR}\right) &= \frac{dP}{dZ} - \frac{1}{4(1-N)^2}\left(\pm\frac{Gr}{\mathrm{Re}}\right) \\ \frac{1}{R}\frac{d}{dR}\left(R\frac{dU}{dR}\right) &= C_{mxd} \end{aligned} \tag{4. 48}$$

Integrating equation (4. 48) twice and applying no slip boundary conditions at the walls we get:

$$U_{fd,mxd} = -\frac{C_{mxd}}{4}\left(1 - R^2 - \frac{1-N^2}{\ln N}\ln R\right) \tag{4. 49}$$

where $C_{mxd} = \left(\frac{dP}{dZ}\right)_{fd,mxd} - \frac{1}{4(1-N)^2}\left(\pm\frac{Gr}{\mathrm{Re}}\right)$

Calculation of Critical Value of Gr/Re

The critical value of Gr/Re can be calculated by using the definition of dimensionless axial velocity u/u_o. The average velocity at any cross section of the vertical concentric annular tube for both mixed and forced convection is same. Thus, one can write the average velocity for both mixed and forced convection as:

$$\bar{U}_{fd,mxd} = \bar{U}_{fd,forced} = \left(1-N^2\right)/2$$

By recalling the integral form of continuity equation, the average velocity for both forced convection and mixed convection is written as

$$\int_N^1 U_{fd,mxd}\ R\,dR = \int_N^1 U_{fd,forced}\ R\,dR$$

$$\frac{C_{mxd}}{4}\int_N^1 \left(1-R^2-\frac{1-N^2}{\ln N}\ln R\right)R\,dR = \frac{C_{forced}}{4}\int_N^1 \left(1-R^2-\frac{1-N^2}{\ln N}\ln R\right)R\,dR$$

It is clear from the above integration, that $C_{mxd} = C_{forced}$. Thus one can write:

$$-\left(\frac{dP}{dZ}\right)_{fd,mxd} + \frac{1}{4(1-N)^2}\left(\pm\frac{Gr}{\mathrm{Re}}\right) = -\left(\frac{dP}{dZ}\right)_{fd,forced} \qquad (4.\ 50)$$

It is again worth mentioning here, that the pressure gradient for the fully developed forced convection can be written as:

$$-\left(\frac{dP}{dZ}\right)_{fd,forced} = \left(\frac{4}{A+B}\right) \qquad (4.\ 51)$$

Therefore, the pressure gradient equation after substituting equation (4. 51) into equation (4. 50) can be written as:

$$-\left(\frac{dP}{dZ}\right)_{fd,mxd} = \left(\frac{4}{A+B}\right) - \frac{1}{4(1-N)^2}\left(\pm\frac{Gr}{\mathrm{Re}}\right) \qquad (4.\ 52)$$

Critical value is the value of Gr/Re at which the pressure starts to build up and for buoyancy aiding flow the value can be calculated by equating the equation (4. 52) to zero. The result is:

$$\left(\frac{Gr}{\mathrm{Re}}\right)_{crt} = 4(1-N)^2\left(\frac{4}{A+B}\right) \qquad (4.\ 53)$$

Table 4.5 Critical values of Gr/Re for a given radius ratio N of vertical concentric annulus under the thermal BC of third kind

N ⟶	0.1	0.2	0.3	0.4	0.5	0.6	0.7	0.8	0.9
$(Gr/Re)_{crt}$ ⟶	44.69	46.18	46.92	47.36	47.63	47.79	47.9	47.96	47.99

Substituting equation (4. 52) into equation (4. 49) the fully developed velocity profile can be expressed as:

$$U_{fd,mxd} = \left(\frac{1}{A+B}\right)\left[1 - R^2 - \frac{1-N^2}{\ln N}\ln R\right] \tag{4. 54}$$

From the above expression, it is clear that the fully developed velocity profile is independent of the buoyancy parameter $(\pm Gr/\mathrm{Re})$. This means that for any value of $(\pm Gr/\mathrm{Re})$, the fully developed velocity profile remains unaffected or unchanged.

4.2.3 Fundamental solutions for the thermal boundary condition of fourth kind

Solution for Case 4.I

This is one of the two cases of the fourth kind thermal boundary condition where the inner wall and the outer wall are maintained at UHF and UWT respectively. The solution for energy equation can be obtained by integrating the equation (4. 32) and applying the fourth kind thermal boundary condition given in the Table 3.2.3 (b), the fully developed temperature profile is given as:

$$\theta = -\left(\frac{N}{1-N}\right)\ln R \tag{4. 55}$$

The above temperature profile is used to obtain the fully developed velocity profile. By substituting equation (4. 55) into strongly coupled axial momentum equation, and can be expressed as:

$$\frac{1}{R}\frac{d}{dR}\left(R\frac{dU}{dR}\right)=\left(\frac{dP}{dZ}\right)_{fd,mxd}+\frac{1}{4\left(1-N\right)^{2}}\left(\pm\frac{Gr}{\mathrm{Re}}\right)\frac{N}{1-N}\ln R \qquad (4.\ 56)$$

Integrating twice and applying no slip boundary conditions at the walls, the equation (4. 56) yields to:

$$U_{fd,mxd}=\left(\frac{C_2-C_1}{4}\right)\left[1-R^2-\frac{1-N^2}{\ln N}\ln R\right]+\frac{C_2}{4}\ln R\left(R^2-N^2\right) \qquad (4.\ 57)$$

where $C_1=\left(\frac{dP}{dZ}\right)_{fd,mxd}$, $C_2=\frac{1}{4\left(1-N\right)^{2}}\left(\pm\frac{Gr}{\mathrm{Re}}\right)\frac{N}{1-N}$

Calculation of Critical Value of Gr/Re

According the definition of the dimensionless axial velocity for forced and mixed convection as u/u_o where u_o is the uniform inlet velocity, the average axial velocity at any section of the channel will be the same for both forced and mixed convection and is equal to $\left(1-N^2\right)/2$. Thus, one can write:

$$\bar{U}_{fd,mxd}=\bar{U}_{fd,forced}=\left(1-N^2\right)/2$$

Therefore, the integral form of continuity equation for both forced convection and mixed convection can be written as:

$$\int_N^1 U_{fd,mxd}\ RdR=\int_N^1 U_{fd,forced}\ RdR$$

$$\int_N^1 \left(\frac{C_2-C_1}{4}\right)\left[1-R^2-\frac{1-N^2}{\ln N}\ln R\right]+\frac{C_2}{4}\ln R\left(R^2-N^2\right)=\int_N^1 -\frac{C_3}{4}\left[1-R^2-\frac{1-N^2}{\ln N}\ln R\right]RdR$$

After integrating and rearranging the terms, the above expression reduced to:

$$-C_1 + C_2\left(\frac{A+B+D+E}{A+B}\right) = -C_3$$

where C_3 represents the pressure gradient for forced convection given by $\left(-dP/dZ\right)_{fd,forced}$

Therefore, the pressure gradient equation for fully developed mixed convection can be written as:

$$-\left(\frac{dP}{dZ}\right)_{fd,mxd} = \left(\frac{4}{A+B}\right) - \frac{1}{4(1-N)^2}\left(\pm\frac{Gr}{\mathrm{Re}}\right)\left[\left(\frac{N}{1-N}\right)\left(\frac{A+B+D+E}{A+B}\right)\right] \qquad (4.\ 58)$$

Critical value of buoyancy parameter (Gr/Re) for which the pressure gradient becomes zero can be evaluated by equating the equation (4. 58) to zero and is equal to:

$$\left(\frac{Gr}{\mathrm{Re}}\right)_{crt} = \frac{4(1-N)^2}{\left[\left(\frac{N}{1-N}\right)\left(\frac{A+B+D+E}{A+B}\right)\right]}\left(\frac{4}{A+B}\right) \qquad (4.\ 59)$$

Table 4.6 Critical values of Gr/Re for a given radius ratio N of vertical concentric annulus, Case 4.I

N ⟶	0.1	0.2	0.3	0.4	0.5	0.6	0.7	0.8	0.9
$(Gr/Re)_{crt}$ ⟶	691.6	371.0	259.6	202.5	167.7	144.1	127.1	114.2	104.1

Fully developed velocity profile

Substituting equation (4. 58) into equation (4. 57) leads to the final form of the fully developed velocity profile:

$$U_{fd,mxd} = \left[\frac{1-\frac{C_2}{4}(D+E)}{A+B}\right]\left[1-R^2-\frac{1-N^2}{\ln N}\ln R\right] + \frac{C_2}{4}\ln R\left(R^2-N^2\right) \qquad (4.\ 60)$$

Solution for Case 4.O

For this case with inner wall and outer wall maintained at UWT and UHF respectively, the fully developed temperature profile is obtained by integrating the energy equation twice and applying the appropriate boundary conditions that are discussed in the fourth kind boundary condition we obtained the final expression for temperature profile as:

$$\theta = \frac{1}{1-N}\left[\ln\left(\frac{R}{N}\right)\right] \tag{4. 61}$$

Substituting the above obtained temperature profile into the equation (4. 31) and integrating with respect to radius R, the solution for the fully developed velocity profile after applying the no slip boundary conditions is expressed as:

$$U_{fd,mxd} = \left(\frac{C_2 - C_1}{4}\right)\left[1 - R^2 - \frac{1-N^2}{\ln N}\ln R\right] + \frac{C_2}{4}\ln R\left(R^2 - N^2\right) \tag{4. 62}$$

where $C_1 = \left(\frac{dP}{dZ}\right)_{fd,mxd} - \frac{1}{4(1-N)^2}\left(\pm\frac{Gr}{\mathrm{Re}}\right)\left[-\frac{\ln N}{1-N}\right]$, $C_2 = -\frac{1}{4(1-N)^2}\left(\pm\frac{Gr}{\mathrm{Re}}\right)\frac{1}{1-N}$

Calculation of Critical Value of Gr/Re

Similar procedure followed in Case 4.I is adopted here to calculate the critical value of buoyancy parameter Gr/Re for Case 4.O. Therefore the pressure gradient for the fully developed mixed convection for Case 4.O can be written as:

$$-\left(\frac{dP}{dZ}\right)_{fd,mxd} = \left(\frac{4}{A+B}\right) - \frac{1}{4(1-N)^2}\left(\pm\frac{Gr}{\mathrm{Re}}\right)\left[-\frac{1}{1-N}\left(\frac{A+B+D+E}{A+B}\right) - \frac{\ln N}{1-N}\right] \tag{4. 63}$$

Thus the critical value of buoyancy parameter $(Gr/Re)_{crt}$ for buoyancy aided flow is given as:

$$\left(\frac{Gr}{\mathrm{Re}}\right)_{crt} = \frac{4(1-N)^2}{\left[-\frac{1}{1-N}\left(\frac{A+B+D+E}{A+B}\right)-\frac{\ln N}{1-N}\right]}\left(\frac{4}{A+B}\right) \qquad (4.\ 64)$$

Table 4.7 Critical values of Gr/Re for a given radius ratio N of vertical concentric annulus, Case 4.O

N →	0.1	0.2	0.3	0.4	0.5	0.6	0.7	0.8	0.9
$(Gr/Re)_{crt}$ →	23.37	33.23	41.99	50.25	58.21	65.98	73.62	81.16	88.61

Fully developed velocity profile

The fully developed velocity profile after substituting equation (4. 63) into equation (4. 62) can be written as:

$$U_{fd,mxd} = \left[\frac{1-\frac{C_2}{4}(D+E)}{A+B}\right]\left[1-R^2-\frac{1-N^2}{\ln N}\ln R\right]+\frac{C_2}{4}\ln R\left(R^2-N^2\right) \qquad (4.\ 65)$$

Note: The definition of parameters N, A, B, D, and E for the above calculations is given in the Table 4.2.

4.4 Eccentric Annulus

Consider a steady Newtonian fluid with constant properties entering the vertical channel open at both ends. Under the assumptions discussed in the section 3.2.4, the region far away from the channel inlet, the flow is assumed to be hydrodynamically fully developed. In addition to the assumptions, for hydrodynamic full development, $V = W = 0$ and $\partial U/\partial Z = 0$ is considered everywhere making the flow to be invariant in the axial direction. Therefore, the resulting two simultaneous equations of motion and energy are:

Z- Momentum Equation

$$-\left(\frac{dP}{dZ}\right)_{fd,mxd}+\left(\pm\frac{Gr}{\mathrm{Re}}\right)\theta+\frac{1}{H^2}\left[\frac{\partial^2 U}{\partial\xi^2}+\frac{\partial^2 U}{\partial\eta^2}\right]=0 \tag{4. 66}$$

Energy Equation

$$\frac{\partial^2\theta}{\partial\xi^2}+\frac{\partial^2\theta}{\partial\eta^2}=0 \tag{4. 67}$$

The above equation is typically a steady conduction equation with no internal heat generation.

4.4.1 Fundamental solutions for the thermal boundary condition of first kind

Obtaining analytical solutions for this kind of thermal boundary is difficult. Utilizing the thermal boundary conditions for this kind, Mokheimer [35] obtained the solution for the fully developed energy equation given as:

Solution for Case 1.I

$$\theta=\frac{\eta-\eta_o}{\eta_i-\eta_o} \tag{4. 68}$$

Substituting equation (4. 68) into equation (4. 66), the fully developed axial momentum equation can be written as:

$$-\left(\frac{dP}{dZ}\right)_{fd,mxd}+\left(\pm\frac{Gr}{\mathrm{Re}}\right)\left(\frac{\eta-\eta_o}{\eta_i-\eta_o}\right)+\frac{1}{H^2}\left[\frac{\partial^2 U}{\partial\xi^2}+\frac{\partial^2 U}{\partial\eta^2}\right]=0$$

After rearranging the terms, the above equation reduces to:

$$\frac{\partial^2 U}{\partial\xi^2}+\frac{\partial^2 U}{\partial\eta^2}=(C_1-C_2\eta)H^2 \tag{4. 69}$$

where $C_1=\left(\frac{dP}{dZ}\right)_{fd,mxd}+\left(\pm\frac{Gr}{\mathrm{Re}}\right)\left(\frac{\eta_o}{\eta_i-\eta_o}\right)$ and $C_2=\left(\pm\frac{Gr}{\mathrm{Re}}\right)\left(\frac{1}{\eta_i-\eta_o}\right)$

Solution for Case 1.O

$$\theta = \frac{\eta - \eta_i}{\eta_o - \eta_i} \tag{4. 70}$$

The fully developed axial momentum equation can be written as:

$$-\left(\frac{dP}{dZ}\right)_{fd,mxd} + \left(\pm\frac{Gr}{\mathrm{Re}}\right)\left(\frac{\eta - \eta_i}{\eta_o - \eta_i}\right) + \frac{1}{H^2}\left[\frac{\partial^2 U}{\partial \xi^2} + \frac{\partial^2 U}{\partial \eta^2}\right] = 0$$

Rearranging the terms, the above expression reduces to:

$$\frac{\partial^2 U}{\partial \xi^2} + \frac{\partial^2 U}{\partial \eta^2} = (C_1 - C_2\eta)H^2 \tag{4. 71}$$

where $C_1 = \left(\frac{dP}{dZ}\right)_{fd,mxd} + \left(\pm\frac{Gr}{\mathrm{Re}}\right)\left(\frac{\eta_i}{\eta_o - \eta_i}\right)$ and $C_2 = \left(\pm\frac{Gr}{\mathrm{Re}}\right)\left(\frac{1}{\eta_o - \eta_i}\right)$

It is difficult to obtain an analytical solution for the above equations due to the mathematical difficulties inherent in it. Moreover, an analytical solution is also difficult because the fully developed pressure gradient $(dP/dZ)_{fd,\ mxd}$ is not known. Thus the only way to evaluate the $(dP/dZ)_{fd,\ mxd}$ is to solve the developing region flow problem till the fully developed conditions. Different values of buoyancy parameter Gr/Re with fine tuning will be used to obtain the $(dP/dZ)_{fd,\ mxd.}$ At one particular value of buoyancy parameter Gr/Re, the $(dP/dZ)_{fd,\ mxd}$ becomes zero indicating the critical value of buoyancy parameter Gr/Re = $(Gr/Re)_{crt}$ beyond which the pressure build up will take place. Details of the numerical solution are given in the following Chapter 5.

Chapter 5

NUMERICAL APPROACH AND METHOD OF SOLUTION

This chapter discusses the numerical technique employed and the method of solution to solve the boundary layer equations that govern the flow and heat transfer for the developing region laminar mixed convection in different vertical channel geometries under different isothermal boundary conditions.

5.1 Numerical Approach

As mentioned in Chapter 3, obtaining closed form analytical solutions to the governing equations of the developing flow for all the geometries considered are quite difficult and for some cases are not possible yet. On the other hand, numerical technique provides solutions with accuracies approaching that of the analytical solution. Many numerical methods exists that can solve these governing equations such as finite difference methods, finite element methods, finite volume methods etc. In the present work, an implicit finite difference scheme is developed using the techniques explained in [38] to solve the governing equations for the flow and heat transfer parameters. The finite difference formulations of the governing equations for different vertical channels are described in the following sections.

5.1.1 Parallel Plates

Figure 5.1 shows the numerical grid of the geometry. Mesh points numbered consecutively from the arbitrary origin with the '*k*' progressing in the direction (Y) perpendicular to the flow (Z) direction, with *k* = 1, 2, , n+1. In this domain *k* = 1 represents the left wall, *k* = n+1 represents the right wall. It is worth mentioning that 'n' being the number of segments in the Y-direction, ΔY and ΔZ are the increments in Y-direction and Z-direction respectively. The solution is marching in the direction of flow (Z) in the form of axial steps. Hence, the quantity for example $U(Y)$ is replaced by $U(k)$.

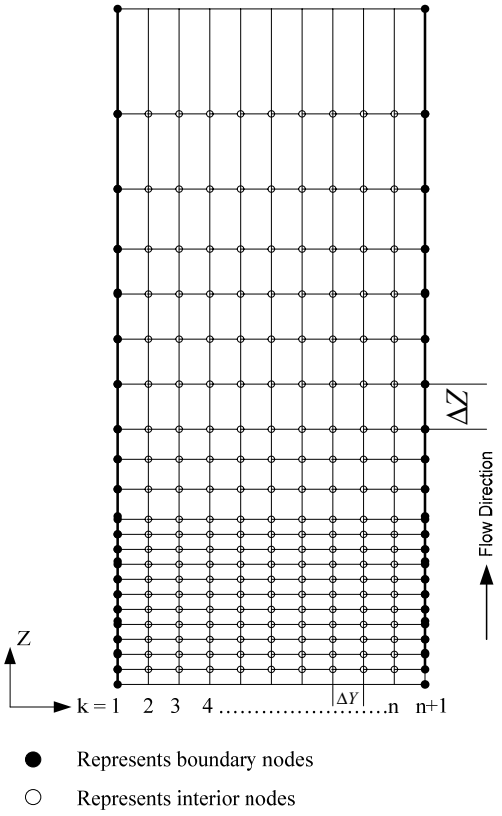

Figure 5.1 Finite difference domain of a two-dimensional vertical channel between parallel plates

Finite Difference Formulation of Continuity Equation

$$\frac{-\left[U(k+1)+U(k)-U^*(k+1)-U^*(k)\right]Y+\left[U(k-1)+U(k)-U^*(k+1)-U^*(k-1)\right](1-Y)}{2\Delta Z} + \frac{V(k)-V(k-1)}{\Delta Y}=0$$

Rearranging the terms, the above finite difference equation takes the following form;

$$V(k)=V(k-1)+\frac{\Delta Y}{2\Delta Z}\left[U(k+1)+U(k)-U^*(k+1)-U^*(k)\right]Y - \frac{\Delta Y}{2\Delta Z}\left[U(k)+U(k-1)-U^*(k-1)-U^*(k)\right](1-Y)+V(k+1) \tag{5. 1}$$

Finite Difference Formulation of the Axial Momentum Equation

$$U^*(k)\left[\frac{U(k)-U^*(k)}{\Delta Z}\right]+V^*(k)\left[\frac{U(k+1)-U(k-1)}{2\Delta Y}\right] = -\left[\frac{P(k)-P^*(k)}{\Delta Z}\right]+\left(\pm\frac{Gr}{\mathrm{Re}}\right)\theta(k)+\left[\frac{U(k+1)-2U(k)+U(k-1)}{(\Delta Y)^2}\right]$$

$$\frac{U^*(k)}{\Delta Z}U(k)-\frac{\left(U^*(k)\right)^2}{\Delta Z}+U(k+1)\frac{V^*(k)}{2\Delta Y}-U(k-1)\frac{V^*(k)}{2\Delta Y}=-\frac{P(k)}{\Delta Z}+\frac{P^*(k)}{\Delta Z}$$

$$+\left(\pm\frac{Gr}{\mathrm{Re}}\right)\theta(k)+\frac{U(k+1)}{\Delta Y^2}-\frac{U(k-1)}{\Delta Y^2}-2\frac{U(k)}{(\Delta Y)^2}$$

$$-U(k)\left[U^*(k)\frac{(\Delta Y)^2}{\Delta Z}+2\right]+U(k+1)\left[1-V^*(k)\frac{\Delta Y}{2}\right]+U(k-1)\left[V^*(k)\frac{\Delta Y}{2}+1\right]$$

$$-P(k)\frac{(\Delta Y)^2}{\Delta Z}=-P^*(k)\frac{(\Delta Y)^2}{\Delta Z}-\frac{\left[U^*(k)\Delta Y\right]^2}{\Delta Z}-\left(\pm\frac{Gr}{\mathrm{Re}}\right)(\Delta Y)^2\theta(k)$$

$$\boxed{aU(k)+bU(k+1)+cU(k-1)+S_PP(k)=R} \tag{5. 2}$$

where

$$a=-\left[U^*(k)\frac{(\Delta Y)^2}{\Delta Z}+2\right]$$

$$b=1-V^*(k)\frac{\Delta Y}{2}$$

$$c=1+V^*(k)\frac{\Delta Y}{2}$$

$$S_P=-\frac{(\Delta Y)^2}{\Delta Z}$$

$$R=-\frac{(\Delta Y)^2}{\Delta Z}\left[P^*(k)+\left(U^*(k)\right)^2\right]-\left(\pm\frac{Gr}{\mathrm{Re}}\right)(\Delta Y)^2\theta(k)$$

Finite Difference Formulation of Energy Equation

$$U^*(k)\frac{\theta(k)-\theta^*(k)}{\Delta Z}+V^*(k)\left[\frac{\theta(k+1)-\theta(k-1)}{2\Delta Y}\right]=\frac{1}{\mathrm{Pr}}\left[\frac{\theta(k+1)-\theta(k-1)-2\theta(k)}{(\Delta Y)^2}\right]$$

$$\theta(k)\left[U^*(k)\frac{(\Delta Y)^2}{\Delta Z}\mathrm{Pr}+2\right]+\theta(k+1)\left[\mathrm{Pr}V^*(k)\frac{\Delta Y}{2}-1\right]+\theta(k-1)\left[-\mathrm{Pr}V^*(k)\frac{\Delta Y}{2}-1\right]$$
$$=\mathrm{Pr}U^*(k)\theta^*(k)\frac{(\Delta Y)^2}{\Delta Z}$$

$$-\left[2+\mathrm{Pr}U^*(k)\frac{(\Delta Y)^2}{\Delta Z}\right]\theta(k)+\theta(k+1)\left[1-\mathrm{Pr}V^*(k)\frac{\Delta Y}{2}\right]+\theta(k-1)\left[1+\mathrm{Pr}V^*(k)\frac{\Delta Y}{2}\right]$$
$$=-\mathrm{Pr}U^*(k)\theta^*(k)\frac{(\Delta Y)^2}{\Delta Z}$$

$$\boxed{a\theta(k)+b\theta(k+1)+c\theta(k-1)=R} \qquad (5.3)$$

where

$$a = -\left[2 + \Pr U^*(k)\frac{(\Delta Y)^2}{\Delta Z}\right]$$

$$b = 1 - \Pr V^*(k)\frac{\Delta Y}{2}$$

$$c = 1 + \Pr V^*(k)\frac{\Delta Y}{2}$$

$$R = -\Pr U^*(k)\theta^*(k)\frac{(\Delta Y)^2}{\Delta Z}$$

Note:

* represents the previous axial step value and **plus** and **minus** in the term $(\pm Gr/\mathrm{Re})$ indicates the buoyancy aiding and buoyancy opposing flow.

Numerical Representation of the Integral Continuity Equation

The integral continuity equation can be represented by employing a trapezoidal rule of numerical integration and is as follows.

$$\left[\sum_{k=2}^{n} U(k) + 0.5\left(U(1) + U(n+1)\right)\right]\Delta Y = 1$$

However, from the no slip boundary conditions

$$U(1) = U(n+1) = 0$$

Therefore, the integral equation reduces to:

$$\left[\sum_{k=2}^{n} U(k)\right]\Delta Y = 1 \qquad (5.4)$$

5.1.2 Circular Tube

Finite Difference Formulation of the Continuity Equation

$$\frac{V(k+1)-V(k)}{\Delta R}+\frac{V(k+1)+V(k)}{2\left[\left(k-\frac{1}{2}\right)\Delta R\right]}+\frac{U(k+1)+U(k)-U^{*}(k+1)-U^{*}(k)}{2\Delta Z}=0$$

$$\frac{V(k+1)}{\Delta R}-\frac{V(k)}{\Delta R}+\frac{V(k+1)}{(2k-1)\Delta R}+\frac{V(k)}{(2k-1)\Delta R}+\frac{U(k+1)+U(k)-U^{*}(k+1)-U^{*}(k)}{2\Delta Z}=0$$

$$V(k+1)=V(k)\left[\frac{k-1}{k}\right]-\left[\frac{(2k-1)}{k}\right]\left[\frac{U(k+1)+U(k)-U^{*}(k+1)-U^{*}(k)}{4}\right]\frac{\Delta R}{\Delta Z}$$

(5. 5)

Finite Difference Formulation of the Axial Momentum Equation

$$V^{*}(k)\left[\frac{U(k+1)-U(k-1)}{2\Delta R}\right]+U^{*}(k)\left[\frac{U(k)-U^{*}(k)}{\Delta Z}\right]=-\left[\frac{P(k)-P^{*}(k)}{\Delta Z}\right]+K_1\theta(k)$$

$$+\left[\frac{U(k+1)+U(k-1)-2U(k)}{(\Delta R)^2}\right]+\frac{1}{(k-1)\Delta R}\left[\frac{U(k+1)-U(k-1)}{2\Delta R}\right]$$

$$U(k)\left[\frac{U^{*}(k)}{\Delta Z}+\frac{2}{(\Delta R)^2}\right]+U(k+1)\left[\frac{V^{*}(k)}{2\Delta R}-\frac{1}{(\Delta R)^2}-\frac{1}{(k-1)\Delta R}\frac{1}{2\Delta R}\right]$$

$$+U(k-1)\left[-\frac{V^{*}(k)}{2\Delta R}-\frac{1}{(\Delta R)^2}+\frac{1}{(k-1)\Delta R}\frac{1}{2\Delta R}\right]+P(k)\left[\frac{1}{\Delta Z}\right]=\frac{\left(U^{*}(k)\right)^2}{\Delta Z}+\frac{P^{*}(k)}{\Delta Z}+K_1\theta(k)$$

$$\boxed{aU(k)+bU(k+1)+cU(k-1)+S_P P(k)=R} \qquad (5.\ 6)$$

where

$$a = \frac{U^*(k)}{\Delta Z} + \frac{2}{(\Delta R)^2}$$

$$b = \frac{1}{\Delta R}\left[\frac{V^*(k)}{2} - \frac{1}{\Delta R} - \frac{1}{2(k-1)\Delta R}\right]$$

$$c = \frac{1}{\Delta R}\left[\frac{-V^*(k)}{2} - \frac{1}{\Delta R} + \frac{1}{2(k-1)\Delta R}\right]$$

$$S_p = \frac{1}{\Delta Z}$$

$$R_k = \frac{\left(U^*(k)\right)^2}{\Delta Z} + \frac{P^*(k)}{\Delta Z} + K_1\ \theta(k)$$

$$K_1 = \pm\frac{Gr}{\mathrm{Re}}$$

Finite Difference Formulation of the Energy Equation

$$V^*(k)\left[\frac{\theta(k+1)-\theta(k-1)}{2\Delta R}\right] + U^*(k)\left[\frac{\theta(k)-\theta^*(k)}{\Delta Z}\right] = \frac{1}{\mathrm{Pr}}\left[\begin{array}{c}\dfrac{\theta(k+1)+\theta(k-1)-2\theta(k)}{(\Delta R)^2} \\ +\dfrac{1}{(k-1)\Delta R}\dfrac{\theta(k+1)-\theta(k-1)}{2\Delta R}\end{array}\right]$$

$$\theta(k)\left[\frac{U^*(k)}{\Delta Z} + \frac{2}{\mathrm{Pr}(\Delta R)^2}\right] + \theta(k+1)\left[\frac{V^*(k)}{2\Delta R} - \frac{1}{\mathrm{Pr}(\Delta R)^2} - \frac{1}{\mathrm{Pr}}\frac{1}{(k-1)\Delta R}\ \frac{1}{2\Delta R}\right]$$
$$+\ \theta(k-1)\left[\frac{-V^*(k)}{2\Delta R} - \frac{1}{\mathrm{Pr}}\frac{1}{(\Delta R)^2} + \frac{1}{\mathrm{Pr}}\frac{1}{(k-1)\Delta R}\ \frac{1}{2\Delta R}\right]$$

$$\boxed{a\,\theta(k) + b\,\theta(k+1) + c\,\theta(k-1) = R} \qquad (5.\ 7)$$

where

$$a = \frac{U^*(k)}{\Delta Z} + \frac{2}{\Pr(\Delta R)^2}$$

$$b = \frac{V^*(k)}{2\Delta R} - \frac{1}{\Pr}\frac{1}{(\Delta R)^2} - \frac{1}{\Pr(k-1)}\frac{1}{\Delta R}\frac{1}{2\Delta R}$$

$$c = \frac{-V^*(k)}{2\Delta R} - \frac{1}{\Pr}\frac{1}{(\Delta R)^2} + \frac{1}{\Pr(k-1)}\frac{1}{\Delta R}\frac{1}{2\Delta R}$$

$$R = \frac{U^*(k)\theta^*(k)}{\Delta Z}$$

Numerical Representation of the Integral Continuity Equation

By introducing the trapezoidal rule of numerical integration, the integral continuity equation can be reduced to the following form.

$$\left[\sum_{k=2}^{n} U(k)R(k) + 0.5\left(U(1)R(1) + U(n+1)R(n+1)\right)\right]\Delta R = \frac{1}{2}$$

$$R(1) = 0 \Rightarrow U(1)R(1) = 0$$
$$U(n+1) = 0$$

$$\left[\sum_{k=2}^{n} U(k)R(k)\right]\Delta R = \frac{1}{2} \qquad (5.\ 8)$$

where $R(k) = (k-1)\Delta R$

5.1.3 Concentric Annulus

Figure 5.2 shows finite difference domain superimposed on a half section of the annular geometry. Since the flow is symmetrical, it is a function of (R, Z) only. The mesh points intersecting at the grid lines are represented by index '*k*' progressing in the radial direction, with $k = 1, 2, 3 \ldots$ n+1. In this domain $k = 1\,(R = N)$ indicates the inner wall, k = n+1 $(R = 1)$ indicates the outer wall. On the other hand, Z = 0 indicates the channel inlet, ΔR and ΔZ are the increments in the radial and axial directions respectively. Integer 'n' indicates the number of radial segments. At the intersection of grid lines, the mesh points designated by filled dots represent the boundary nodes and the mesh points designated by unfilled dots represent the interior nodes where the solution for the unknown variables like (U, V, θ) are calculated.

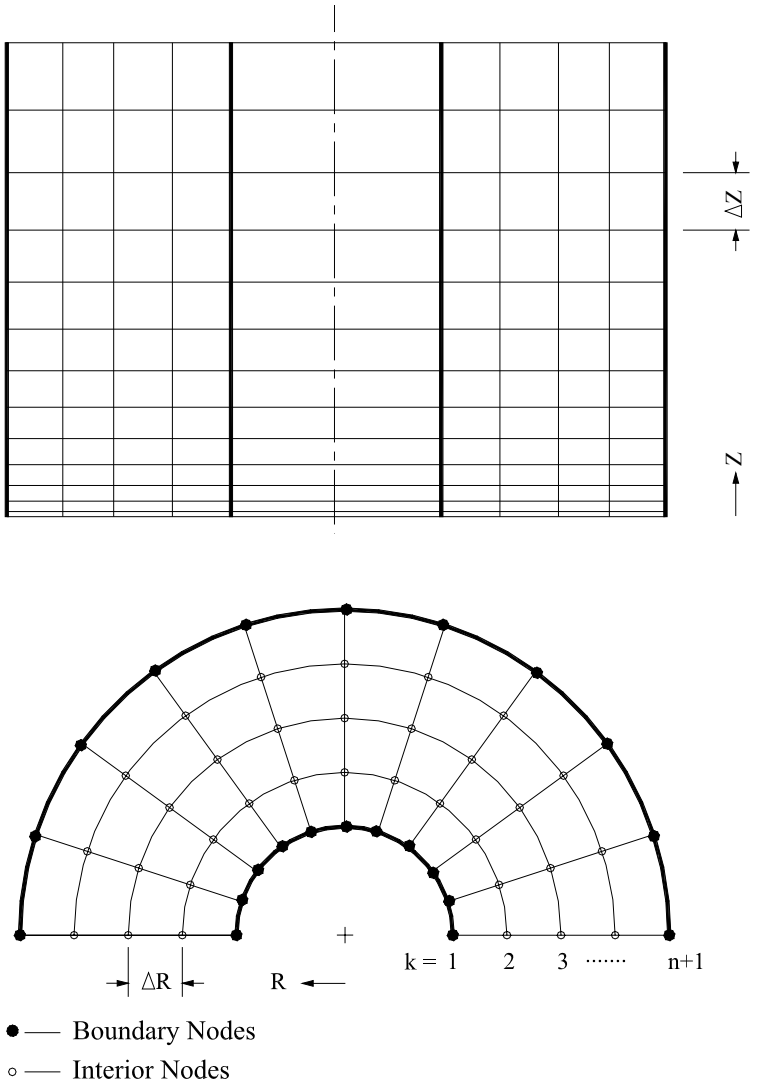

Figure 5.2 Finite difference domain of half-section of vertical concentric annulus

Finite Difference Formulation of the Continuity Equation

$$\frac{V(k+1)-V(k)}{\Delta R}+\frac{V(k+1)+V(k)}{2\left[N+(k-1/2)\Delta R\right]}+\frac{U(k+1)+U(k)-U^*(k+1)-U^*(k)}{2\Delta Z}=0$$

After simplifying and rearranging the above equation we get:

$$V(k+1)=V(k)\frac{N+(k-1)\Delta R}{N+k\Delta R}-\left[\frac{2N+(2k-1)\Delta R}{N+k\Delta R}\right]\left[\frac{U(k+1)+U(k)-U^*(k+1)-U^*(k)}{4\Delta Z}\right]\Delta R$$

(5. 9)

Finite Difference Formulation of the Axial Momentum Equation

$$V^*(k)\left[\frac{U(k+1)-U(k-1)}{2\Delta R}\right]+U^*(k)\left(\frac{U(k)-U^*(k)}{\Delta Z}\right)=\frac{P^*(k)-P(k)}{\Delta Z}$$
$$+K_2\theta^*(k)+\frac{U(k+1)-2U(k)+U(k-1)}{(\Delta R)^2}+\frac{1}{N+(k-1)\Delta R}\frac{U(k+1)-U(k-1)}{2\Delta R}$$

After rearranging the terms, the above expression can be written as:

$$U(k)\left[U^*(k)+\frac{2\Delta Z}{(\Delta R)^2}\right]+U(k-1)\left[-\frac{V^*(k)\Delta Z}{2\Delta R}-\frac{\Delta Z}{(\Delta R)^2}+\frac{\Delta Z}{N+(k-1)\Delta R}\frac{1}{2\Delta R}\right]$$
$$+U(k+1)\left[\frac{V^*(k)\Delta Z}{2\Delta R}-\frac{\Delta Z}{(\Delta R)^2}-\frac{\Delta Z}{N+(k-1)\Delta R}\frac{1}{2\Delta R}\right]+P(k)=P^*(k)+\left(U^*(k)\right)^2+K_2\theta^*(k)\Delta Z$$

$$\boxed{aU(k)+bU(k+1)+cU(k-1)+S_pP(k)=R} \qquad (5.\ 10)$$

where

$$a = U^*(k) + \frac{2\Delta Z}{(\Delta R)^2}$$

$$b = \frac{V^*(k)\Delta Z}{2\Delta R} - \frac{\Delta Z}{(\Delta R)^2} - \frac{\Delta Z}{N + (k-1)\Delta R}\frac{1}{2\Delta R}$$

$$c = -\frac{V^*(k)\Delta Z}{2\Delta R} - \frac{\Delta Z}{(\Delta R)^2} + \frac{\Delta Z}{N + (k-1)\Delta R}\frac{1}{2\Delta R}$$

$$S_P = 1.0$$

$$R = P^*(k) + \left(U^*(k)\right)^2 + K_2\theta^*(k)\Delta Z$$

$$K_2 = \pm\frac{1}{4(1-N)^2}\frac{Gr}{\mathrm{Re}}$$

Finite Difference Formulation of the Energy Equation

$$V^*(k)\left[\frac{\theta(k+1)-\theta(k-1)}{2\Delta R}\right] + U^*(k)\left(\frac{\theta(k)-\theta^*(k)}{\Delta Z}\right) = \frac{1}{\mathrm{Pr}}\left[\frac{\theta(k+1)-2\theta(k)+\theta(k-1)}{(\Delta R)^2} + \frac{1}{N+(k-1)\Delta R} + \frac{\theta(k+1)-\theta(k-1)}{2\Delta R}\right]$$

Rearranging the terms, the equation becomes:

$$\theta(k-1)\left[\frac{-V^*(k)}{2\Delta R} - \frac{1}{\mathrm{Pr}(\Delta R)^2} + \frac{1}{\mathrm{Pr}\left(N+(k-1)\Delta R\right)}\frac{1}{2\Delta R}\right] + \theta(k)\left[\frac{U^*(k)}{\Delta Z} + \frac{2}{\mathrm{Pr}(\Delta R)^2}\right] + \theta(k+1)\left[\frac{V^*(k)}{2\Delta R} - \frac{1}{\mathrm{Pr}(\Delta R)^2} - \frac{1}{2\Delta R}\frac{1}{\mathrm{Pr}\left(N+(k-1)\Delta R\right)}\right] = \frac{U^*(k)\theta^*(k)}{\Delta Z}$$

$$\boxed{a\theta(k) + b\theta(k+1) + c\theta(k-1) = R} \qquad (5.\ 11)$$

where

$$a=\frac{U^{*}(k)}{\Delta Z}+\frac{2}{\Pr(\Delta R)^{2}}$$

$$b=\frac{V^{*}(k)}{2\Delta R}-\frac{1}{\Pr(\Delta R)^{2}}-\frac{1}{2\Delta R}\frac{1}{\Pr\left(N+(k-1)\Delta R\right)}$$

$$c=-\frac{V^{*}(k)}{2\Delta R}-\frac{1}{\Pr(\Delta R)^{2}}+\frac{1}{\Pr\left(N+(k-1)\Delta R\right)}\frac{1}{2\Delta R}$$

$$R=\frac{U^{*}(k)\theta^{*}(k)}{\Delta Z}$$

* represents the previous axial step value

Numerical Representation of the Integral Continuity Equation

By introducing the trapezoidal rule of numerical integration, the integral continuity equation can be reduced to the following form.

$$\left[\sum_{k=2}^{n}U(k)R(k)+0.5\left(U(1)R(1)+U(n+1)R(n+1)\right)\right]\Delta R=\frac{1-N^{2}}{2}$$

$$U(1)=U(n+1)=0$$

$$\left[\sum_{k=2}^{n}U(k)R(k)\right]\Delta R=\frac{1-N^{2}}{2} \qquad (5.\ 12)$$

where $R(k)=N+(k-1)\Delta R$

5.1.4 Eccentric Annulus

Due to symmetry, (i.e. for $0 \le \xi \le \pi$), equations (3. 41)-(3. 44), subject to the boundary conditions given in Table 3.3 and equations (3. 46)-(3. 48) have been solved numerically by means of linearized implicit finite difference scheme which depends on the application of equations (3. 42)-(3. 45) at each cross section all the values of V in equation (3. 42) will be deliberately taken at the previous axial step in order to make this equation locally uncoupled from the continuity equation (3. 41) and make equations (3. 41)-(3. 45) sufficient to obtain the five unknowns (U, V, W, P and θ).

Mesh points are numbered consecutively; i is progressing in the η-direction with i =1,2,3,....., n+1 from the outer wall and j is progressing in the ξ-direction with j = 1,2,3,..... m+1 from the wide side of the annulus (at $\xi = 0$). Consequently, there are (n+1) (m+1) grid points per axial step including the boundary points (on the inner and outer cylindrical surfaces and the lines of symmetry, $\xi = 0$ and $\xi = \pi$). $\Delta\xi$, $\Delta\eta$ and ΔZ are the increments in the respective directions.

Finite Difference Formulation of the Continuity Equation

$$\frac{H(i,j+1)W(i,j+1)-H(i,j-1)W(i,j-1)}{2\Delta\xi}+\frac{H(i,j)V(i,j)-H(i-1,j)V(i-1,j)}{\Delta\eta} + H(i,j)^2\left[\frac{U(i,j)-U^*(i,j)}{\Delta Z}\right]=0 \qquad (5.\ 13)$$

Finite Difference Formulation of the Axial Momentum Equation

$$\frac{W^*(i,j)}{H(i,j)}\left[\frac{U(i,j+1)-U(i,j-1)}{2\Delta\xi}\right]+\frac{V^*(i,j)}{H(i,j)}\left[\frac{U(i+1,j)-U(i-1,j)}{2\Delta\eta}\right]+U^*(i,j)\left[\frac{U(i,j)-U^*(i,j)}{\Delta Z}\right]$$
$$=-\left(\frac{P(i,j)-P^*(i,j)}{\Delta Z}\right)\pm\frac{Gr}{\mathrm{Re}}\theta(i,j)+\frac{1}{H(i,j)^2}\left[\begin{array}{l}\dfrac{U(i,j+1)-2U(i,j)+U(i,j-1)}{(\Delta\xi)^2}\\ +\dfrac{U(i+1,j)-2U(i,j)+U(i-1,j)}{(\Delta\eta)^2}\end{array}\right] \qquad (5.\ 14)$$

Finite Difference Formulation of ξ-Momentum Equation

$$\frac{W^*(i,j)}{H(i,j)}\left[\frac{W(i,j+1)-W(i,j-1)}{2\Delta\xi}\right]+\frac{V^*(i,j)}{H(i,j)^2}\left[\frac{H(i+1,j)W(i+1,j)-H(i-1,j)W(i-1,j)}{2\Delta\eta}\right]$$
$$+U^*(i,j)\left[\frac{W(i,j)-W^*(i,j)}{\Delta Z}\right]-\frac{V^*(i,j)^2}{H(i,j)^2}\left[\frac{H(i,j+1)-H(i,j-1)}{2\Delta\xi}\right]$$
$$=\frac{1}{H(i,j)^3}\left[\begin{array}{l}\dfrac{H(i,j+1)W(i,j+1)-2H(i,j)W(i,j)+H(i,j-1)W(i,j-1)}{(\Delta\xi)^2}\\ +\dfrac{H(i+1,j)W(i+1,j)-2H(i,j)W(i,j)+H(i-1,j)W(i-1,j)}{(\Delta\eta)^2}\end{array}\right]$$
$$+\frac{2}{H(i,j)^2}\left[\frac{H(i,j+1)-H(i,j-1)}{2\Delta\xi}\right]\left[\frac{U(i,j)-U^*(i,j)}{\Delta Z}\right] \qquad (5.\ 15)$$
$$+\frac{2}{H(i,j)^4}\left[\frac{H(i+1,j)-H(i-1,j)}{2\Delta\eta}\right]\left[\begin{array}{l}\dfrac{H(i,j+1)V(i,j+1)-H(i,j-1)V(i,j-1)}{2\Delta\xi}\\ -\dfrac{H(i+1,j)W(i+1,j)-H(i-1,j)W(i-1,j)}{2\Delta\eta}\end{array}\right]$$

Finite Difference Formulation of the Energy Equation

$$\frac{W^*(i,j)}{H(i,j)}\left[\frac{\theta(i,j+1)-\theta(i,j-1)}{2\Delta\xi}\right]+\frac{V^*(i,j)}{H(i,j)}\left[\frac{\theta(i+1,j)-\theta(i-1,j)}{2\Delta\eta}\right]$$
$$+U^*(i,j)\left[\frac{\theta(i,j)-\theta^*(i,j)}{\Delta Z}\right]=\frac{1}{\mathrm{Pr}}\frac{1}{H(i,j)^2}\left[\begin{array}{l}\dfrac{\theta(i,j-1)-2\theta(i,j)+\theta(i,j+1)}{(\Delta\xi)^2}\\ +\dfrac{\theta(i-1,j)-2\theta(i,j)+\theta(i+1,j)}{(\Delta\eta)^2}\end{array}\right] \qquad (5.\ 16)$$

Numerical Representation of the Integral Continuity Equation

The integral continuity equation (3. 45) can be written in a numerical form as:

$$\frac{8(1-N)}{\pi(1+N)}\left(0.5\sum_{i=2}^{n}U(i,1)\left(H(i,1)\right)^2+U(i,m+1)\left(H(i,m+1)\right)^2+\sum_{j=2}^{m}\sum_{i=2}^{n}U(i,j)\left(H(i,j)\right)^2\right)\Delta\eta\Delta\xi=\bar{U} \qquad (5.\ 17)$$

5.2 Method of Solution

The numerical solution of these set of parabolic equations for the aforesaid geometries is obtained by first selecting the parameters that are involved such as Pr, Gr/Re and θ_T for parallel plates, Pr, Gr/Re for circular tubes and Pr, Gr/Re, N and θ_T for annulus. The algorithm of solution is as follows:

1. Initially, inlet boundary conditions are set at the nodes of the finite difference domain under study $\left(\text{i.e. } U_0 = 1 \text{ and } V = P = \theta = 0\right)$.
2. Setting the hydrodynamic and thermal boundary conditions for the given case at the nodes representing the walls of the geometry under study.
3. Initializing the unknown variables (U, V, θ) at the first axial step.
4. Creating a tri-diagonal matrix to solve for temperature at the nodes. Since, the energy equation is independent of the equation of motion in the flow direction; it can be solved initially. A sample tri-diagonal matrix is shown as an example.
5. Applying Thomas Algorithm [38] to obtain the solution for the tri-diagonal matrix created in step 4.
6. After that, the axial momentum equation along with integral continuity equation is solved for velocity and pressure variation. This can be achieved by creating a matrix and applying Gauss Jordan Elimination technique [38] to solve this matrix. A sample matrix is shown as an example.
7. Next, the differential continuity equation is solved for transverse velocity component by direct substitution of the values obtained in steps 4-6.

8. The values of the variables at the previous axial step are updated with the new axial step values that are calculated in steps 4-7.
9. A convergence criterion or condition is imposed to achieve the desired solution. The criterion is the attainment of the fully developed velocity conditions within 1% deviation from the corresponding analytical solution.

Matrix form of step 4

Tri-diagonal matrix showing '*n*' number of segments consider in the direction perpendicular to the flow.

$$\begin{bmatrix} a & b & 0 & 0 & . & . & . & . & 0 & 0 \\ c & a & b & 0 & . & . & . & . & . & 0 \\ 0 & c & a & b & 0 & . & . & . & . & . \\ 0 & 0 & c & a & b & 0 & . & . & . & . \\ . & . & . & . & . & . & . & . & . & . \\ . & . & . & . & . & . & . & . & . & 0 \\ . & . & . & . & . & . & . & . & . & 0 \\ . & . & . & . & . & . & . & . & . & 0 \\ 0 & . & . & . & . & . & . & c & a & b \\ 0 & 0 & . & . & . & . & 0 & 0 & c & a \end{bmatrix} \begin{bmatrix} \theta(2) \\ \theta(3) \\ \theta(4) \\ \theta(5) \\ . \\ . \\ . \\ . \\ \theta(n-1) \\ \theta(n) \end{bmatrix} = \begin{bmatrix} R_2 \\ R_3 \\ R_4 \\ R_5 \\ . \\ . \\ . \\ . \\ . \\ R_n \end{bmatrix}$$

where a, b, c are the coefficients of the unknowns and R_i where $i = 2,.....n$ are the R.H.S. of the corresponding set of parabolic equations given for the problem under consideration.

Matrix form of step 6

Matrix showing a set of *n* parabolic equations, (*n*-1) equations is used to solve the velocity at the respective nodes and n^{th} equation is used to solve the pressure, which assumes to be constant at each axial step.

$$\begin{bmatrix} 1 & 1 & 1 & 1 & 1 & 1 & 1 & 1 & 1 & 0 \\ a & b & 0 & 0 & . & . & . & . & 0 & s_p \\ c & a & b & 0 & . & . & . & . & . & s_p \\ 0 & c & a & b & 0 & . & . & . & . & s_p \\ 0 & 0 & c & a & b & 0 & . & . & . & s_p \\ . & . & . & c & a & b & 0 & . & . & s_p \\ . & . & . & . & . & . & . & . & . & s_p \\ . & . & . & . & . & . & . & . & 0 & s_p \\ . & . & . & . & . & 0 & c & a & b & s_p \\ 0 & 0 & . & . & . & . & 0 & c & a & s_p \end{bmatrix} \begin{bmatrix} U(2) \\ U(3) \\ U(4) \\ U(5) \\ . \\ . \\ . \\ . \\ U(n-1) \\ U(n) \end{bmatrix} = \begin{bmatrix} R_{cont} \\ R_2 \\ R_3 \\ R_4 \\ . \\ . \\ . \\ . \\ . \\ R_n \end{bmatrix}$$

The elements in the first row of the matrix represent the coefficients of the unknowns of the integral continuity equation for vertical parallel plates. a, b, c are the coefficients of the unknowns, R_{cont} and R_i where $i = 2,.....n$ are the R.H.S. of the corresponding set of parabolic equations.

5.3 Selection of Marching Step

It has been stated in the above algorithm that the solution is marching in the direction of flow. So the purpose is to select a proper marching step that will improve the accuracy of the solution. The axial marching step is to be very small near the entrance where the large gradients exist and can be longer downstream of the channel.

There are several ways of selecting the marching steps namely linear increment step, exponential increment step and hyperbolic increment step etc. In the present study, emphasis will be given to linear increment step and exponential increment step.

Linear Increment Step

In this increment step technique, an increment is given step-by-step along the length of the channel. A constant value of axial step increment $\Delta Z = 10^{-5}$ is given for the first 1000 axial steps for the case of parallel plates, circular tube and concentric annulus, and for eccentric annulus, the technique developed by Mokheimer [35] is directly used. After the first given number of axial steps the increment remains 10^{-3} for each of the geometry under consideration. Figures (5. 3 & 5. 4) show the variation of linear increment and total axial distance with respect to the axial steps. The solid lines in the figures show that sudden jump in the increment results into large fluctuations in the derivatives of the variables that exist at the entrance region of the channel. These fluctuations provide less accuracy in the solution.

Exponential Increment Step

In exponential increment step, the increment is smooth following an exponentially increasing along the channel length. A function that describes the exponential increment step is given below for the case of parallel plates, circular tubes and concentric annulus

$$\Delta Z = a * 10^{-6} Exp\left(\sqrt{b * Z}\right)$$

whereas for the eccentric annulus, the exponential function is given as:

$$\Delta Z = a * 10^{-10} Exp\left(\sqrt{b * Z}\right)$$

ΔZ = axial step increment

Z = No. of axial steps

a , b are constants

As an objective of having the step increment $\Delta Z = 10^{-3}$ after the given no. of axial steps for each of the geometry considered, several tests have been performed on the exponential function for different values of constants a, b. After analyses the values of constants a and b are taken as 1.1 and 0.0464 respectively for parallel plates, circular tube and concentric annulus, while for eccentric annulus the values are 1.1 and 2.567.

The dashed lines in the Figures (5.3 & 5.4) illustrate that due to smooth increment in the axial step, the variations in the derivatives of the variables encountered in the entrance region of the channel are reduced and the percentage of accuracy in the solution can be increased compared to linear increment step.

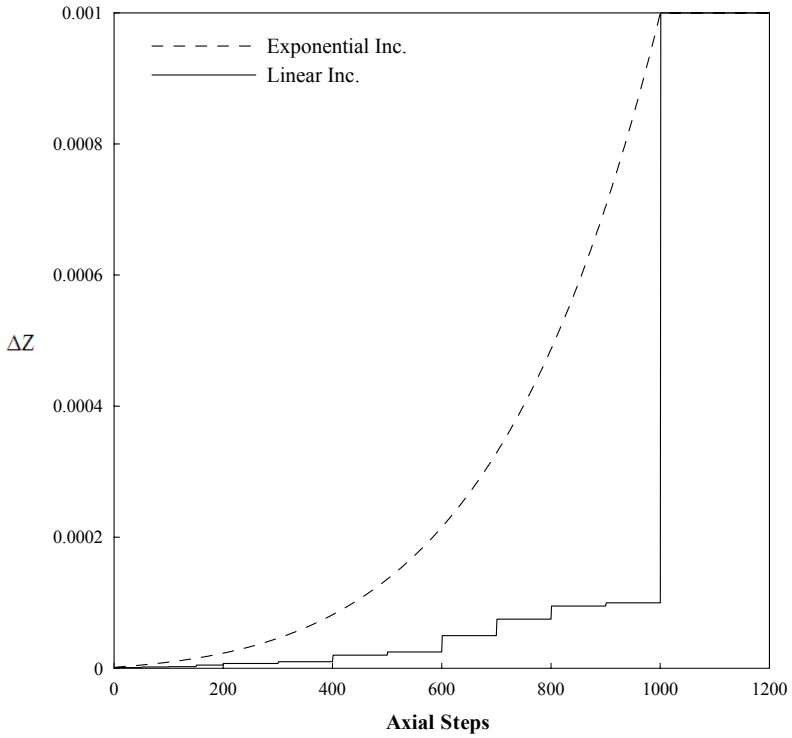

Figure 5.3 Variation of axial step increment with respect to axial steps

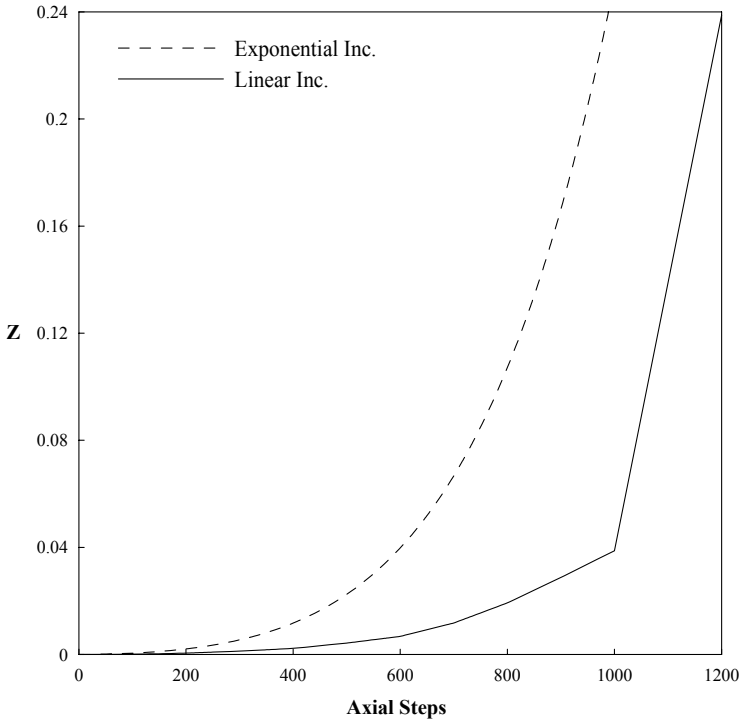

Figure 5.4 Variation of total axial distance with respect to axial steps

It is clear from the Figures (5.3 & 5.4), that an exponential function provides smooth change of the axial step. This is reflected to the avoidance of having step change on the hydrodynamic and heat transfer parameters due to the step change in the axial step. So it is selected as the marching step in the present study.

5.4 Grid Independence Test

As a matter of fact, the numerical methods especially finite difference methods suffer mainly from approximation and simplification represented by the truncation errors. So there is a probability of having numerical inaccuracy in the solution. In any numerical scheme, the numerical inaccuracy that results from truncation errors can be reduced via mesh refinement. If the mesh size is coarse, the truncation errors will be prominent. On the other hand, if the mesh size or grid points are fined, the solution results into accurate

approaching to the analytical solution which is completely based on several numerical tests. At some stage, as the number of grid points increases, there will be no change in the accuracy of the solution. This is called Grid Independence solution.

In the present numerical tests, the grid independence test is carried out for hydrodynamic fully development lengths for each number of grid points taken in the Y direction of the parallel plates. Different grid points are investigated to verify this fact. Figure 5.5 shows the grid independence test for vertical channel between parallel plates. It is observed that for coarse grid points or nodes, the value of hydrodynamic fully development length is high and as the number of nodes increases in the Y-direction, the hydrodynamic fully development length decreases. No more significant variation in the value of fully developed length was reported for the grid points or nodes greater than 50. This was also confirmed for other parameters, which imply that there is no variation in the accuracy of the solution. Mesh of 50 grid points was used to obtain all the results. The same number of grid points is considered in the respective directions for the rest of the geometries (circular tube and concentric annulus).

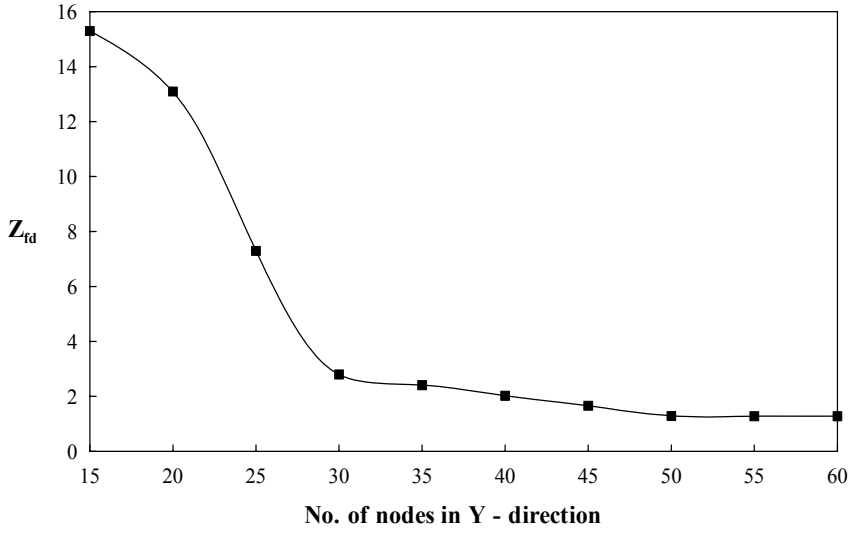

Figure 5.5 Graphical representation of grid independence test

Chapter 6

VALIDATION OF CODE

6.1 Introduction

The mathematical model that describes the behavior of the system under consideration consists of set of differential equations. The solutions to this set of equations can be obtained either by analytical or numerical methods. The numerical model can be validated by comparing the results with the previously published work. In the present study, the validation of code has been done for the following geometries under fully developed and developing conditions for the given thermal boundary conditions.

6.2 Parallel Plates

The numerical code is validated by comparing the results with the work of Aung and Worku [8] for the thermal boundary condition of first kind with asymmetric wall heating in the developing laminar mixed convection. The code is also validated for the forced convection by comparing the results reported by Shah and London [36] and by analytical solutions. The present results are obtained for the fluid of Prandtl number 0.7 for the sake of comparison.

Comparison with fully developed forced convection in vertical channel between parallel plates

The Nusselt number obtained by numerical code presented in the Table 6.1 for the fully developed forced convection for the thermal boundary conditions of 1st, 3rd and 4th kinds show good agreement with the results reported by Shah & London [36] having less than 1% difference.

Table 6.1 Comparison of numerical results with the available results of fully developed forced convection between vertical parallel plates

Fully Developed Forced Convection (Gr/Re= 0)									
Nusselt no.	**1st kind BC**			**3rd kind BC**			**4th kind BC**		
	Present results	Shah & London [36]	deviation %	Present results	Shah & London [36]	deviation %	Present results	Shah & London [36]	deviation %
Nu_h	4.0047	4	0.1175	4.860	4.861	0.02008	4.014	4	0.35
Nu_c	3.9951	4	0.1225				3.979	4	0.525

Comparison of results with the available numerical results for the developing laminar mixed convection between vertical parallel plates

The present numerical code is also validated for the developing laminar mixed convection with the work of Aung and Worku [8]. Figure 6.1 show the comparison of velocity profiles between the present results and Aung and Worku [8] for Gr/Re = 0 & 100 and for θ_T= 0.5 at an axial length of Z = 0.04. Figures (6.2 & 6.3) show the variation of pressure and mean temperature along the channel length (Z). The graphical results show excellent agreement with the work of Aung and Worku [8].

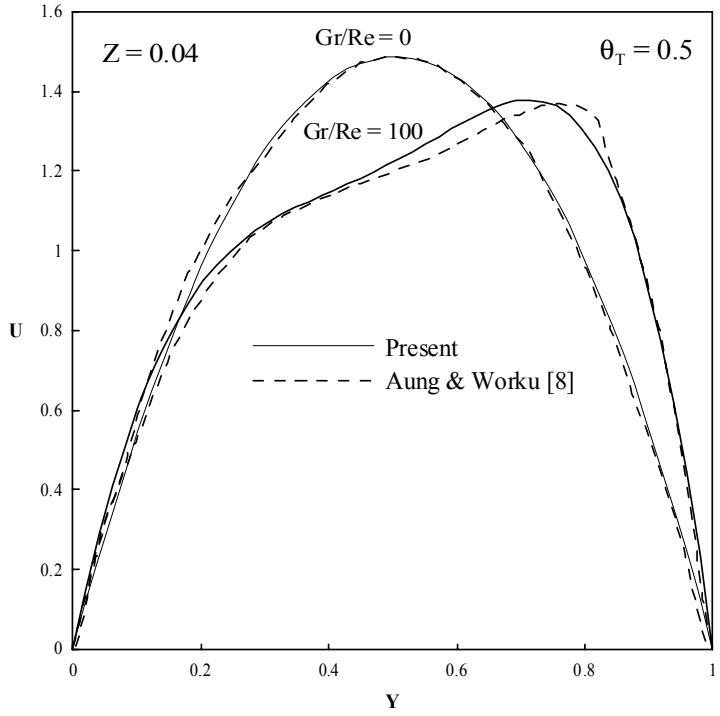

Figure 6.1 Comparison of velocity profiles between present results and Aung & Worku [8] for Gr/Re = 0 & 100 and for θ_T= 0.5 at dimensionless channel height Z = 0.04 between vertical parallel plates

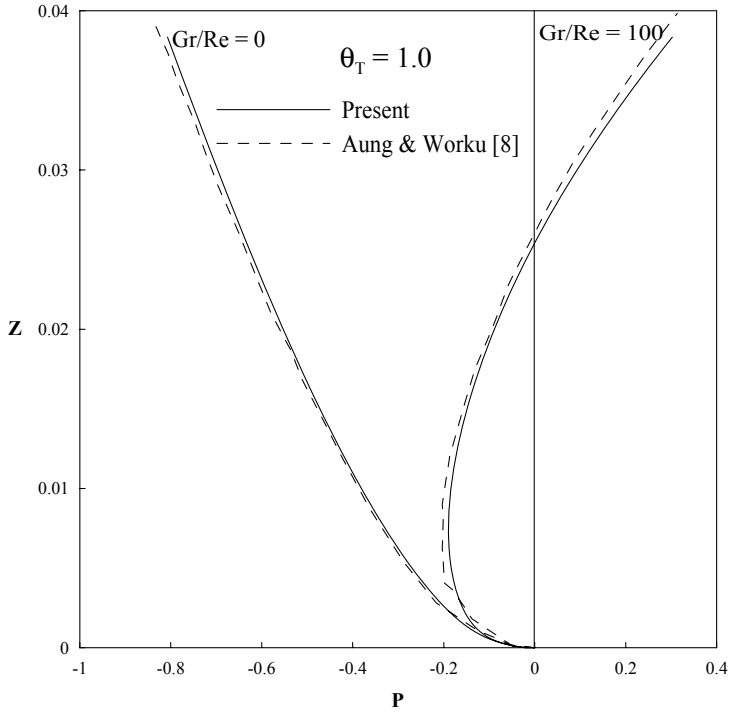

Figure 6.2 Comparison of pressure variation between the present results and Aung & Worku [8] for Gr/Re = 0 & 100 and for θ_T= 1.0 along the channel height (Z) between vertical parallel plates

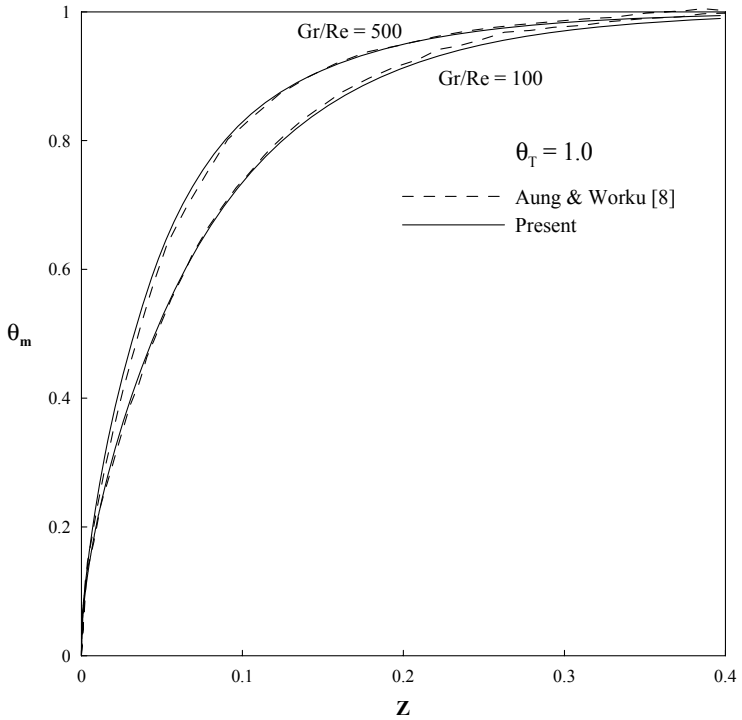

Figure 6.3 Comparison of mean temperature between the present results and Aung & Worku [8] for Gr/Re = 100 & 500 and for θ_T= 1.0 along the channel height (Z) between vertical parallel plates

6.3 Circular Tube and Concentric Annulus

In this section of the chapter, the code is validated for the circular geometries (circular tube and concentric annulus) for fully developed forced convection as well as for developing laminar mixed convection.

The asymptotic Nusselt number for circular tube for fully developed forced convection flow obtained numerically, Nu =3.665041 shows excellent agreement less than 1% of the result of Shah and London [36] who presented the value as 3.66. For the concentric annulus, the code is validated by comparing the present numerical results for friction factor and Nusselt number for forced convection. The results are presented in the Table 6.2 which shows excellent agreement less than 1% deviation in the results reported Shah and London [36] for fully developed forced convection. On the other hand, the

numerical results obtained in the developing region for laminar mixed convection for pressure along the axial direction shows good agreement with the work of Sharaawi and Sarhan [37]. Figure 6.4 shows the results of [37] obtained for different Gr/Re for the thermal boundary condition of 3rd kind and for radius ratio N = 0.9.

Table 6.2 Comparison of friction factor and Nusselt numbers on both walls for different radius ratio, N

N	fRe			Nu_i			Nu_o		
	Present results	Shah & London [36]	deviation %	Present results	Shah & London [36]	deviation %	Present results	Shah & London [36]	deviation %
0.1	23.346	23.343	0.013	10.463	10.459	0.038	3.124	3.095	0.937
0.3	23.462	23.461	0.004	5.967	5.966	0.017	3.301	3.319	0.545
0.5	23.815	23.813	0.008	4.879	4.889	0.205	3.501	3.520	0.540
0.7	23.952	23.949	0.013	4.391	4.391	0.000	3.708	3.715	0.188
0.9	23.994	23.996	0.008	4.104	4.103	0.012	3.904	3.906	0.051

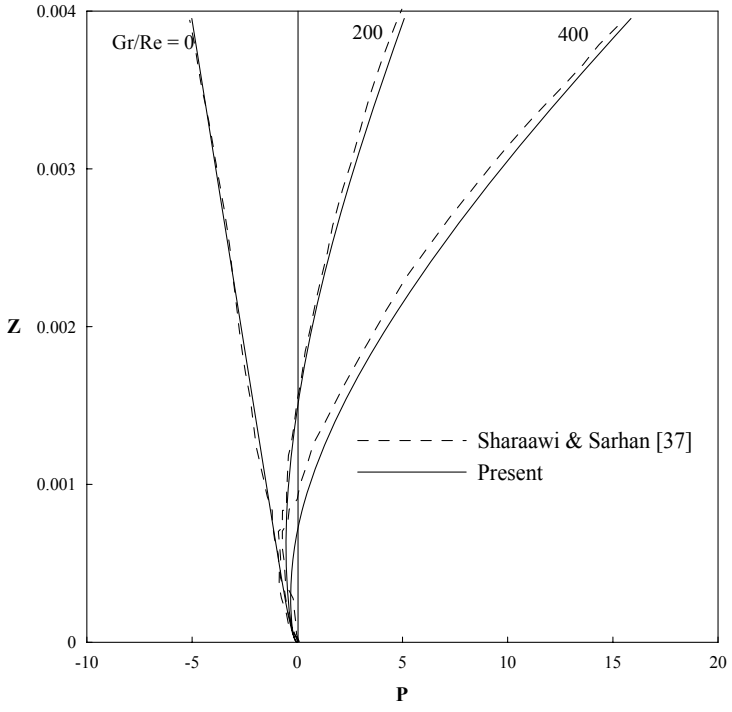

Figure 6.4 Comparison of pressure variation between the present results and Sharaawi & Sarhan [37] for different Gr/Re along the channel height (Z), for radius ratio N = 0.9, Case 3.I

6.4 Eccentric Annulus

The finite difference equations mentioned in Chapter 5 of the respective section for vertical eccentric annulus was solved by Mokheimer [35] who developed a FORTRAN code by first selecting values of Gr/Re for an annulus of given radius ratio N and dimensionless eccentricity E and a fluid of a given Pr. The code has been well validated as reported in [34]. However, a special run of the present code was conducted for a fluid of Pr = 1 in an eccentric annulus of radius ratio N = 0.5 and eccentricity E = 0.5 under thermal boundary conditions of the first kind with the outer wall heated (case 1.O). This special case was conducted for the sake of comparison of the results obtained via the present code and those obtained and published by Ingham and Patel [32] for this particular case. Such a comparison of the developing pressure gradient obtained by the present code with that obtained by Ingham and Patel [32] for the above mentioned case is shown in Fig. 6.5 below.

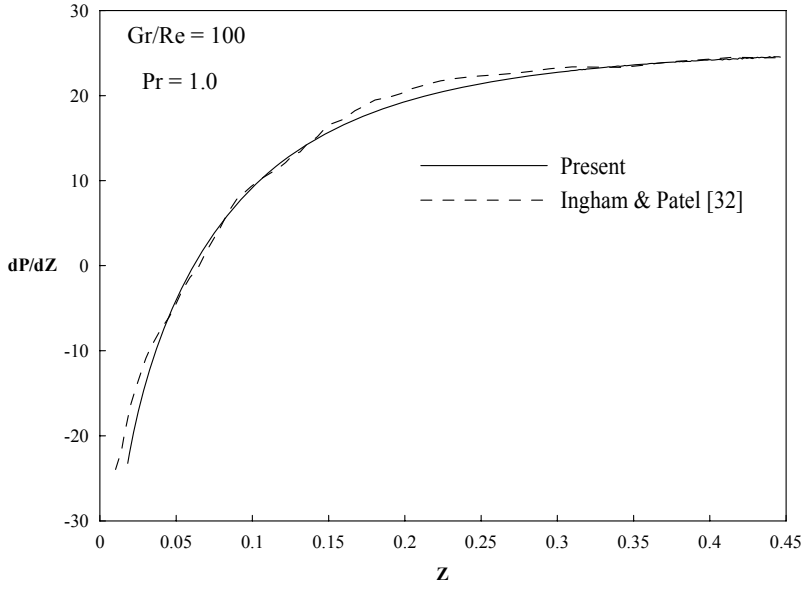

Figure 6.5 Comparison of present results with the results published by Ingham and Patel [32] for pressure gradient along the channel height (Z)

Other comparisons have been conducted between the fully developed pressure gradient for the special case of Gr/Re = 0, i.e., forced convection in eccentric annuli, obtained via the present code for all cases under consideration with the pertinent values obtained by Shah and London [36]. Such comparisons are tabulated hereunder.

Table 6.3 Comparison between the fully developed pressure gradient in eccentric annuli obtained through the present code and the previously published results for Gr/Re = 0

E	**$(dP/dZ)_{fd}$ = 2 x fRe**		
	Present results	Shah & London [36]	deviation %
0.1	47.36	46.96	0.852
0.3	42.60	42.30	0.709
0.5	35.51	35.34	0.481
0.7	28.60	28.51	0.316

The above comparisons, shown in Fig. 6.5 and Table 6.3, reveal excellent agreement between the results of the present work and the previously published results.

Chapter 7

RESULTS AND DISCUSSION ON DEVELOPING LAMINAR MIXED CONVECTION BETWEEN VERTICAL PARALLEL PLATES

7.1 Introduction

Having the mathematical model as well as the developed computer codes, validated for each case under consideration, these codes have been used to investigate the hydrodynamics and heat transfer characteristics of the developing laminar mixed convection in the entry region of vertical channels under consideration. This chapter is devoted to present and discuss the obtained results for laminar developing mixed convection in the entry region of a vertical channel between two parallel plates.

The existence of a critical value of buoyancy parameter Gr/Re at which the pressure gradient for mixed convection in a vertical channel equals to zero was demonstrated analytically. Moreover the values of these $(Gr/Re)_{crt}$ for different geometries under different isothermal boundary conditions were also analytically obtained in Chapter 4.

This chapter is devoted to obtain and present numerical solutions for the laminar developing mixed convection in the entry region of a vertical channel between parallel plates. First, numerical results for the development of pressure gradient and pressure along the channel from its entrance till the fully developed region will be obtained and presented for different values of buoyancy parameter Gr/Re.

This is to demonstrate that for $Gr/Re < (Gr/Re)_{crt}$ no pressure build up will take place downstream of the channel entrance. Thus, after this demonstration, in this chapter, emphasis is concentrated on buoyancy aided flow, a situation in which buoyancy effects result in positive pressure gradient and consequently pressure build up. The plots that present the development of the pressure gradient and the local pressure along the channel height show clearly the effects of the buoyancy on the flow hydrodynamic behavior in the entry region and show clearly how the buoyancy effects aid the flow to overcome the viscous friction and eventually results in pressure build up along the channel for buoyancy-aided flows with the buoyancy parameter (Gr/Re) greater than the critical values obtained and presented in chapter 4 for different channel geometries. Moreover, the development of other important heat transfer parameters such as the mean bulk fluid temperature and the averaged Nusselt number are also presented and discussed.

The results presented in this chapter are those obtained via the numerical investigation for the developing laminar mixed convection in the entry region of a vertical channel between parallel plates under three different fundamental isothermal thermal boundary conditions, which are namely; thermal boundary conditions of the first, third and fourth kinds. The investigation covers a wide range of the buoyancy parameter (Gr/Re) from 0 to 600. Moreover, quantitative information about the effects of buoyancy on the hydrodynamic parameters in mixed convection in the entry region between vertical parallel plates for fluids of different Prandtl number are presented. In this regard, the results obtained and presented are for fluids of Pr number of 0.7, 1, 10 and 100.

It is worth repeating here that this chapter is exclusively dedicated to study the hydrodynamic parameters, namely, pressure and pressure gradient which are greatly

affected by the buoyancy parameter Gr/Re as well as the fluid type (Prandtl Number). Some important information that can be obtained from the variation of these two parameters along the channel are the location at which the buoyancy forces balance the viscous forces and the pressure gradient changes from negative to positive (the location at which $dP/dZ = 0$), the location of the onset of pressure build up and the location of the onset of flow reversal. Another very important parameter is the fully developed length that is defined as the length beyond which the hydrodynamic and thermal flow fields become invariant. The development of the thermal flow field represented by the development of the temperature profiles are used to obtain the development of the local and averaged dimensionless heat transfer coefficient represented by Nusselt number. The effect of the controlling parameters on the above mentioned hydrodynamic and thermal parameters are presented and discussed hereunder.

The controlling parameters for the mixed convection in the entry region between two parallel plates are the buoyancy parameter Gr/Re, Prandtl number and the ratio of the dimensionless temperature of the two plates θ_T for thermal boundary conditions of the first kind. The values of θ_T for the thermal boundary conditions of the first kind that have been used for the present computations are given in section 4.1.

Due to its importance in understanding the physics of the problem under consideration, the velocity and temperature profiles of the flow fields in the entry region are presented and discussed first for a sample of the investigated cases. This sample is selected such that it helps in shedding light on the physics of the developing laminar mixed convection between parallel plates under isothermal boundary conditions.

7.2 Results for thermal boundary conditions of the first kind

Examples of the obtained results for the developing axial velocity profiles from the channel entrance up to the fully developed region are shown in Figs. 7.1 (a) and 7.1 (b) for buoyancy-aided flow with the buoyancy parameter Gr/Re = 50 and 100, respectively, under thermal boundary conditions of the first kind with $\theta_T = 0$ (i.e., for asymmetrically heated channel, one wall is isothermally heated and one wall is kept isothermally cold). Figure 7.1 (c) depicts the development of the velocity profiles along the channel under thermal boundary conditions of the first kind with $\theta_T = 1$ (i.e., for symmetrically heated channel, the two walls are isothermally heated at the same elevated temperature). These profiles together with non-presented profiles show the following. Very near to the entrance, as indicated by profiles # 1,2 in all of the three figures, Figs. 7.1 (a)-(c), the fluid decelerates near the two walls of the channel (due to the formation of the two boundary layers on the walls) and accelerates in the core region as a result of the continuity principle. However, further downstream, heating one of the walls, cases represented by Figs 7.1(a) and (b), or heating of the two walls symmetrically, the case represented by Fig. 7.1(c), shifts the location of the velocity-profile peaks towards the heated wall, as indicated by profiles # 4, 5, 6 and 7 in Figs. 7.1(a) and (b). On the other hand, Figure 7.1(c) shows velocity profiles, # 4, 5, 6 7, 8 and 9 of two peaks near the two heated walls and a minimum near the core of the channel where the heating and consequentially the buoyancy effects did not penetrate yet. This represents a clear distortion of the velocity profiles due to the buoyancy effects, which deviate the velocity profiles from its parabolic shape. However, the peaks for symmetric heating cases,

represented in Fig. 7.1 (c) are shifted again towards the middle of the gap reflecting that the flow is approaching full-development.

The flow reaches thermal full development before hydrodynamic full-development for cases of Pr < 1. After reaching thermal full development, the flow will behave similar to a pure forced flow and continue developing to reach the fully developed parabolic velocity profile. More development will take place with clear change in the peak of the velocity profile until hydrodynamic full-development is achieved and the velocity U throughout the channel attains its fully developed value (U_{fd}). For cases of asymmetric heating, the peak of the velocity profile will be closer to the heated wall. Moreover, for high heating rates represented by large values of Gr/Re, such as the case represented in Fig. 7.1(b), the velocity profile will suffer a permanent distortion and will never restore its fully developed parabolic velocity profile due to the flow reversal occurrence. In such situations, the flow reversal takes place at the cold wall to compensate for the high flow velocities generated near the heated walls as a result of the high buoyancy forces resulted from the high heating rates at the heated wall and thus satisfying the continuity principle. On the other hand, for a symmetrically heated channel, Fig. 7.1 (c), flow reversal will never take place at either wall and the highly distorted velocity profile will develop and eventually achieve its fully developed parabolic velocity profile.

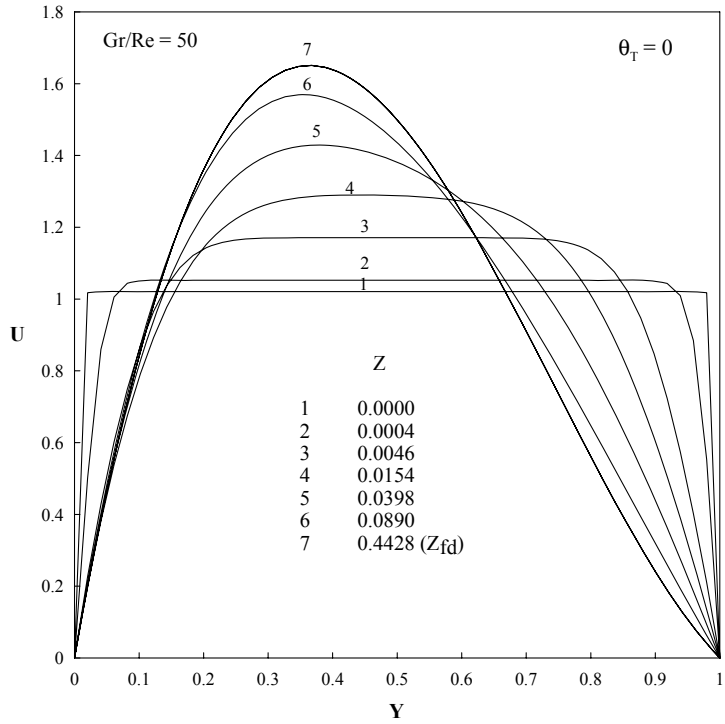

Figure 7.1(a) Variation of velocity distribution at different locations of channel height (Z) for Gr/Re = 50 and for θ_T= 0 (asymmetric wall heating) for the first kind thermal boundary condition in vertical parallel plates

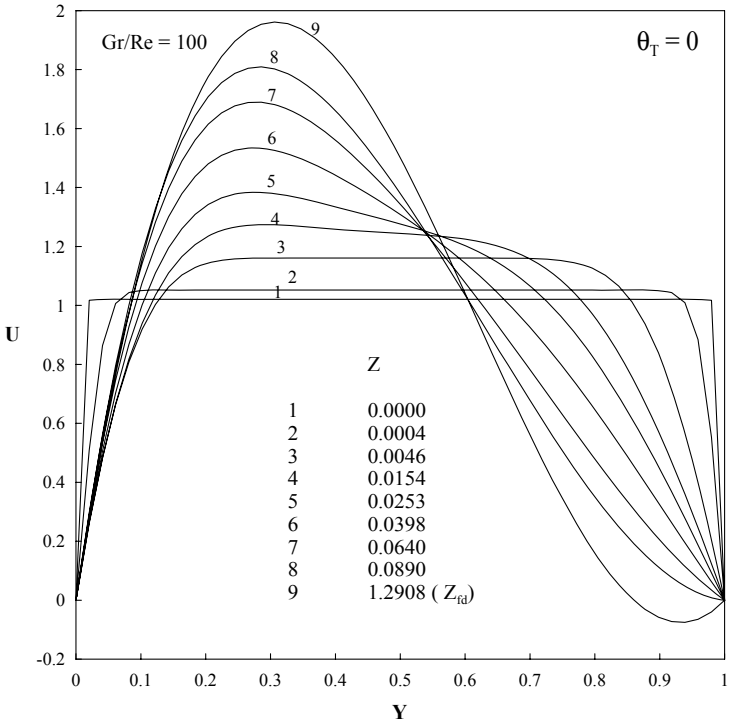

Figure 7.1(b) Variation of velocity distribution at different locations of channel height (Z) for Gr/Re = 100 and for θ_T = 0 (asymmetric wall heating) for the first kind thermal boundary condition in vertical parallel plates

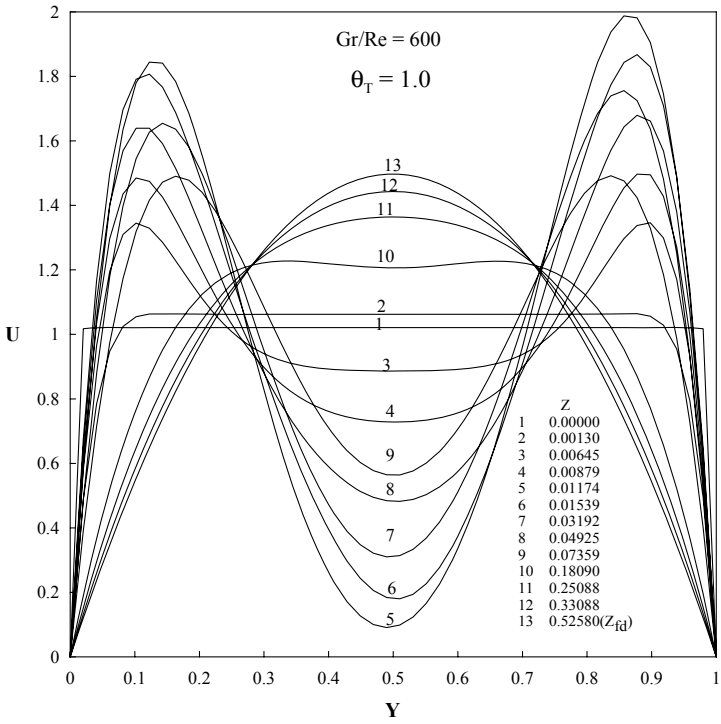

Figure 7.1 (c) Streamwise velocity distributions as a function of axial distance (Z) of Gr/Re = 600 for θ_T =1.0 (symmetric wall heating) for the first kind thermal boundary condition in vertical parallel plates

The location of the flow reversal onset, if any, has been defined as the location at which the velocity gradient becomes ≤ 0. Thus, the velocity gradient has been continuously monitored, especially at the walls, and the locations of flow reversal onset are recorded and presented in Table 7.1 for a wide range of the operating buoyancy parameter Gr/Re and 5 different cases of thermal boundary conditions of the first kind with θ_T varies from 0 to 1. It is worth reporting here that the location of flow reversal is greatly affected by the type of the applied thermal boundary conditions, represented here by the value of θ_T, (e.g., for the case of θ_T = 1, flow reversal will never take place). This location is also affected by the value of the buoyancy parameter Gr/Re under the same thermal boundary conditions. It is clear that the flow reversal will take place for asymmetrically heated channels with high values of the buoyancy parameter Gr/Re.

Values of the buoyancy parameter Gr/Re that represents heating rates that are high enough to create severe flow reversal at the cooler wall in asymmetrically heated channels usually results in a flow instability and consequentially numerical instability. The locations of the flow and numerical instabilities for such cases are also reported in Table 7.1. Table 7.1 shows that the location of flow and numerical instabilities are always preceded by the occurrence of flow reversal.

Another important hydrodynamic parameter that is also recorded in Table 7.1 for all the cases under consideration is the fully developed length. The fully developed length has been defined in the present work, as well as in most of the pertinent published work in the literature, as the location at which the developing velocity profile approaches its analytically obtained fully developed velocity profile within 1 % deviation. It is worth mentioning here that the flow will develop to its fully developed conditions if the channel is high enough and the heating rates are not so high such that flow reversal takes place for asymmetric heated channels. For situations of high heating rates that result in mild flow reversal, the flow overcomes the distortion in its developing velocity profile and eventually achieves its fully developed velocity profiles that are obtained analytically within 1 % deviation but at relatively far locations from the channel entrance as indicated in Table 7.1. Table 7.1 shows clearly that the fully developed length monotonically increases with the buoyancy parameter Gr/Re which implies that the increase of the heating rates represented by the buoyancy parameter Gr/Re results in more distortion of the velocity profiles which requires more time (length) from the flow to overcome this distortion to fully develop restoring its analytically obtained velocity profile. It is worth noting here that the monotonically increasing fully developed channel length (height)

with the buoyancy parameter Gr/Re reaches almost asymptotic values with the high values of Gr/Re. However, for situations of mild flow reversal where full development conditions are achievable, the fully developed length will oscillate around its asymptotic value. This is attributed to the fact that the flow in such situations suffers from mild flow instability, which might also result in a mild numerical instability and consequentially less numerical accuracy in predicting the fully developed length in such situations. Thus, it is recommended to take the reported values of the fully developed length for such situations as a rough numerical estimation for such a length. For asymmetric heating with high enough heating rates resulting in severe flow reversal at the cooler wall, fully developed conditions will never be achieved. On the other hand, for symmetric heating, fully developed conditions are always achieved.

Temperature profiles developments are shown in Fig. 7.2(a) for asymmetric heating under thermal boundary conditions of the first kind with $\theta_T = 0$ and Gr/Re = 100 and in Fig. 7.2(b) for symmetric heating under thermal boundary conditions of the first kind with $\theta_T = 1$. These two figures show how the temperature profiles are developing approaching their invariant analytical fully developed profiles. For the asymmetric heating conditions the temperature profile will develop from the entrance till approach its linear profile at the fully developed region where the fluid flows in laminated layers and all the heat transferred from the heated wall goes to the cold wall through the fluid laminated layers by pure conduction. Higher temperature near the heated wall result in buoyancy aiding effect for upward flow while the cooling effects of the cold wall results in opposite buoyancy effects and for large asymmetrical heating conditions flow reversal might take place at the cold wall. This was reported during the present work via the

velocity profiles for high values of the heating rates represented by the buoyancy parameter Gr/Re. For the symmetric heating conditions, Fig. 7.2(b) shows the development of the temperature profiles that have its maximum at the two symmetrically heated walls and the minimum at the core of the channel. This type of developing temperature profiles is consistent with the pertinent developing velocity profiles that have two peaks near the two heated walls and minimum velocities near the core of the channel where that heat did not penetrate yet. These profiles show clearly how is heat takes time (distance) until it penetrates the fluid layers reaching to the core at large enough distances from the channel entrance till it reaches fully developed region where all the fluid layers will attain the same temperature of a dimensionless value of 1. This implies that all the heat supplied via the two walls is totally absorbed by the fluid in the entry region and no more heat to be absorbed by the fluid in the fully developed region at which the flow will behave exactly as an isothermal forced flow. The temperature profiles have been developed for all cases under consideration. These profiles have been used to obtain the most important heat transfer parameter, which is namely the local Nusselt number. The local Nusselt number is simply obtained from the temperature gradient, of the dimensionless temperature profiles, at the walls and the other thermal parameter namely mean temperature are explained later in this chapter.

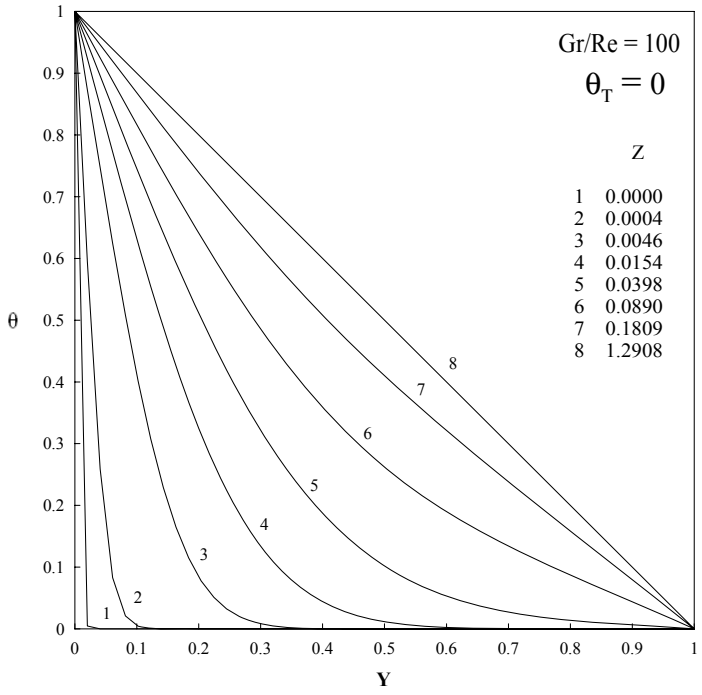

Figure 7.2 (a) Developing temperature profiles for thermal boundary condition of first kind for Gr/Re = 100 and for $\theta_T = 0$ at different axial locations (Z) between vertical parallel plates

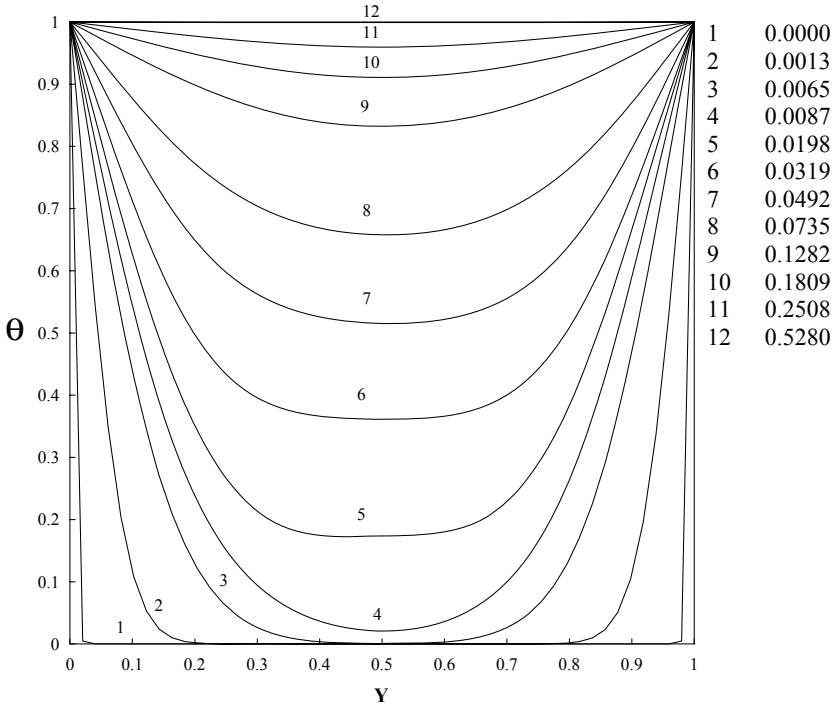

Figure 7.2 (b) Developing temperature profiles for thermal boundary condition of first kind for Gr/Re = 600 and for $\theta_T = 1.0$ at different axial locations (Z) between parallel plates

Engineers are not frequently concerned with the velocity or temperature profiles and they are rather interested in the pressure drop and the heat transfer parameters such as the Nusselt number. Therefore, more emphasis is devoted hereafter to study the hydrodynamic behavior of the flow in the developing entrance region between vertical parallel plates. In this regard, the development of the pressure gradient and pressure from the channel entrance till the fully developed region is recorded for all cases under investigation over a wide range of the operating parameters and the thermal boundary conditions. These developing profiles for the pressure and pressure gradient for mixed convection in vertical channel between parallel plates, which are similar to pertinent results that are available in the literature, are discussed in the present work from an angle that was not looked at before. Moreover, results that are not available in the literature are extracted from theses profiles and presented here for the first time in the literature.

According to the problem formulation given in Chapter 3, mixed convection in vertical channels can be generally categorized into two main categories, which are namely, buoyancy-aided flow and buoyancy-opposed flow. For buoyancy aided flow, the buoyancy-force term in the right hand side of the vertical momentum equation has a positive sign implying that the buoyancy is working in the same direction of the main flow. On the other hand, for buoyancy-opposed flow the buoyancy-force term has a negative sign implying that the buoyancy is working in an opposite direction to that of the forced flow. Having this understanding, the buoyancy parameter Gr/Re with positive values will be used to express buoyancy-aided flow situations while negative values of Gr/Re are used to represent buoyancy-opposed flow situations.

Figures 7.3 (a) and (b) depict the developments of the pressure gradient (dP/dZ) and the pressure (P), respectively, through the entrance region of a vertical channel between parallel plates under thermal boundary conditions of first kind with $\theta_T = 0$ for a wide range of the buoyancy parameter Gr/Re for buoyancy-opposed flows ($-90 \leq Gr/Re \leq 0$) and for buoyancy-aided flows ($0 < Gr/Re \leq 90$). These two figures show that the dimensionless pressure develops from zero at the channel entrance with a very high negative pressure gradient at the entrance acquiring negative values due to the friction between the walls and the fluid which results in building up two boundary layers over the two walls due to the viscous effects of the fluid. These negative values of the pressure will continue increasing due to the corresponding negative pressure gradient for the cases of pure forced convection ($Gr/Re = 0$) and the buoyancy-opposed flow cases with negative values of Gr/Re. For pure forced convection and relatively low negative values of Gr/Re for buoyancy-opposed flows, the pressure gradient develops from a very high negative value at the entrance and continues negative with a decreasing negativity till it reaches asymptotically to its fully developed negative value. For highly-opposed-flows (flows with large negative values of Gr/Re), the pressure gradient of high negative value at the entrance will develop with a decreasing negativity after the entrance reaching a minimum negative value then it will increase again in negativity with a decreasing rate till it reaches asymptotically its fully developed negative value as illustrated in Fig. 7.3(a). This behavior of pressure gradient shows that both viscous forces and buoyancy forces act in the same direction opposing the forced flow direction trying, both, to retard the flow. The direct result of the act of these two forces for buoyancy-opposed flow is to create and develop more negative pressure in the flow direction which is evidently

presented for cases of Gr/Re ≤ 0 in Fig. 7.3 (b). It is worth mentioning here that large values of the opposing buoyancy parameters lead to flow reversal and consequentially it leads faster to flow instability. On the other hand, for buoyancy-aided flow situations that have positive values of he buoyancy term and represented by the positive values of Gr/Re in Figs. 7.3(a) and (b), the pressure develops from its zero value at the entrance acquiring negative value downstream due to the high negative pressure gradient at the entrance for all values of the buoyancy parameter Gr/Re. This negative pressure gradient with large negative values at the entrance develops downstream with a decreasing negativity approaching asymptotically its negative value for relatively low values of the buoyancy parameter Gr/Re. However, for large values of the buoyancy parameter Gr/Re for buoyancy-aided flow situations the pressure gradient develops from its very high negative value at the entrance with a decreasing negativity with an increasing rate such that it will reach zero and then continue increasing reaching asymptotically it's fully developed positive value as shown in Fig. 7.3(a).

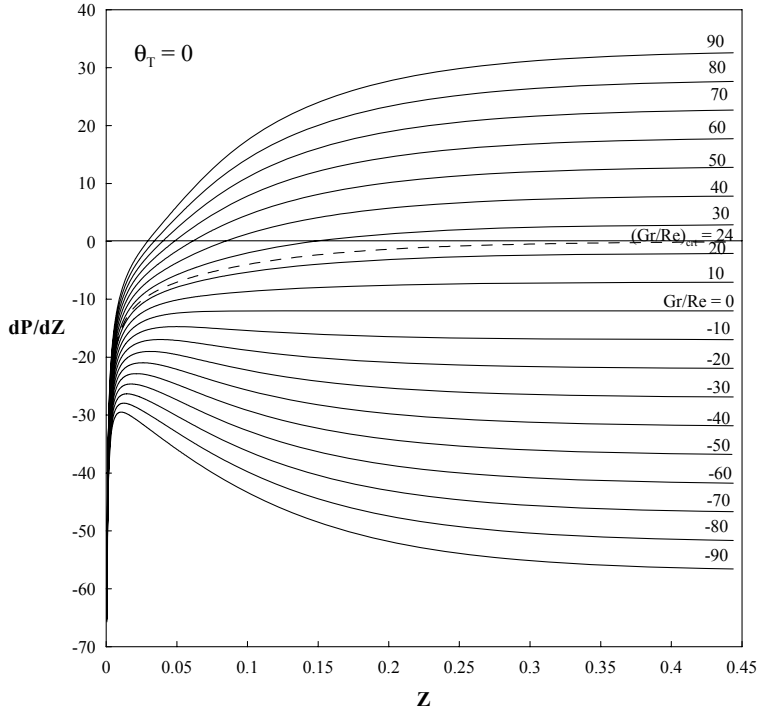

Figure 7.3 (a) Variation of pressure gradient along the channel height for positive and negative values of Gr/Re under the thermal BC of first kind and for $\theta_T = 0$ between vertical parallel plates

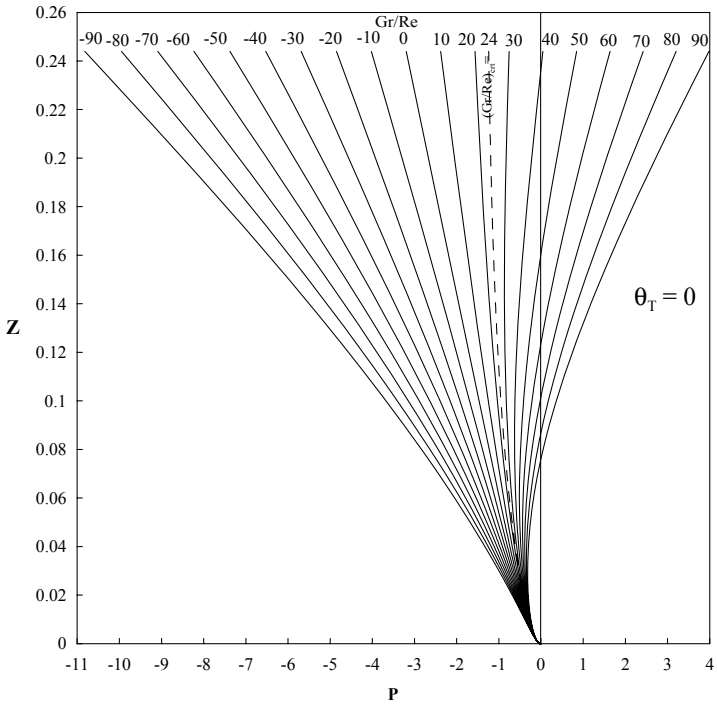

Figure 7.3 (b) Pressure variation along the channel height for positive and negative values of Gr/Re under the thermal BC of first kind and for $\theta_T = 0$ between vertical parallel plates

For such situation of buoyancy-aided flow with relatively low positive values of the buoyancy parameter Gr/Re, the buoyancy forces act in the same flow direction aiding the flow to overcome the viscous effects and the development of the pressure looks similar to that of pure forced convection but with lower negative values in the fully developed region (i.e. with less pressure drop along the channel). However, for buoyancy-aided flows with relatively large values of the buoyancy parameter Gr/Re, the buoyancy forces aiding the flow will develop downstream not only balancing the viscous forces but also overcome viscous forces resulting in pressure build up. Thus, the pressure will develop further from the negative values, acquired downstream the channel entrance as a result of the viscous effects due to the presence of the two walls, with a positive pressure gradient reaching the value of zero then continues building up positive pressure that monotonically increases downstream as shown in Fig. 7.3(b). Within this positive range of the buoyancy parameter Gr/Re for buoyancy-aided flows, there exists a value of the buoyancy parameter at which the pressure gradient will develop from the usual very high negative value at the entrance to asymptotic value of exactly zero. This particular value of the Gr/Re, at which ($dP/dZ = 0$) exists only for buoyancy-aided flow as shown in Fig. 7.3(a).

This particular value has been named as the critical value of Gr/Re, $(Gr/Re)_{crt}$. The existence of these critical values of Gr/Re has been mathematically demonstrated and its values were analytically obtained, in Chapter 4, for all the cases under consideration. The developments of the pressure gradient and the pressure for buoyancy-aided flow with the buoyancy parameter equals to $(Gr/Re)_{crt}$ are shown as dotted lines in Figs. 7.3(a) and (b), respectively for the mixed convection in a vertical channel under thermal boundary

conditions of the first kind with $\theta_T = 0$. For this particular case, the dimensionless pressure is developing from its zero value at the entrance acquiring a negative value due to the dominant viscous effects at this region. Further downstream and due to the continuous heating, the buoyancy effects participate in controlling the flow and its effect develops in the flow direction till it balances exactly the viscous forces resulting in exactly a zero pressure gradient in the fully developed region as shown in Fig. 7.3(a) and consistently constant but negative pressure throughout the channel height till the fully developed conditions achieved as shown in Fig. 7.3 (b).

For buoyancy-aided flows with $Gr/Re > (Gr/Re)_{crt}$, the buoyancy forces working in the flow direction are not effective directly after the channel entrance due to the time needed for the heat to penetrate and alter the fluid density resulting in a developing effect of the buoyancy forces which eventually overcome the viscous forces after distances that depend on the value of Gr/Re (heating rates). These distances are nothing but the distance from the entrance to the locations at which the developing negative pressure gradient crosses the line of zero value and inverts its sign to be a positive pressure gradient. For such situations, the dimensionless pressure will also develop from its zero value at the entrance acquiring negative value due to the friction at the entrance. This is a direct result of the viscous effects at the entrance, which will be gradually balanced and eventually overcome by the developing buoyancy forces. This results in a build up of the pressure making it develop gradually with a decreasing negativity till it crosses the line of zero value and continue building up creating a monotonically increasing positive pressure as shown in Fig. 7.3(b). On the other hand for values of $Gr/Re < (Gr/Re)_{crt,,}$ both the

pressure gradient and the pressure acquire negative values throughout the downstream of the channel entrance.

It is clear from the above two figures and the above discussion that pressure build up will take place down stream a vertical channel due mixed convection effects only for buoyancy-aided flow. Thus from now on, the discussion will be devoted only to buoyancy-aided flow with the buoyancy parameter $Gr/Re \geq 0$ for all the geometries under consideration. More analysis that focuses on the development of the pressure gradient as well as the pressure along the channel height from the entrance up to the fully developed region for all the cases under consideration is presented hereunder. The objective of such analysis is to extract the hydrodynamic parameters of practical importance such as the locations of changing the developing pressure gradient from negative to positive values, the locations of the onset of pressure build up, the locations of flow reversal onset if any, the locations of flow and numerical instability and the fully developed length.

Figures 7.3 (c) and (d) focus more on the development of the pressure gradient (dP/dZ) and pressure (P), respectively, for buoyancy-aided flow situations ($Gr/Re > 0$) in the entry region of a vertical channel between two parallel plates under thermal boundary conditions of the first kind with $\theta_T = 0$. Similar results but for the case of $\theta_T = 1$ are shown in Figs. 7.3(e) and (f), respectively. These four figures are only sample of the results obtained from the investigated cases under thermal boundary conditions of the first cases. The considered cases that investigated the effect of θ_T on the hydrodynamic and thermal performance of the buoyancy aided flow in a vertical channel between two parallel plates under thermal boundary conditions of the first kind are namely, $\theta_T = 0$, 0.25, 0.5, 0.75 and 1.

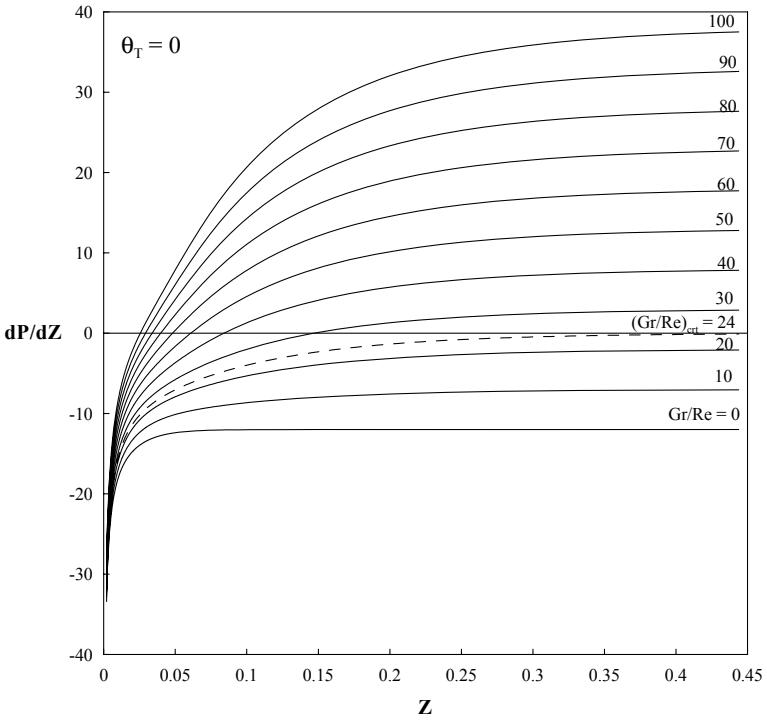

Figure 7.3(c) Variation of pressure gradient along the channel height for different Gr/Re for the thermal boundary condition of first kind and for $\theta_T = 0$ between vertical parallel plates

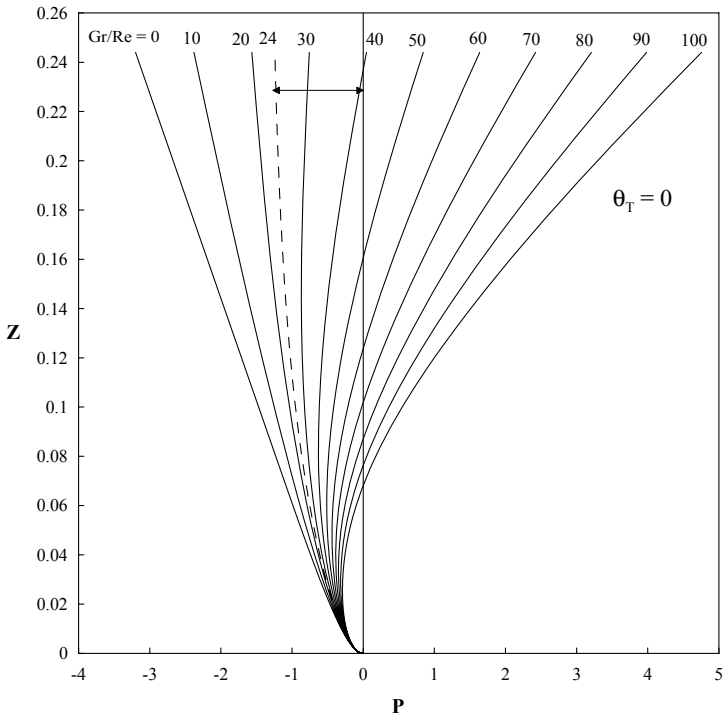

Figure 7.3(d) Pressure variation along the channel height for different Gr/Re for the thermal boundary condition of first kind and for $\theta_T = 0$ between vertical parallel plates

In all the investigated cases the developments of the pressure and the pressure gradient for buoyancy-aided flows have the same trends shown in Figures 7.3(c-f).

Figure 7.3 (c) clearly shows that for the buoyancy-aided flow with the buoyancy parameter $Gr/Re = (Gr/Re)_{crt} = 24$, under thermal boundary conditions of first kind with $\theta_T = 0$, the pressure gradient (shown by the dotted line) develops from a high negative value at the entrance with a decrease in negativity approaching it's a asymptotic fully developed value of exactly zero. This zero pressure gradient is confirmed by the asymptotically constant value attained by the developing pressure profile for the pertinent case as shown by the dotted line in Fig. 7.3(c). For buoyancy-aided flows under the same thermal boundary conditions but with $Gr/Re > (Gr/Re)_{crt}$, the pressure gradients profiles for all cases develops from its very high negative value at the entrance with decreasing negativity crossing the line of zero value and eventually approaching asymptotically its fully developed positive value. Similar results and trends have been obtained for the buoyancy-aided flow in vertical channels between two parallel plates under thermal boundary conditions of the first kind with different values of the two plates dimensionless temperature ratio, $\theta_T = 0$, 0.25, 0.5, 0.75, and 1. Figures 7.3(e) and (f) give, as another example, the development of pressure gradients and pressure for different values of Gr/Re for the case of $\theta_T = 1$.

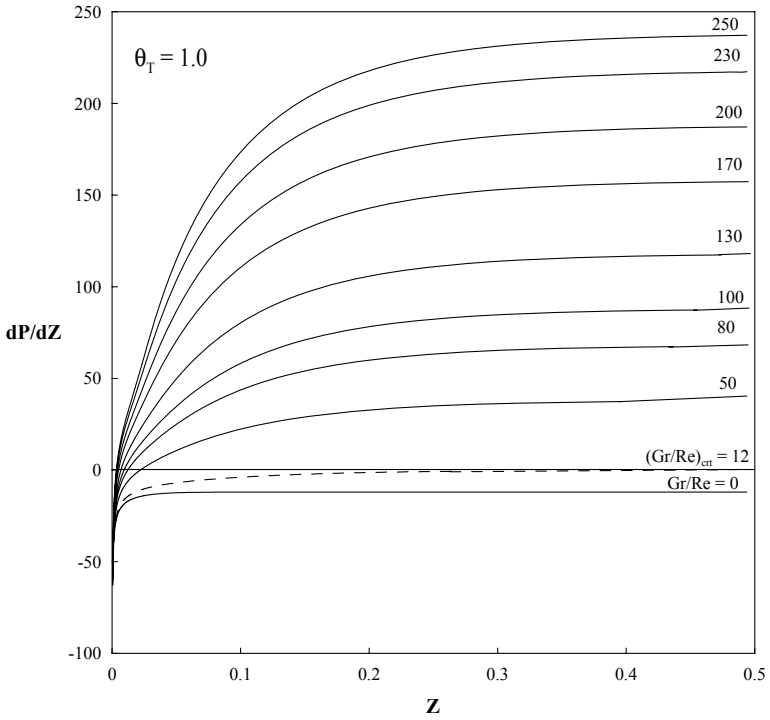

Figure 7.3(e) Variation of pressure gradient along the channel height for different Gr/Re for the thermal boundary condition of first kind and for $\theta_T = 1.0$ between vertical parallel plates

For buoyancy aided flows with $Gr/Re > (Gr/Re)_{crt}$ the pressure build up due to the buoyancy effects explained earlier results in monotonically increasing positive pressure. For situations with Gr/Re is higher than $(Gr/Re)_{crt}$, the buoyancy effects acts in the flow direction aiding the flow, to overcome the friction due to the fluid viscous effects. This would definitely results in reducing the load on the pumping device (pump for liquid and compressor for gases). For relatively higher values of Gr/Re, the channel would have higher buoyancy forces that make the channel, due to high heating rates, act as a diffuser and the pumping device in such cases might work as a flow regulator (this was noticed and reported by Han [20]).

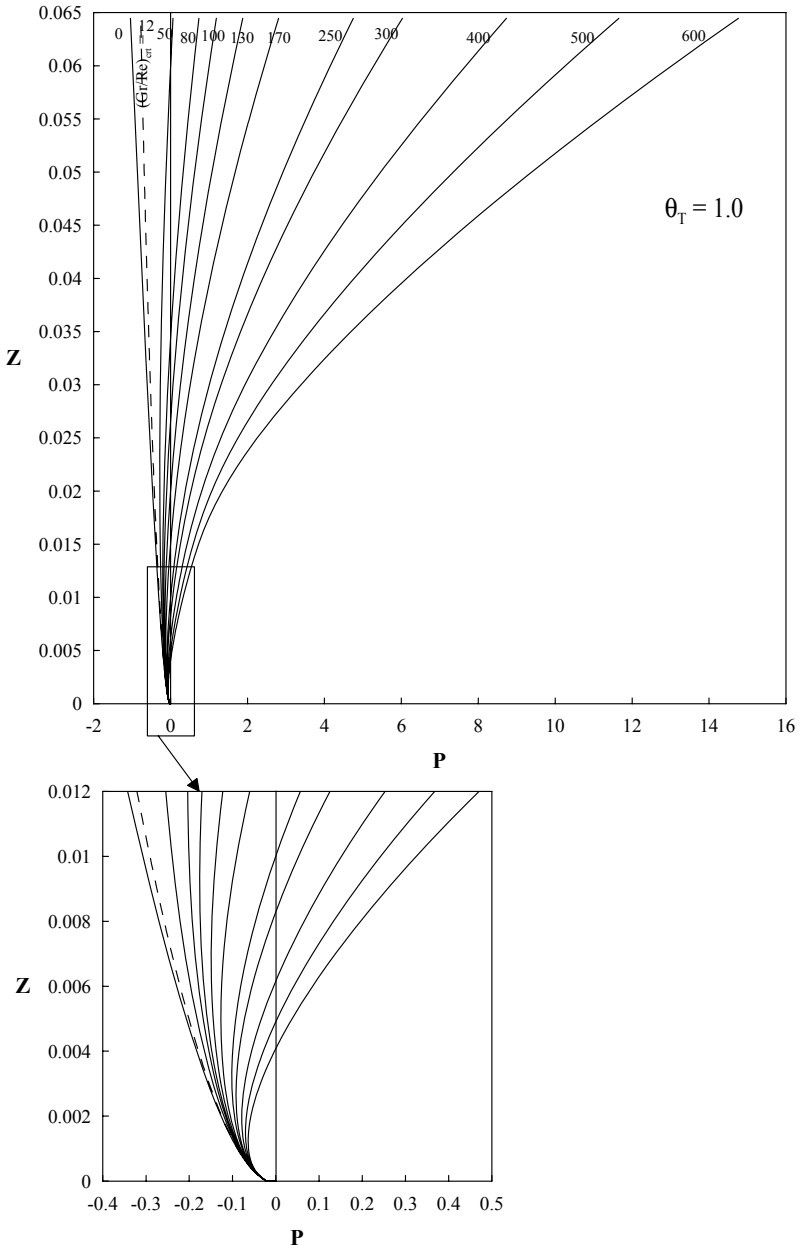

Figure 7.3(f) Pressure variation along the channel height for different Gr/Re for the thermal boundary condition of first kind and for $\theta_T = 1.0$ between vertical parallel plates

However, for very high heating rates the pressure build up due to the buoyancy-aiding effects might result in a back pressure that is high enough to prevent the fluid particles to continue flowing downstream the vertical channel. In such situations, flow reversal takes place especially near the cold wall (for cases of asymmetric heating) where the buoyancy

effects are weaker. The locations of the flow reversal onset in such situation was defined as the locations at which the velocity gradient at the wall $\partial U / \partial Y \leq 0$. These locations (if any) are reported for all the investigations cases in Table 7.1. Increasing more the heating rate (Gr/Re), the flow reversal become severe and the flow will suffer from flow instability, which directly leads to numerical instability and the computer code stops, since it is not formulated to solve flow instability problem. The locations of the flow and numerical instability are indicated also in Table 7.1.

Two more important hydrodynamic parameters are recorded in Table 7.2 for all the investigated cases. These two parameters are the location at which the pressure gradient, for buoyancy aided flow with the buoyancy parameter Gr/Re > $(Gr/Re)_{crt}$, crosses the line of zero value changing its sign from negative pressure gradient to positive pressure gradient (Z_I). This represents the location at which pressure build up started. This pressure build-up results in increasing the pressure from the negative value downstream the entrance with a positive pressure gradient such that it reaches zero at a location (Z_{II}) where it increases monotonically and positively downstream. These locations are obtained for all the investigated cases and are reported in Table 7.2. These locations represent the height beyond which a vertical channel with buoyancy aided flow condition can act as a diffuser under given thermal boundary conditions. Caution should be taken in determining the operating heating rates represented in terms of the buoyancy parameter Gr/Re such that flow reversal due to pressure build-up can be avoided. This type of the obtained and presented information for different isothermal boundary conditions for different values of Gr/Re would be of prime importance to the designer of heat transfer and flow equipment. Such information would definitely help the designer to properly

size the pump or compressor needed to pump the fluid through channels subjected to buoyancy-aided flow situations. It is clear that making the design and sizing of the pump based on pure forced flow conditions would result in an oversized pumping device. So, due to its importance, the values of Z_I and Z_{II} for buoyancy-aided flows in a vertical channel between parallel plates under thermal boundary conditions of the first kind are plotted as function of the buoyancy parameter Gr/Re for different values of θ_T in Figs. 7.4(a) and (b), respectively.

Table 7.1 Locations of numerical instability (Z_{in}), onset of flow reversal (Z_{fr}) and the hydrodynamic fully development length (Z_{fd}) between vertical parallel plates under the thermal BC of first kind with different θ_T

Gr/Re	$\theta_T = 0$			$\theta_T = 0.25$			$\theta_T = 0.5$			$\theta_T = 0.75$			$\theta_T = 1.0$		
	Z_{in}	Z_{fr}	Z_{fd}	Z_{in}	Z_{fr}	Z_{fd}	Z_{in}	Z_{fr}	Z_{fd}	Z_{in}	Z_{fr}	Z_{fd}	Z_{in}	Z_{fr}	Z_{fd}
0		NFR	0.06700		NFR	0.06700		NFR	0.06700		NFR	0.06700		NFR	0.06700
10		NFR	0.21430		NFR	0.22320		NFR	0.23246		NFR	0.24007		NFR	0.24591
20		NFR	0.28380		NFR	0.29380		NFR	0.30080		NFR	0.30480		NFR	0.30787
30		NFR	0.33780		NFR	0.34280		NFR	0.34480		NFR	0.34580		NFR	0.34380
40		NFR	0.38880		NFR	0.38480		NFR	0.37980		NFR	0.37480		NFR	0.36880
50		NFR	0.44280		NFR	0.42180		NFR	0.41080		NFR	0.39780		NFR	0.38880
60		NFR	0.51280		NFR	0.46280		NFR	0.43780		NFR	0.41980		NFR	0.40180
70		NFR	0.63680		NFR	0.50080		NFR	0.45980		NFR	0.43780		NFR	0.41480
80		0.20237	0.80980		NFR	0.55280		NFR	0.48780		NFR	0.45080		NFR	0.42780
90		0.12265	1.12380		NFR	0.60780		NFR	0.50780		NFR	0.46680		NFR	0.43680
100		0.09464	1.29080		NFR	0.89380		NFR	0.53780		NFR	0.48080		NFR	0.44280
150	0.20071	0.05322			0.09597	0.95980		NFR	0.73380		NFR	0.53887		NFR	0.47680
200	0.06103	0.04091		0.11570	0.06674			0.16340	0.85480		NFR	0.59380		NFR	0.48480
230	0.06072	0.03669		0.09075	0.05832			0.13050			NFR	0.62380		NFR	0.50180
250	0.04899	0.03453		0.08140	0.05432		24.28700	0.11670			NFR	0.63880		NFR	0.50680
300	0.04340	0.03067		0.06288	0.04698		0.32380	0.09420			0.69980	0.94080		NFR	0.51080
400	0.04047	0.02578		0.05716	0.03813		0.09550	0.07110			0.22140			NFR	0.55380
500	0.03283	0.02288		0.04047	0.03301		0.07010	0.05981		7.50950	0.17490			NFR	0.55980
600	0.02798	0.02075		0.03569	0.02847		0.06640	0.05107		0.34080	0.15130			NFR	0.57380

Table 7.2 Locations of zero pressure gradient (Z_I) and onset of pressure build up (Z_{II}) between vertical parallel plates under the thermal BC of first kind with different θ_T

Gr/Re	$\theta_T = 0$		$\theta_T = 0.25$		$\theta_T = 0.5$		$\theta_T = 0.75$		$\theta_T = 1.0$	
	Z_I	Z_{II}	Z_I	Z_{II}	Z_I	Z_{II}	Z_I	Z_{II}	Z_I	Z_{II}
20			0.28771	*	0.13907	*	0.09791	*	0.07607	0.23046
30	0.13465	0.51268	0.08433	0.26193	0.06176	0.18209	0.04844	0.14082	0.03958	0.11513
40	0.07402	0.22356	0.05210	0.15056	0.03948	0.11435	0.03141	0.09224	0.02587	0.07726
50	0.05219	0.14827	0.03727	0.10707	0.02834	0.08370	0.02265	0.06855	0.01874	0.05797
60	0.04009	0.11224	0.02846	0.08338	0.02169	0.06595	0.01741	0.05439	0.01448	0.04623
70	0.03205	0.09083	0.02263	0.06829	0.01735	0.05430	0.01401	0.04496	0.01170	0.03836
80	0.02621	0.07651	0.01856	0.05776	0.01434	0.04605	0.01163	0.03825	0.00973	0.03275
90	0.02187	0.06615	0.01563	0.04995	0.01215	0.03991	0.00989	0.03326	0.00829	0.02856
100	0.01858	0.05824	0.01342	0.04393	0.01050	0.03517	0.00857	0.02940	0.00718	0.02532
130	0.01252	0.04252	0.00929	0.03202	0.00732	0.02587	0.00598	0.02181	0.00499	0.01889
150	0.01018	0.03574	0.00762	0.02703	0.00601	0.02197	0.00488	0.01861	0.00400	0.01616
200	0.00679	0.02507	0.00508	0.01937	0.00391	0.01595	0.00292	0.01360	0.00122	0.01186
250	0.00493	0.01912	0.00355	0.01506	0.00138	0.01250	0.00100	0.01070	0.00087	0.00934
300	0.00365	0.01542	0.00122	0.01230	0.00093	0.01026	0.00081	0.00880	0.00073	0.00769
400	0.00098	0.01109	0.00080	0.00897	0.00071	0.00752	0.00064	0.00646	0.00059	0.00566
500	0.00077	0.00863	0.00066	0.00703	0.00059	0.00591	0.00054	0.00508	0.00050	0.00445
600	0.00066	0.00704	0.00058	0.00576	0.00052	0.00485	0.00048	0.00418	0.00044	0.00366

* For such cases, the pressure defect did not cross the value of zero before the fully developed conditions.

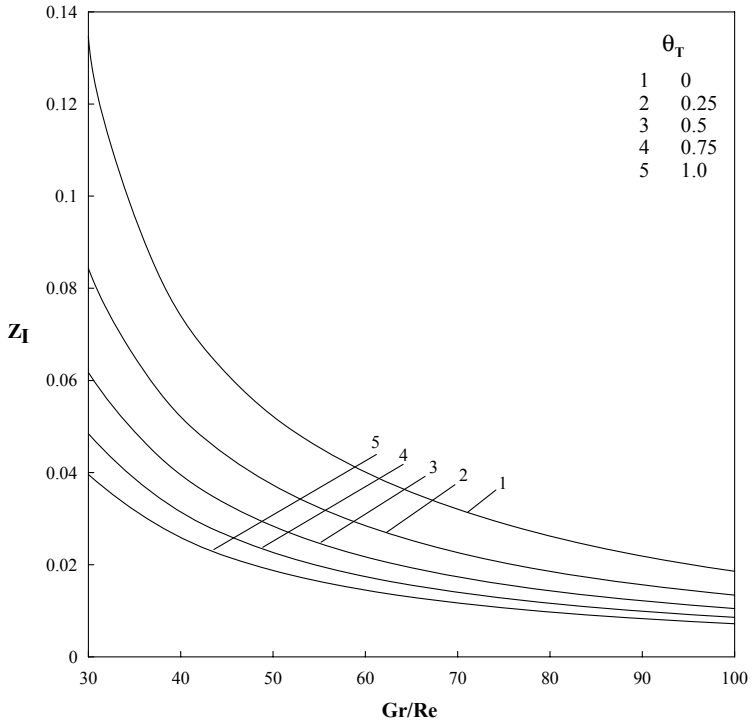

Figure 7.4(a) Graphical representation of location of zero pressure gradient (Z_I) as a function of Gr/Re for different θ_T in vertical parallel plates under the thermal BC of first kind

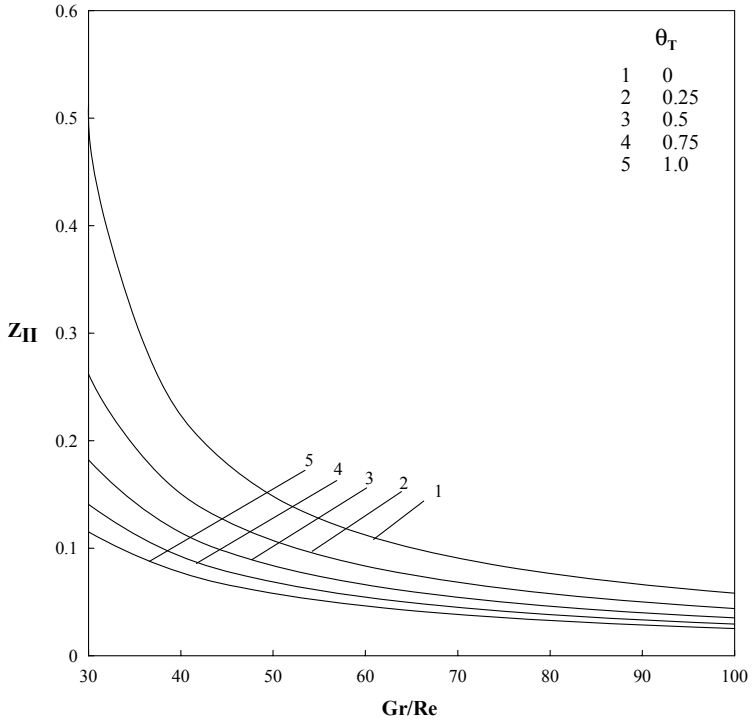

Figure 7.4(b) Graphical representation of location of zero pressure (Z_{II}) as a function of Gr/Re for different θ_T in vertical parallel plates under the thermal BC of first kind

Figure 7.5(a) shows the variation of the mean bulk fluid temperature for $\theta_T = 0$ at different Gr/Re. The mean temperature increases gradually from very small value near the channel entrance to its asymptotic fully developed constant value far downstream of the channel entrance. The asymptotic fully developed mean bulk temperature value is different for different buoyancy parameter Gr/Re and is greater than the forced convection value (Gr/Re = 0). A similar trend is observed for θ_T =1.0, shown in the Figure 7.5(b) except at large values of Z, all the curves converge to the value 1.

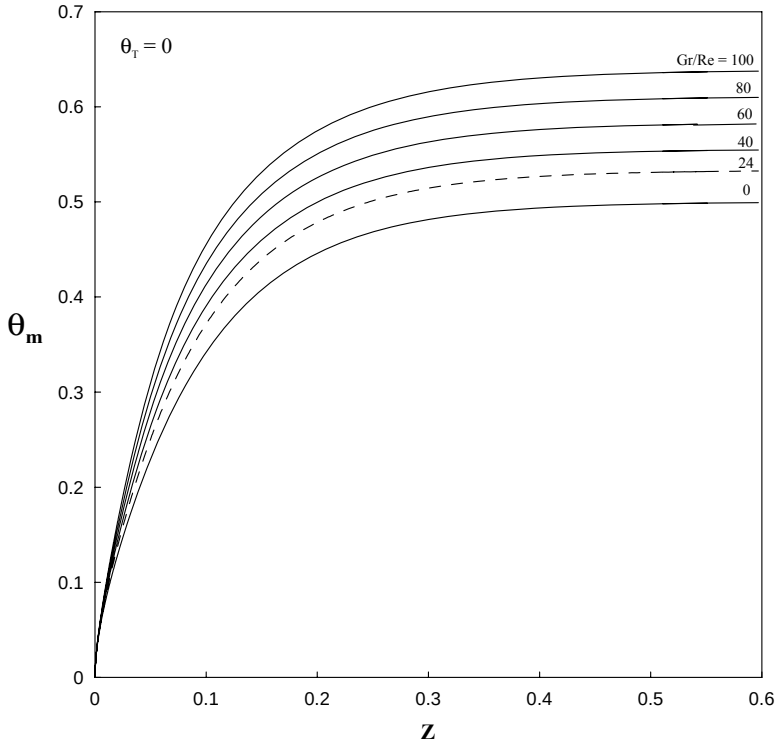

Figures 7.5(a) Mean or bulk temperature along the channel height for different Gr/Re for the thermal boundary condition of first kind and for $\theta_T = 0$ between vertical parallel plates.

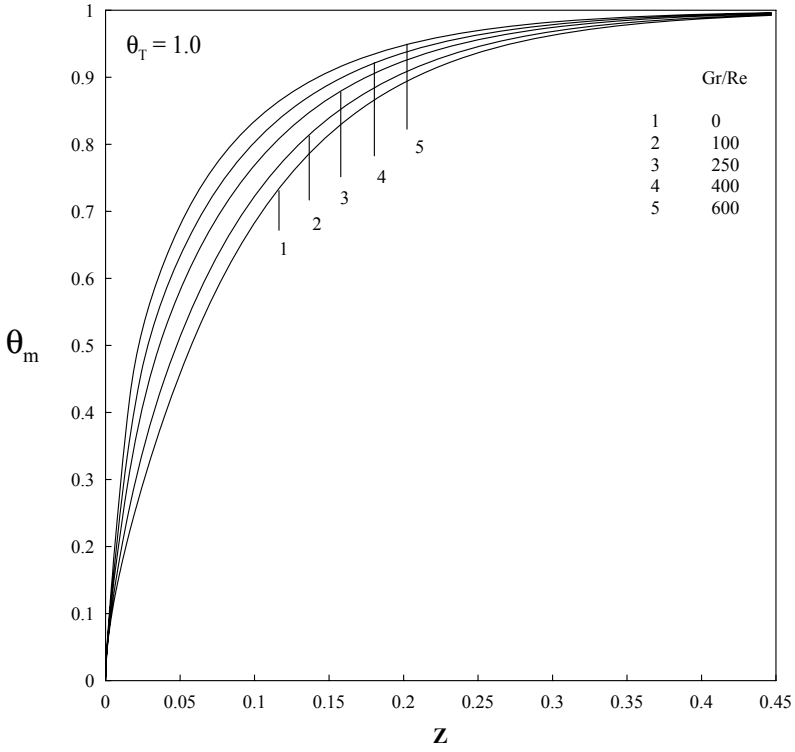

Figure 7.5(b) Mean or bulk temperature along the channel height for different Gr/Re for thermal boundary condition of first kind and for $\theta_T = 1.0$ between vertical parallel plates

The Nusselt number based on the mean temperature is plotted as a function of position (Z) for different buoyancy parameters Gr/Re and for $\theta_T = 0$. Figure 7.5(c) shows the variation of Nusselt number on the heated side of the vertical channel between parallel plates. The figure shows that the Nusselt number, from its high value near the heated region of the channel where the temperature gradients are high enough, falls sharply at the entrance then it gradually decreases and attains its asymptotic fully developed value for all values of buoyancy parameter Gr/Re at the downstream of the channel. The fully developed Nusselt number obtained for a given Gr/Re is greater than the one obtained and reported by Shah and London [36] for the forced convection. Also the Nusselt number under fully developed conditions increases as Gr/Re increases.

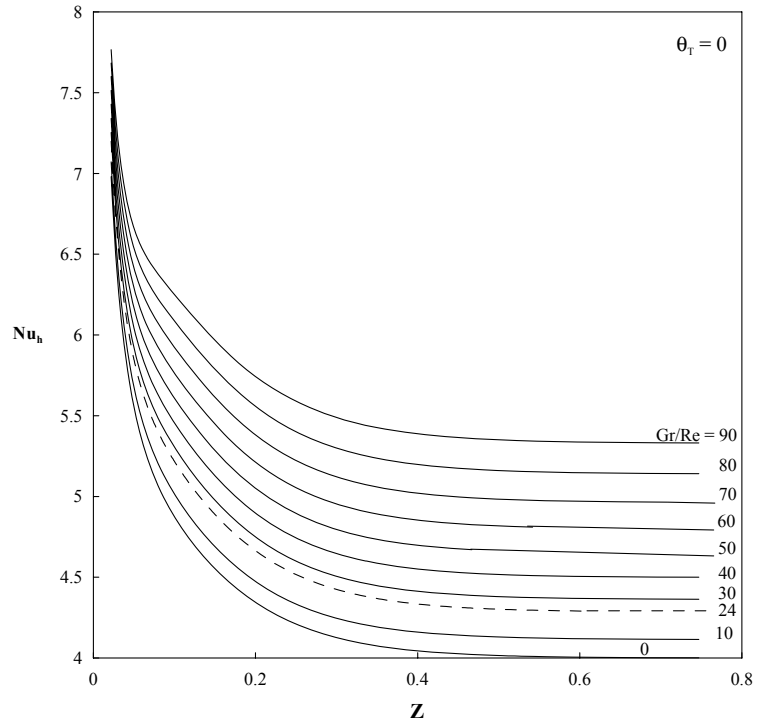

Figure 7.5(c) Variation of Nusselt number on the heated side of the channel versus axial distance for different Gr/Re for the thermal BC of first kind and for $\theta_T = 0$ between vertical parallel plates

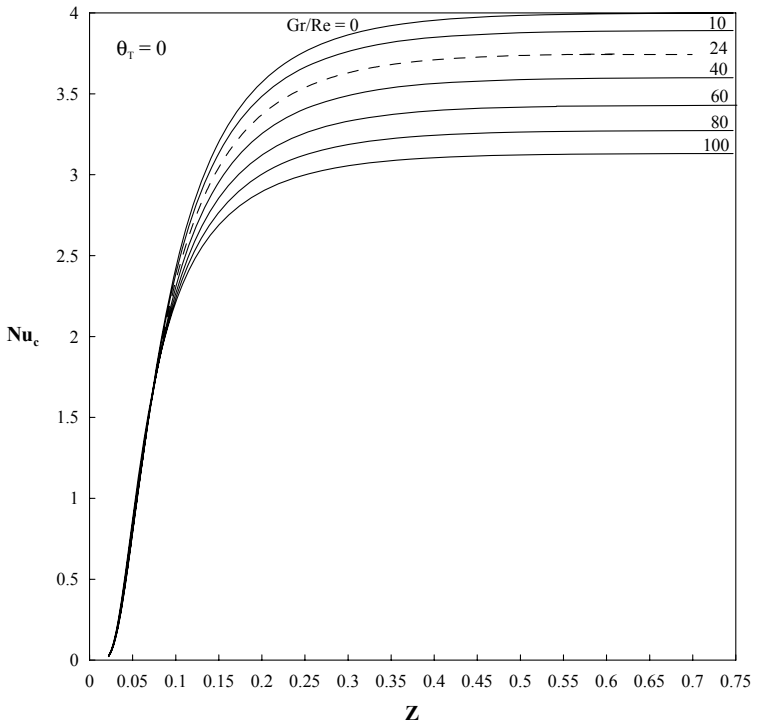

Figure 7.5(d) Variation of Nusselt number on the cold side of the vertical channel versus axial distance (Z) for different Gr/Re for the thermal BC of first kind and for $\theta_T = 0$ between vertical parallel plates

On the other hand, Nusselt number increases gradually from zero close to the channel entrance near the cold wall and attain its asymptotic fully developed value far downstream of the channel entrance where the velocity and temperature profile becomes invariant. This is due to the heat transfer takes place from hot region to the cold region. However, the fully developed Nusselt number is different for different Gr/Re and decreases as the Gr/Re increases. It is clear from the Figure 7.5(d) the fully developed Nusselt number for buoyancy parameter Gr/Re > 0 is less than the forced convection value equal to 4 which was also reported by Shah and London [36].

7.3 Results for the thermal boundary condition of third kind

Sample results of velocity and temperature profiles investigated for laminar developing mixed convection in a vertical channel between parallel plates under thermal boundary condition of third kind with different buoyancy parameters Gr/Re are shown in Figures 7.6(a-c). It is worth mentioning here that these plots are obtained for buoyancy aided flow only. Figures 7.6(a & b) exhibit similar behavior to that observed in the case of first kind thermal boundary condition with $\theta_T = 0$. As can be seen, very close to the channel inlet, the heating effects are not yet felt and further downstream, the heating causes the fluid accelerate near the hot wall and decelerate near the unheated wall (adiabatic wall) resulting in distortion of velocity profile to satisfy the continuity principle. With further increase in heating rates, this distortion becomes more severe and results into flow reversal near the adiabatic wall as shown in Fig. 7.6 (b). However, the velocity profile recovers and attains its asymptotic fully developed parabolic profile.

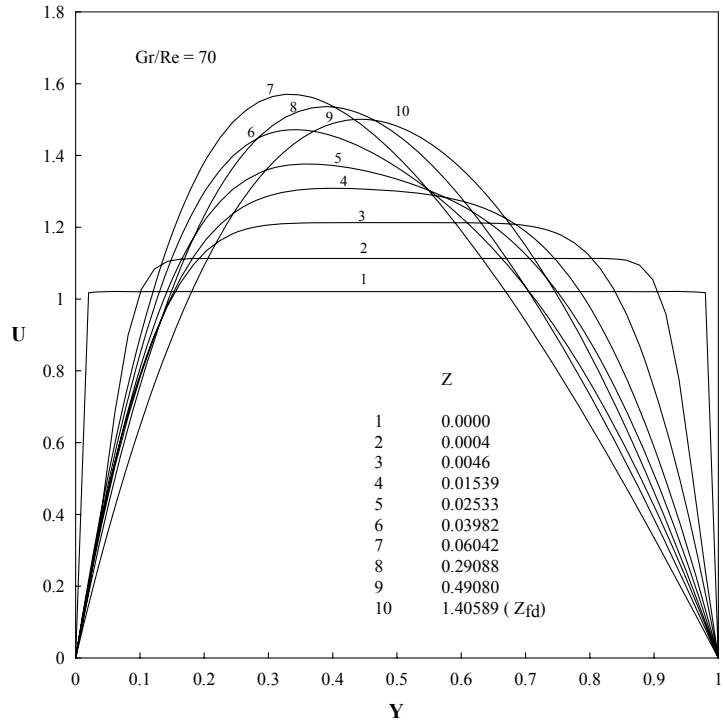

Figure 7.6(a) Variation of velocity distribution at different locations of channel height (Z) for Gr/Re = 70 for third kind boundary condition between vertical parallel plates

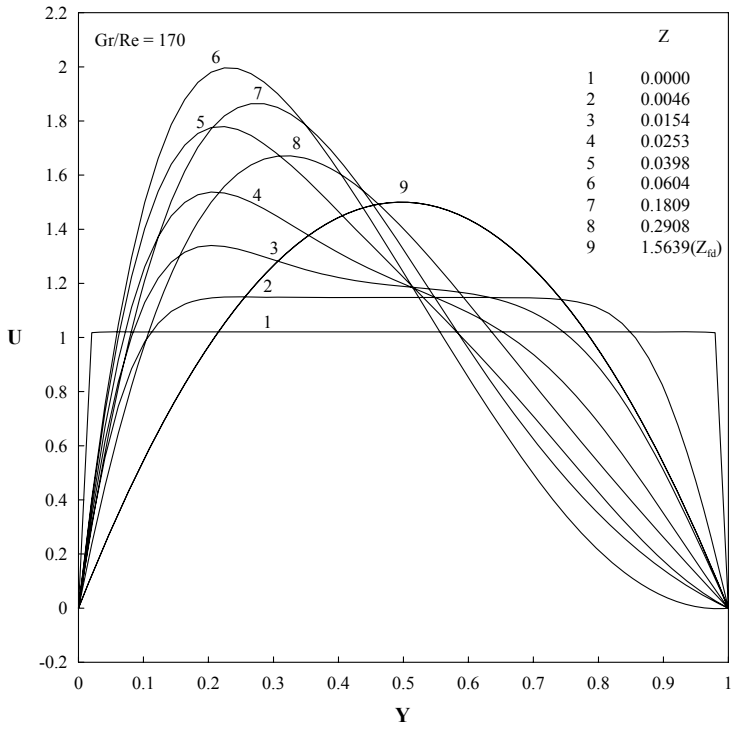

Figure 7.6(b) Variation of velocity distribution at different locations of channel height (Z) for Gr/Re = 170 for third kind boundary condition between vertical parallel plates

Figure 7.6(c) shows the development of temperature profile for buoyancy parameter Gr/Re = 170 under thermal boundary condition of third kind. This figure represents similar behavior to that discussed under thermal boundary condition of first kind when θ_T = 1.0 (symmetrical wall heating conditions).

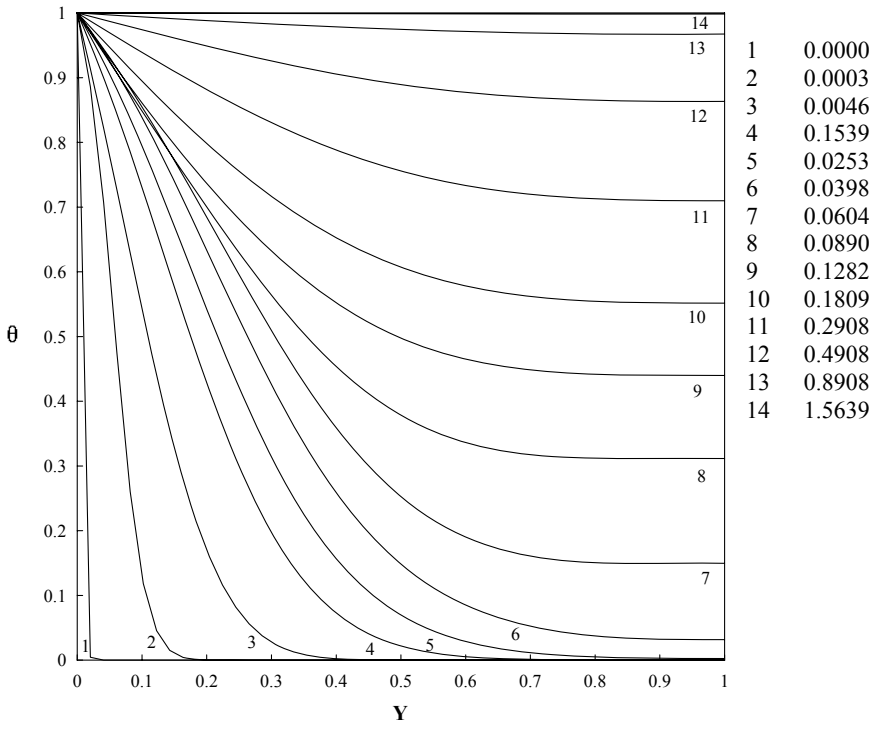

Figure 7.6 (c) Developing temperature profiles for thermal boundary condition of third kind for Gr/Re = 170 at different axial locations (Z) between vertical parallel plates

The developments of pressure gradient and pressure are shown in figures 7.7(a & b) for buoyancy-aided flow under thermal boundary condition of third kind. These two figures show how the two hydrodynamic parameters are developing downstream of the channel at different heating rates represented by buoyancy parameter Gr/Re. The similar discussion reported in the first kind thermal boundary also holds well in this situation.

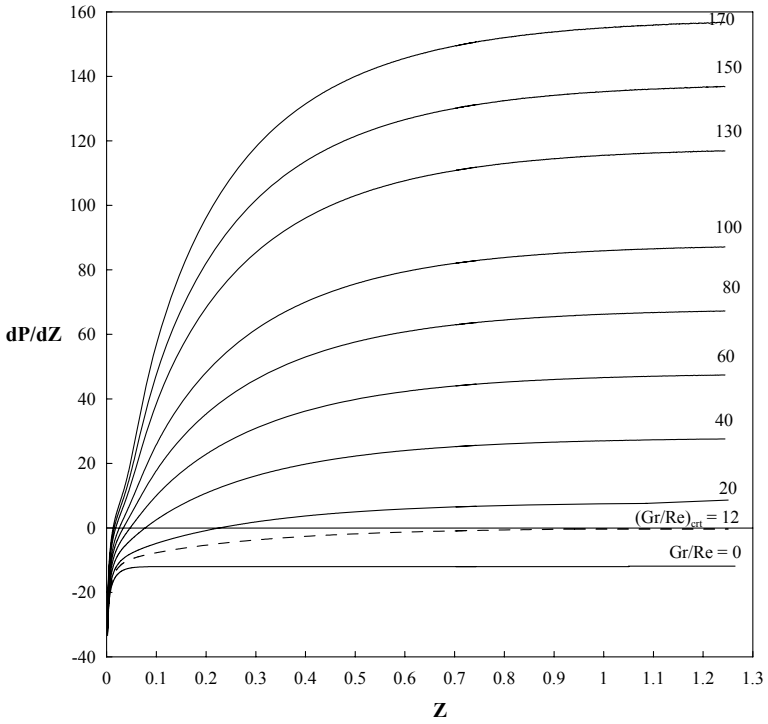

Figure 7.7(a) Variation of pressure gradient along the channel height for different Gr/Re for the thermal boundary condition of third kind between vertical parallel plates

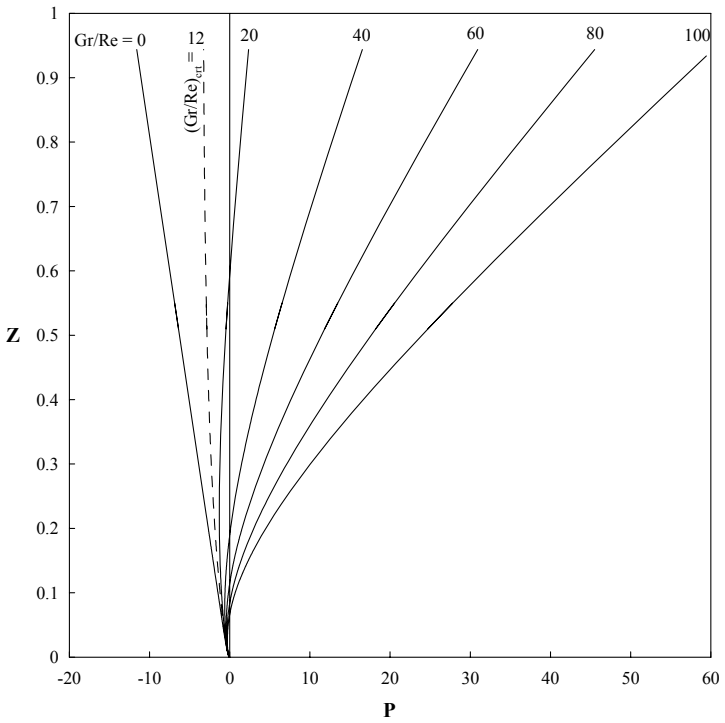

Figure 7.7(b) Pressure variation along the channel height for different Gr/Re for the thermal boundary condition of third kind between vertical parallel plates

Knowing that there is a possibility of incipient of flow reversal as the heating rates Gr/Re increases, which lead to numerical instability in the solution, the locations of onset of flow reversal and numerical instability in addition to location of hydrodynamic fully development lengths at which the velocity profile becomes invariant and attains its asymptotic fully developed profile with 1% deviation from its analytical profile, are presented in Table 7.3.

Table 7.3 Locations of numerical instability (Z_{in}), onset of flow reversal (Z_{fr}) and the hydrodynamic fully development length (Z_{fd}) between vertical parallel plates under the thermal BC of third kind

Gr/Re	**Z_{in}**	**Z_{fr}**	**Z_{fd}**
0		NFR	0.06707
10		NFR	0.91087
20		NFR	1.10088
30		NFR	1.20788
40		NFR	1.27888
50		NFR	1.33389
60		NFR	1.37389
70		NFR	1.40589
80		NFR	1.43589
90		NFR	1.44789
100		NFR	1.48889
130		NFR	1.53890
150		0.06740	1.54090
170		0.05268	1.56390
200	0.06908	0.04340	
230	0.06042	0.03813	
250	0.04798	0.03570	

It is worth mentioning here that there exist certain points, where the pressure gradient (dP/dZ) changes from its negative value to positive value and the pressure from its negative value to positive value resulting in positive pressure build up. These points or locations at which this phenomenon takes place are presented in Table 7.4. The dotted lines in Figures 7.7(a & b) represents the development of pressure gradient and pressure for critical value of $(Gr/Re)_{crt}$. It is clear not only from the figures but also from the table that these locations exists for the buoyancy parameter $Gr/Re > (Gr/Re)_{crt}$. The locations decreases with increase in heating rates Gr/Re as illustrated in Figures 7.8(a & b).

Table 7.4 Locations of zero pressure gradient (Z_I) and onset of pressure build up (Z_{II}) between vertical parallel plates under the thermal BC of third kind

Gr/Re	**Z_I**	**Z_{II}**
20	0.21835	0.58588
30	0.10623	0.27727
40	0.06873	0.17923
50	0.05062	0.13183
60	0.03958	0.10434
70	0.03187	0.08648
80	0.02616	0.07392
90	0.02185	0.06454
100	0.01858	0.05722
130	0.01252	0.04226
150	0.01018	0.03563
170	0.00854	0.03060
200	0.00679	0.02506
230	0.00557	0.02114
250	0.00493	0.01912

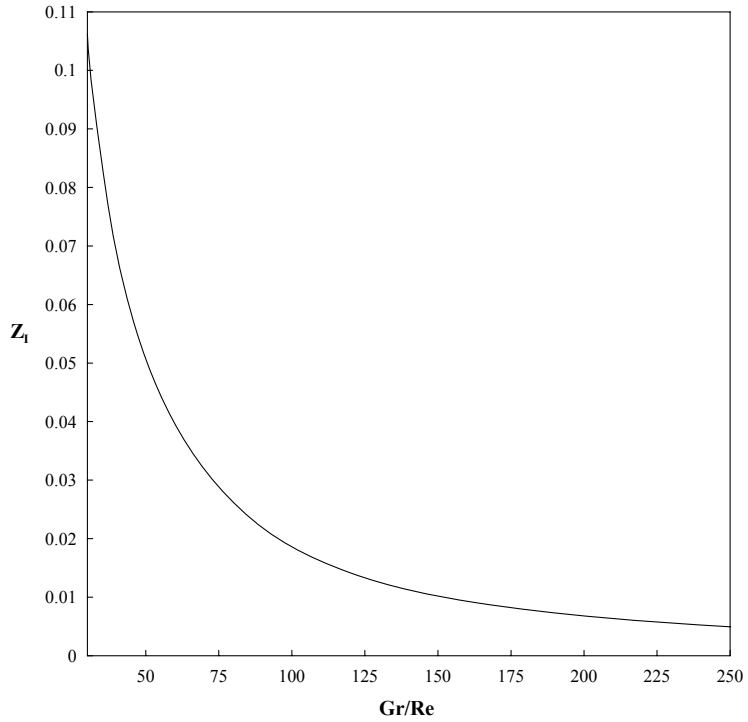

Figure 7.8(a) Graphical representation of location of zero pressure gradient (Z_I) versus Gr/Re in vertical parallel plates under the thermal BC of third kind

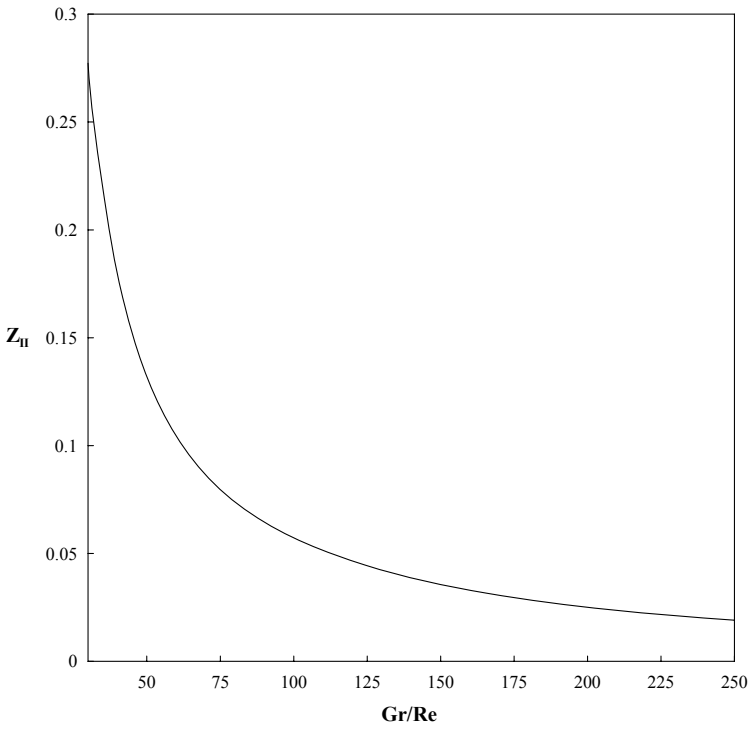

Figure 7.8(b) Graphical representation of location of onset of pressure builds up (Z_{II}) versus Gr/Re in vertical channel between parallel plates under the thermal BC of third kind

Figures 7.9(a) show the variation of mean temperature as a function of axial distance. It is seen that the mean temperature increases from very small value close to the channel entrance and attains fully developed value 1.0 far downstream of the channel for all values of buoyancy parameter Gr/Re. It is clear that at far downstream of the channel the buoyancy parameter Gr/Re has no effect. In other words, under hydrodynamically and thermally fully developed conditions, the buoyancy effects have no significance for this kind of thermal boundary condition.

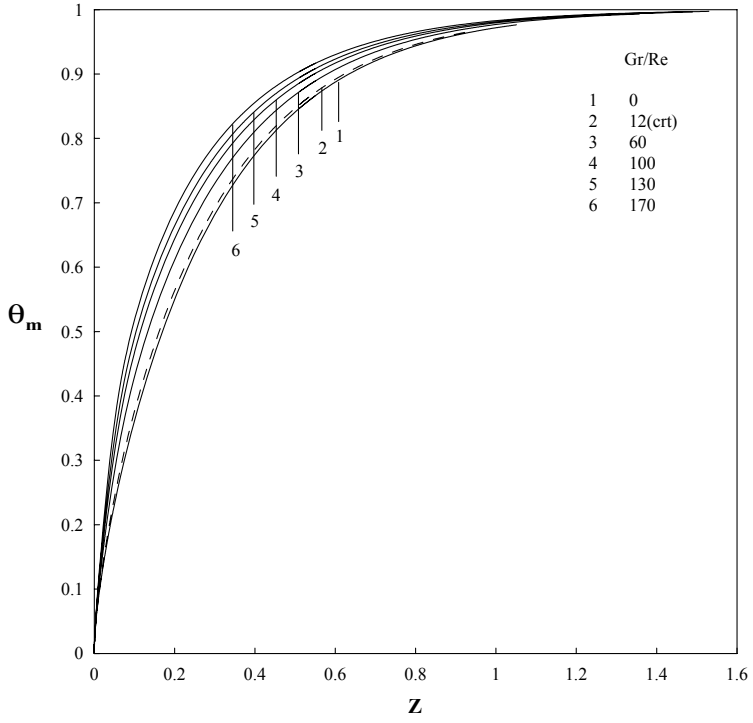

Figure 7.9(a) Mean or bulk temperature along the channel height for different Gr/Re for thermal boundary condition of third kind between vertical parallel plates

The other heat transfer characteristics namely Nusselt number variation is shown in Figure 7.9(b). The figure shows the effect of buoyancy on the Nusselt number as the heating rates increases. It is evident from the figure that the Nusselt number from its high

value near the channel entrance falls sharply and attains the same constant value for all the buoyancy parameters Gr/Re far downstream of the channel since the calculation of Nusselt number is based on the mean temperature that has a fully developed value of 1.0 regardless of the buoyancy effects.

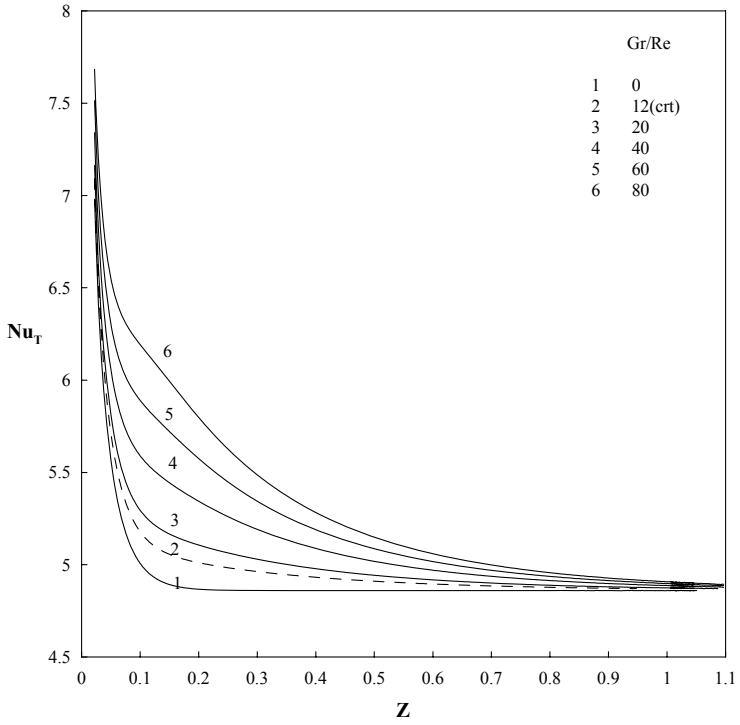

Figure 7.9(b) Variation of Nusselt number on the heated side of the parallel plates along the channel height for different Gr/Re for the thermal boundary condition of third kind

7.4 Results for the thermal boundary condition of fourth kind

The developments of velocity profiles along the axial distance for laminar mixed convection in vertical channel between parallel plates under thermal boundary condition of fourth kind are shown in the Figures 7.10(a & b) for Gr/Re = 24 and 100. These two figures represent only samples of the investigated cases under the thermal boundary condition of fourth kind. Similar explanation can be drawn from the first and third boundary conditions for this boundary condition.

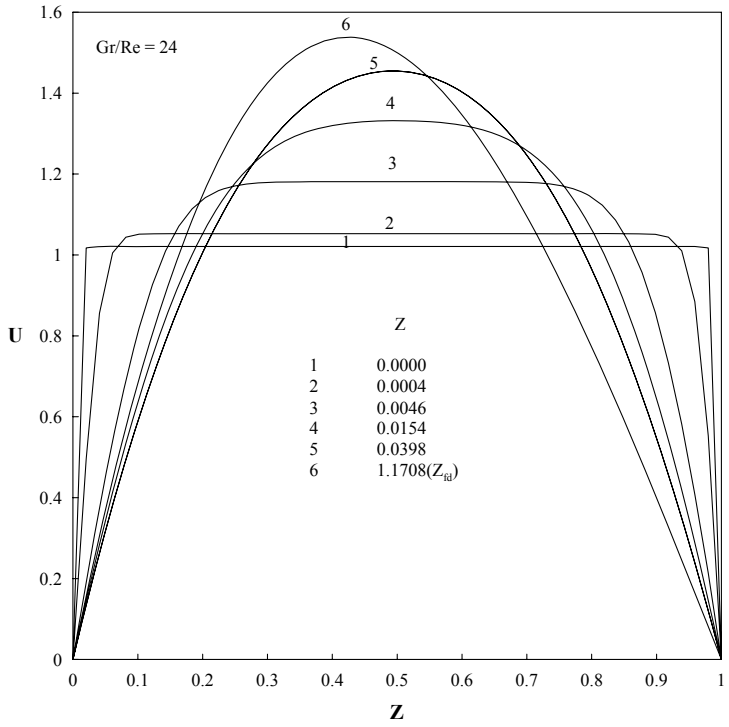

Figure 7.10(a) Variation of velocity distribution at different locations of channel height (Z) for Gr/Re = 24 for the thermal boundary condition of fourth kind between vertical parallel plates

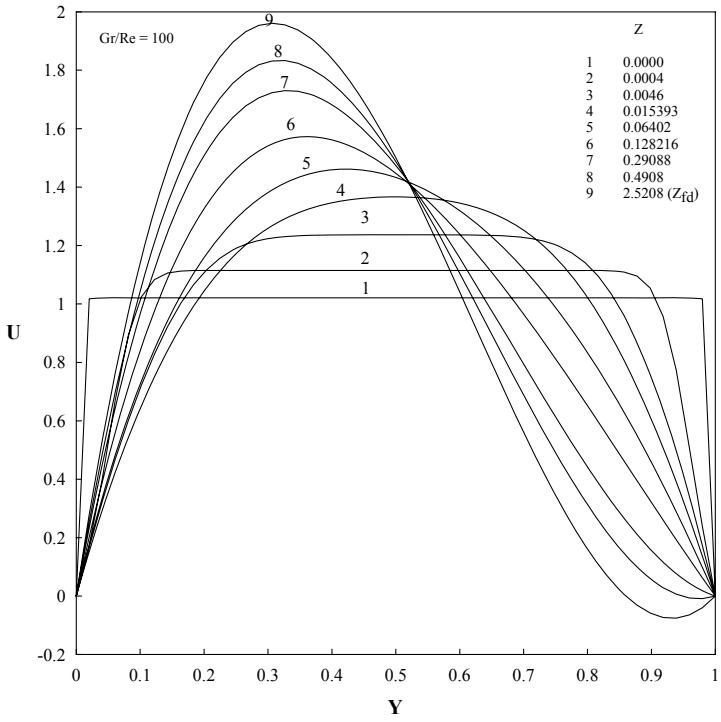

Figure 7.10(b) Variation of velocity distribution at different locations of channel height (Z) for Gr/Re = 100 for the thermal boundary condition of fourth kind between vertical parallel plates

Higher heating rates results in flow reversal due to excessive pressure build up due to buoyancy effect in the flow direction as well as due to the need of satisfying the mass conservation principle. The flow reversal causes the flow unstable and results in possible numerical instability in the solution. It is worth mentioning here that higher heating rates Gr/Re delays the development of velocity profile which in turn increases the hydrodynamic fully development length, a location at which the velocity profile attains its fully developed profile. The locations with possible onset of flow reversal, numerical instability and hydrodynamic fully development length are presented in the Table 7.5.

Table 7.5 Locations of numerical instability (Z_{in}), onset of flow reversal (Z_{fr}) and the hydrodynamic fully development length (Z_{fd}) between vertical parallel plates under the thermal BC of fourth kind

Gr/Re	**Z_{in}**	**Z_{fr}**	**Z_{fd}**
0		NFR	0.06707
10		NFR	0.81087
20		NFR	1.07887
30		NFR	1.27688
40		NFR	1.45989
50		NFR	1.65490
60		NFR	1.87291
70		NFR	2.16791
80		0.86287	2.39789
90		0.54288	
100		0.41188	
130	1.27188	0.24298	
150	0.73487	0.19019	
170	0.53588	0.15731	
200	0.36488	0.12597	
230	0.24201	0.10667	
250	0.25088	0.09731	

Figure 7.10(c) show how the temperature profiles are affected by constant heating of the wall along the axial direction between the vertical parallel plates. The figure is plotted for Gr/Re = 100 under thermal boundary condition of fourth kind (one wall is maintained at constant heat flux and the other is at isothermal condition).

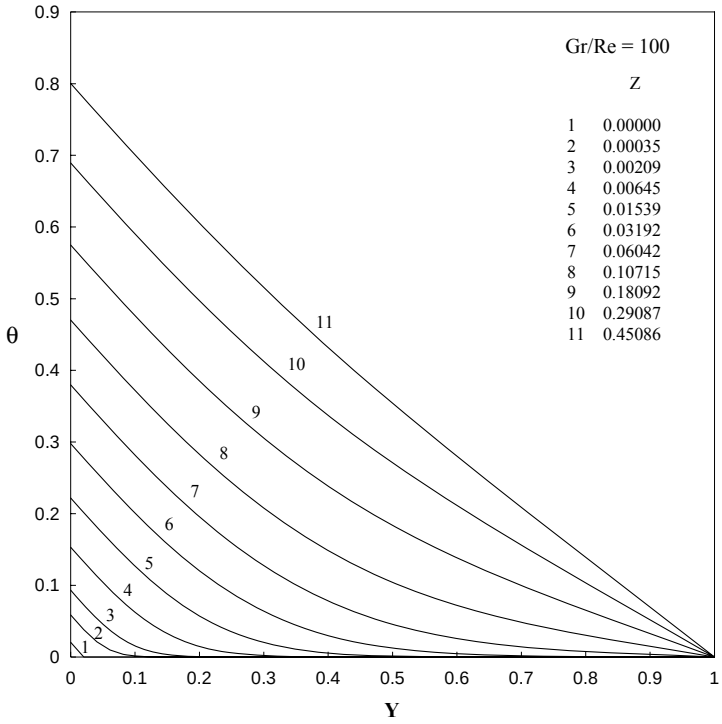

Figure 7.10(c) Developing temperature profiles for thermal boundary condition of fourth kind for Gr/Re = 100 at different axial locations (Z) between vertical parallel plates

Figures 7.11(a & b) depict the variation of pressure gradient and pressure along the axial direction for different buoyancy parameters Gr/Re under the thermal boundary condition of fourth kind. The behavior shown in these two figures is similar to the results obtained in first and third kind boundary conditions. Existences of locations at which the buoyancy forces balance out the viscous forces are shown in Table 7.6. Figures 7.12(a & b) show how the locations get closer to the entrance with increase in buoyancy parameter Gr/Re. These figures explains that higher heating rates causes the buoyancy forces to be felt very close to the channel entrance dominating the forced convection.

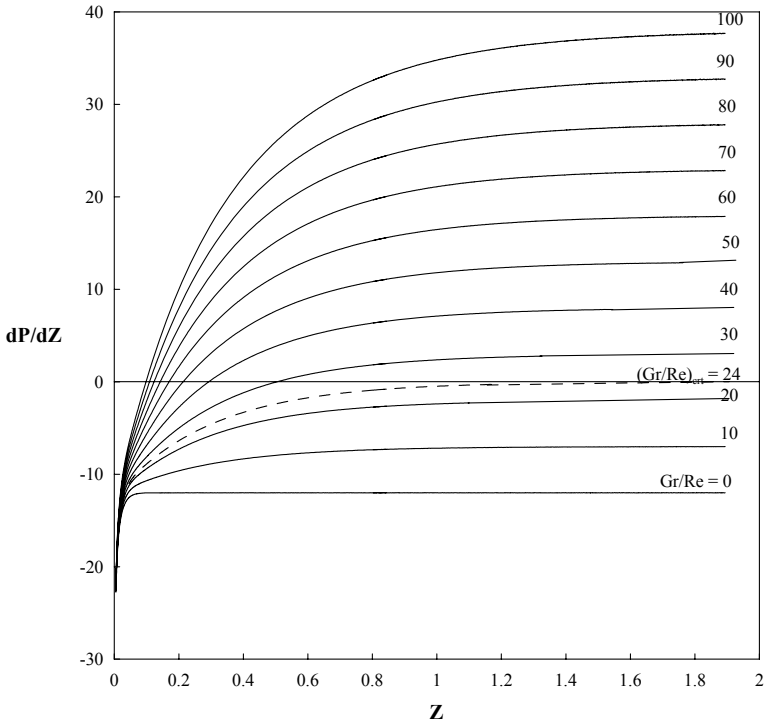

Figure 7.11(a) Variation of pressure gradient along the channel height for different Gr/Re for the thermal boundary condition of fourth kind between vertical parallel plates

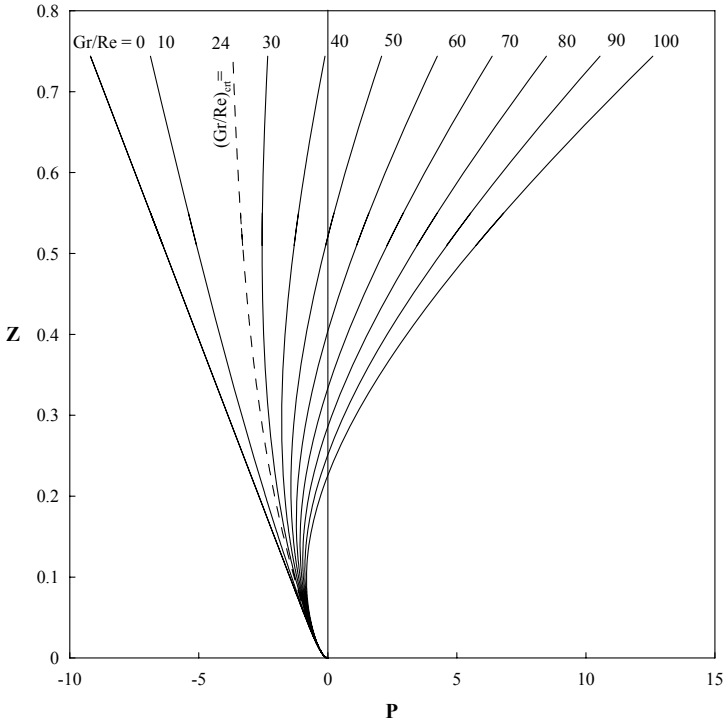

Figure 7.11(b) Pressure variation along the channel height for different Gr/Re for the thermal boundary condition of fourth kind between vertical parallel plates

Table 7.6 Locations of zero pressure gradient (Z_I) and onset of pressure build up (Z_{II}) between parallel plates under the thermal BC of fourth kind

Gr/Re	**Z_I**	**Z_{II}**
30	0.47503	1.58794
40	0.26848	0.71511
50	0.19085	0.48152
60	0.14900	0.36768
70	0.12265	0.29936
80	0.10454	0.25357
90	0.09128	0.22068
100	0.08110	0.19587
130	0.06093	0.14812
150	0.05231	0.12831
170	0.04581	0.11366
200	0.03858	0.09760
230	0.03330	0.08594
250	0.03052	0.07976

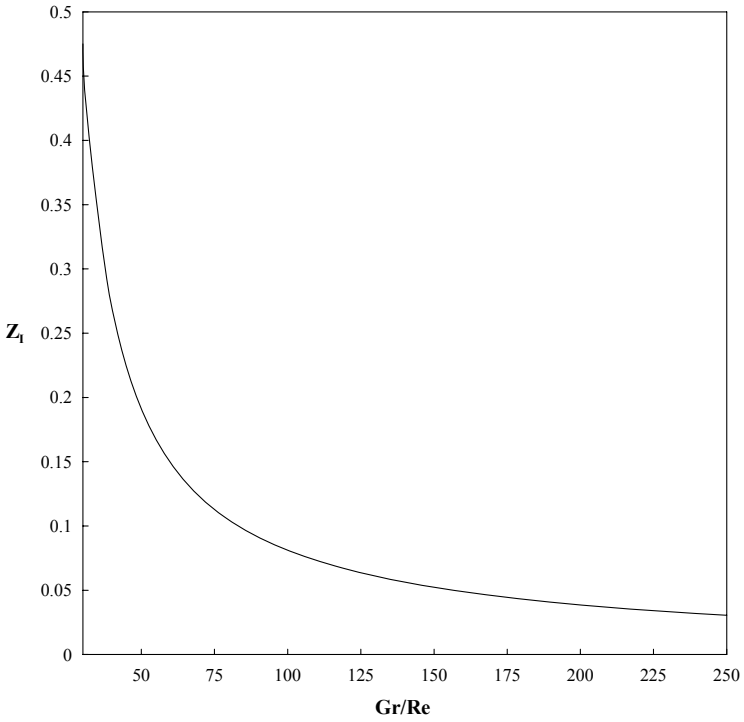

Figure 7.12(a) Graphical representation of location of zero pressure gradient (Z_I) as a function of Gr/Re in vertical parallel plates under the thermal BC of fourth kind

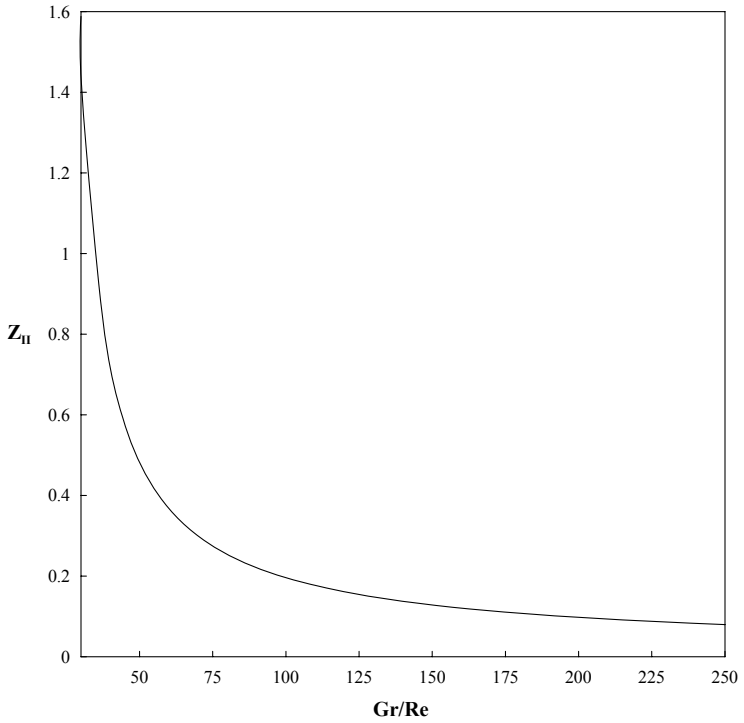

Figure 7.12(b) Graphical representation of location of onset of pressure builds up (Z_{II}) as a function of Gr/Re in vertical parallel plates under the thermal BC of fourth kind

The other two important thermal and heat transfer parameters namely mean temperature and Nusselt number are depicted in Figures 7.13(a) and 7.13(b & c). It is shown in Figure 7.13(a) that for a given buoyancy parameter Gr/Re, the mean temperature increases from very small value at the channel entrance to the fully developed conditions which is similar to the trend observed in the thermal boundary condition of first kind for $\theta_T = 0$. It is also clear from the figure that far downstream of the channel mean temperature attains its constant fully developed value which is different for different values of buoyancy parameter Gr/Re.

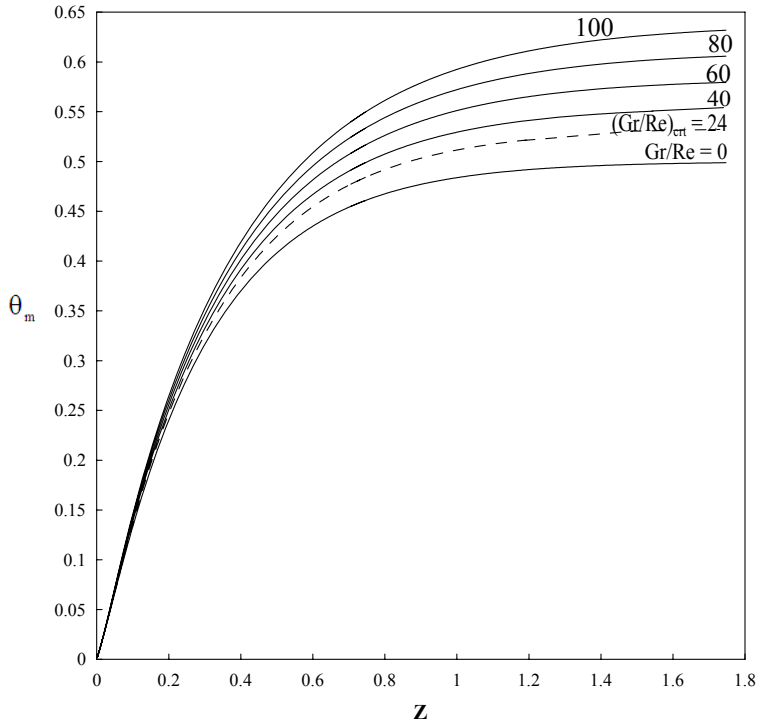

Figure 7.13(a) Mean or bulk temperature varitation along the channel height for different Gr/Re for the thermal boundary condition of fourth kind between vertical parallel plates

Figures 7.13(b & c) show how the Nusselt number is affected by higher heating rates Gr/Re on both constant heated and unheated walls. It is observed that from Fig. 7.13(b), the Nusselt number at fully developed conditions increases with increase in buoyancy parameter Gr/Re. This is due to significant effect of buoyancy forces that causes the fluid accelerates near the heated wall which in turn increases the heat transfer rate. On the other hand, the Nusselt number on the cold wall at fully developed conditions decreases with the increase in buoyancy parameter Gr/Re due to the presence of a decelerating flow near the cold wall as illustrated in Fig. 7.13(c). It is worth mentioning that the deceleration of the flow near the cold wall increases with the buoyancy parameter Gr/Re to offset the acceleration near the hot wall that increase with the increase in the buoyancy effects and satisfy the mass conservation principle.

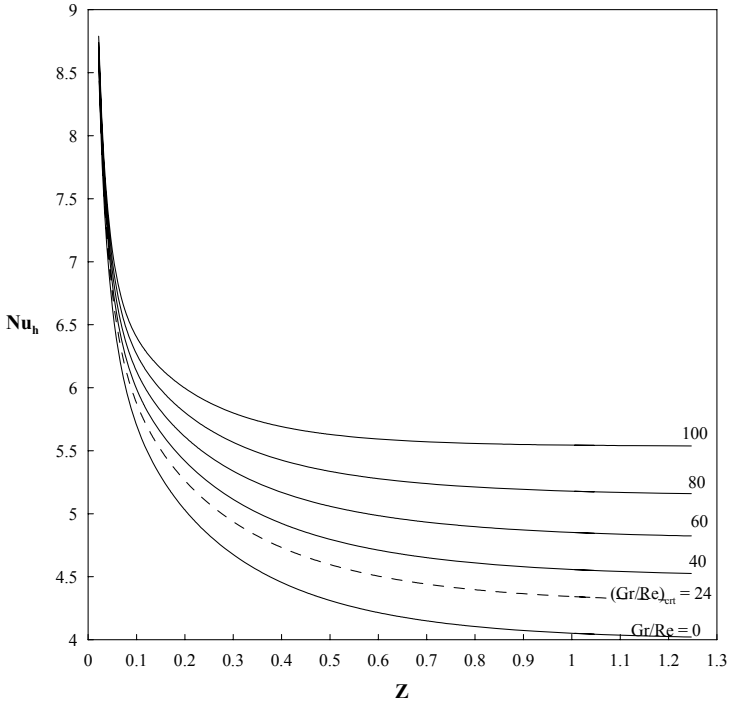

Figure 7.13(b) Variation of Nusselt number on the heated side of the parallel plates along the channel height for different Gr/Re for the thermal boundary condition of fourth kind

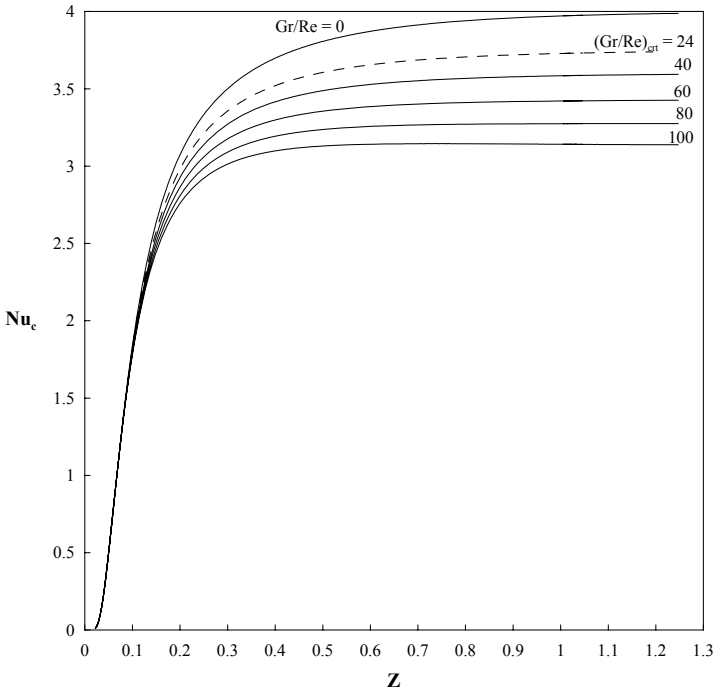

Figure 7.13(c) Variation of Nusselt number on the cold side of the vertical parallel plates verses axial distance (Z) for different Gr/Re for the thermal boundary condition of fourth kind

7.5 Effect of Prandtl number on hydrodynamic parameters

Effect of Prandtl number on the hydrodynamic parameters for laminar mixed convection in vertical channel between parallel plates has been studied by closely investigating the behavior of pressure gradient and pressure. The results were plotted for slightly below and above critical value of buoyancy parameter $(Gr/Re)_{crt}$ for fluid of Pr = 1, 10 and 100 under the thermal boundary condition first kind ($\theta_T = 0$).

Figures 7.14 (a-f) show the variation of pressure gradient and pressure as a function of axial distance for different values of buoyancy parameter Gr/Re for the investigated Prandtl numbers. All the figures exhibit the similar behavior as was seen in the case for Pr = 0.7. In other words, the Prandtl number has no effect on the critical value of $(Gr/Re)_{crt}$ under fully developed conditions (i.e. the critical value remains almost same

for all Prandtl numbers), as proved mathematically. However, locations of onset of pressure build up and incipient of positive pressure gradient above the critical value of buoyancy parameter $(Gr/Re)_{crt}$ are calculated and presented in the Table shown below for the Prandtl numbers investigated.

Pr	**$Gr/Re = 30 > (Gr/Re)_{crt}$ $\theta_T = 0$**	
	Z_I	**Z_{II}**
1	0.2087	0.7155
10	2.0584	6.2967
100	20.2054	62.0514

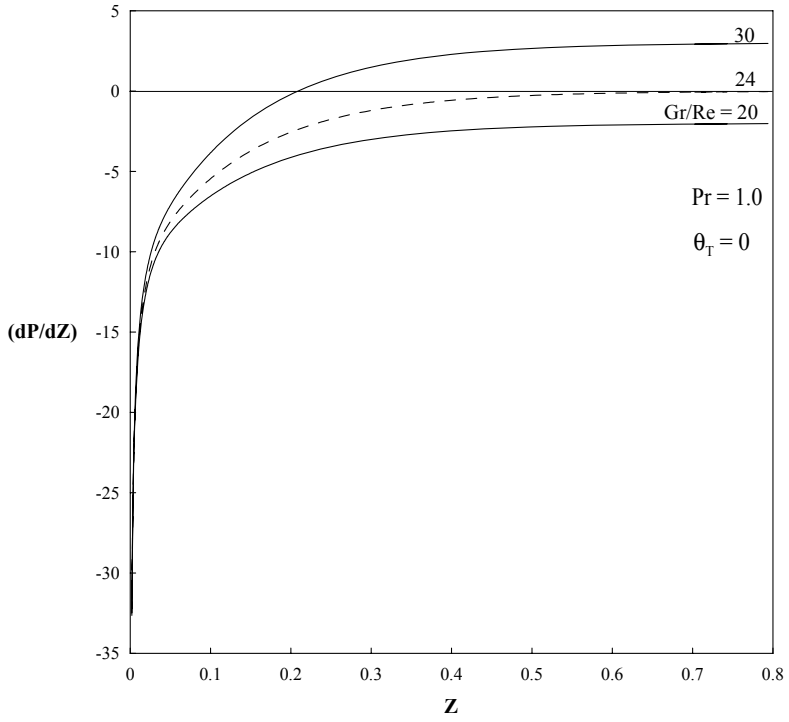

Figure 7.14 (a) Variation of pressure gradient for various Gr/Re for $\theta_T = 0$ and for Pr =1.0 between vertical parallel plates

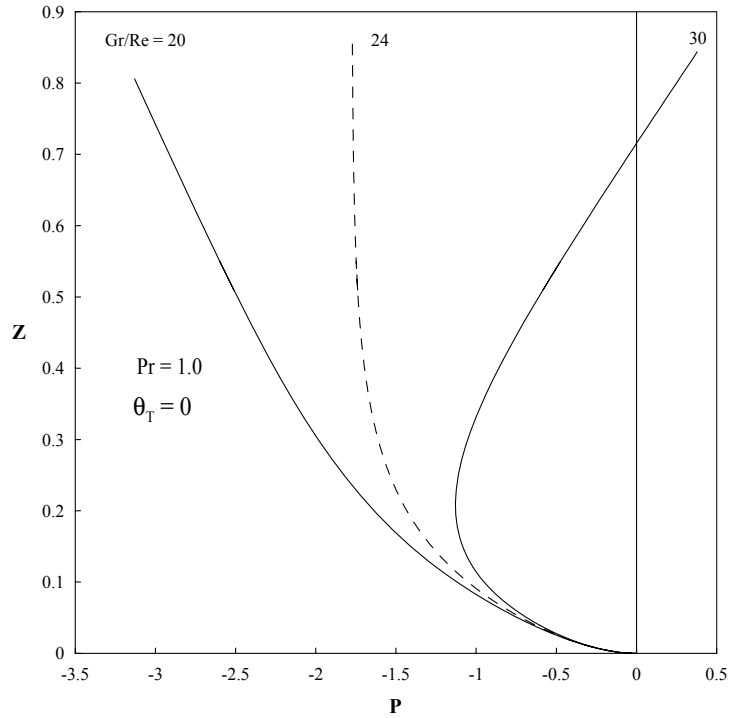

Figure 7.14 (b) Pressure variation for various Gr/Re for $\theta_T = 0$ and for Pr = 1.0 between vertical parallel plates

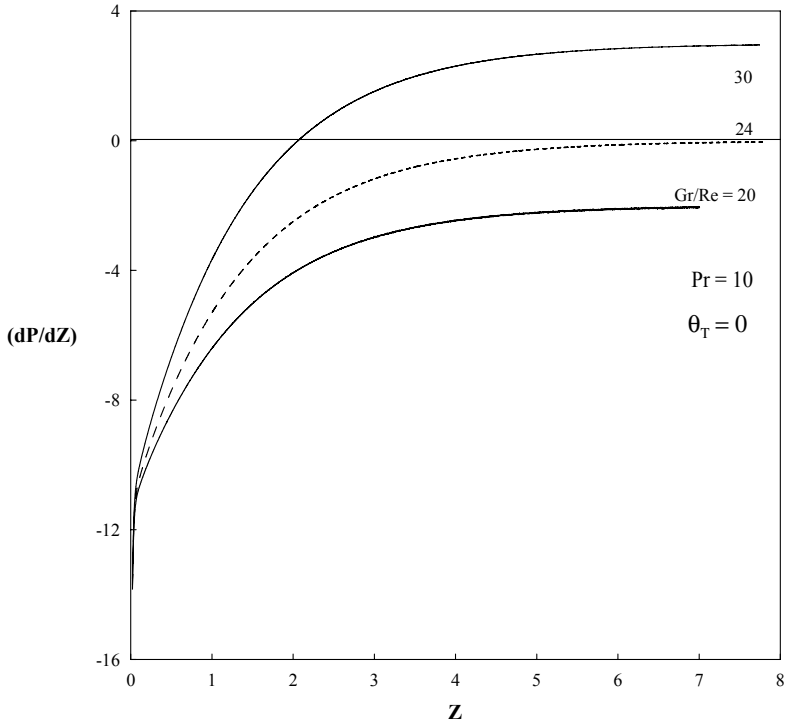

Figure 7.14 (c) Variation of pressure gradient for various Gr/Re for $\theta_T = 0$ and for Pr = 10 between vertical parallel plates

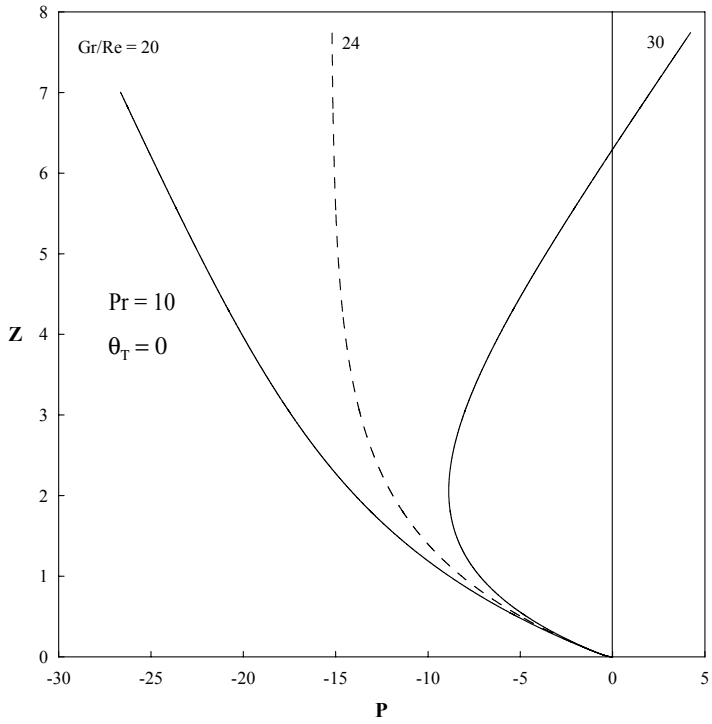

Figure 7.14 (d) Pressure variation for various Gr/Re for $\theta_T = 0$ and for Pr = 10 between vertical parallel plates

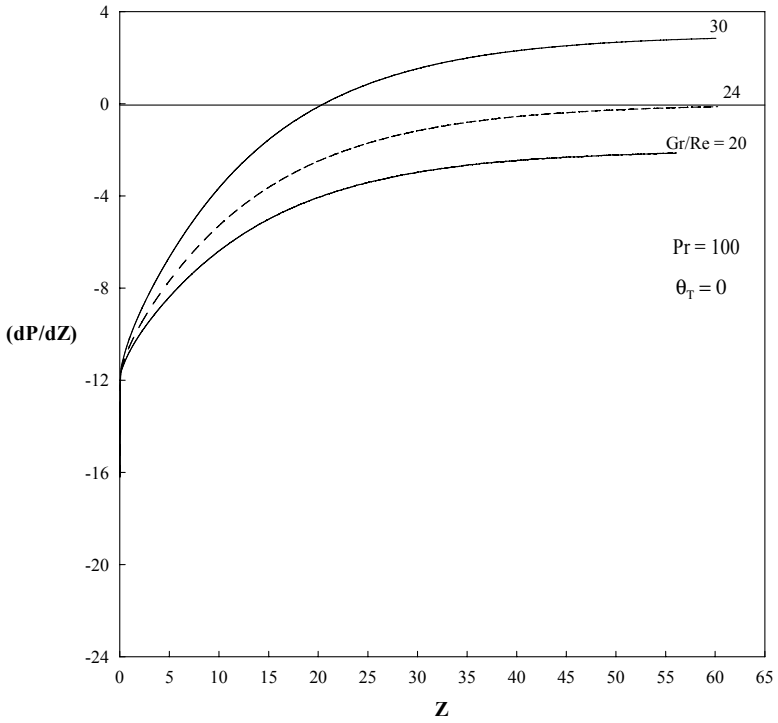

Figure 7.14 (e) Variation of pressure gradient for various Gr/Re for $\theta_T = 0$ and for Pr = 100 between vertical parallel plates

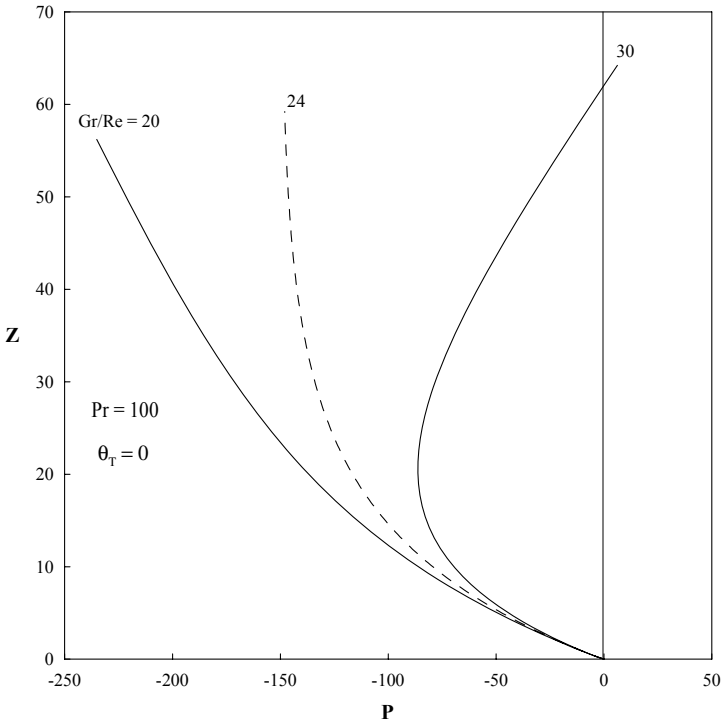

Figure 7.14 (f) Pressure variation for various Gr/Re for $\theta_T = 0$ and for Pr = 100 between vertical parallel plates

Chapter 8

RESULTS AND DISCUSSION FOR LAMINAR MIXED CONVECTION INSIDE VERTICAL CIRCULAR TUBE AND CONCENTRIC ANNULUS

8.1 Introduction

This chapter is devoted to present and to discuss the results that are obtained from the validated codes for developing laminar mixed convection inside vertical circular and concentric cylinders. Emphasis is devoted to discuss the hydrodynamics of the problem under consideration. In addition, thermal and heat transfer characteristics of the problem are also investigated in order to understand the physics of the problem.

The results obtained in this chapter are pertinent to buoyancy aided flow, a situation where buoyancy forces act in the direction of the flow. However sample of results are presented for buoyancy opposed flow to show that the pressure build up will never take place for these flow situation. Quantitative information is given about the effects of buoyancy on the hydrodynamic parameters namely, the development of pressure and pressure gradient. These two important parameters clearly show the effect of buoyancy forces on the hydrodynamic behavior of the fluid flow. The significance of these parameters can be shown by plotting the development of the pressure gradient and local pressure along the channel height, such figure shows how and at what locations the buoyancy forces overcome the viscous forces. The determination of location of channel

height at which the buoyancy forces balance the viscous forces is one of the main objectives of this chapter. The results are obtained and presented for fluid of Pr = 0.7.

The chapter is also devoted to present some quantitative information on the location of onset of flow reversal, where the velocity gradient becomes ≤ 0 and the location of flow instability (a situation where large values of Gr/Re results into turbulence). Another important parameter is the location of hydrodynamic fully development length defined as the length far from the downstream of the channel where hydrodynamic and thermal flow fields become invariant.

The results presented in this chapter are those obtained through the numerical investigation for the developing laminar mixed convection in the entry region of a vertical channel inside vertical circular tube and vertical concentric annulus under the given thermal boundary conditions. Since there exists only two thermal boundary conditions (isothermal and isoflux) for the circular tube, the present investigation is limited to isothermal boundary condition (UWT) and for concentric annulus, of the four available fundamental thermal boundary conditions, results are obtained for the thermal boundary conditions of first kind, (one wall of the annulus is kept at uniform temperature and the other is at fluid inlet temperature). However, fully analytical solutions for the 1^{st}, 3^{rd} and 4^{th} kind thermal boundary conditions are obtained in Chapter 4. It is to remind the reader that first kind thermal boundary condition can be classified into two cases, Case 1.I where inner wall is considered as the heat transfer boundary surface and Case 1.O where outer is considered as the heat transfer boundary surface.

The results are obtained for a wide range of Gr/Re from -400 to 800 and the controlling parameters namely radius ratio N, θ_T and Gr/Re are explicitly used to solve the problem for a given Pr number. The values of controlling parameters θ_T = 0 and radius ratio N = 0.1, 0.3, 0.5, 0.7 and 0.9 are taken for present investigation. But the results are presented for only one of the investigated cases (N = 0.5). In the case of circular tube, the investigation covers a range of buoyancy parameter (Gr/Re) from -100 to 140. Moreover, other important heat transfer parameters namely mean bulk temperature and Nusselt number for these vertical circular channels are presented and discussed.

8.2 Results and Discussion for Vertical Circular Tube

Due to symmetry only half of the cross sectional plane is solved and the results are presented for buoyancy aided flow situation under uniform wall temperature boundary condition.

Figure 8.1 shows the development of axial velocity for buoyancy ratio Gr/Re = 120 at different locations of axial distance. It is very interesting to observe that the profiles are similar to those obtained for mixed convection between parallel plates under the first kind thermal boundary condition when θ_T = 1.0 (symmetric wall heating). There is no flow reversal in the vicinity of the heated wall (R=1). The velocity profile starts to be distorted in the downstream. This distortion becomes severe further downstream of the channel shown in profiles # 2-8. Then it recovers and attains its fully developed asymptotic parabolic profile represented by profile # 13.

Regarding other hydrodynamic parameters, Figures 8.2(a & b) show the development of pressure gradient (dP/dZ) and dimensionless pressure along the channel height Z for positive and negative values of buoyancy parameter Gr/Re. For buoyancy opposed flows, the pressure from zero at the channel entrance increases with negative magnitude as shown in Figure 8.2 (b). This negativity of pressure will continue increasing due to the corresponding increasing negative pressure gradient which attains constant value at fully developed conditions shown in Figure 8.2 (a). Moreover, the negativity of pressure and pressure gradient with decreasing magnitude prevails for some positive values of buoyancy parameter $Gr/Re < (Gr/Re)_{crt}$. For positive values of buoyancy parameter $Gr/Re > (Gr/Re)_{crt}$, the pressure build up will take place and the negativity of pressure gradient vanishes. This is clear that from the Figures 8.2 (a & b), the onset of pressure build up due to buoyancy effects exist only for buoyancy aided flows. The dotted lines shown in these two figures represent the development of pressure gradient and pressure for the critical value of $(Gr/Re)_{crt}$ which was obtained in Chapter 4 of the respective section.

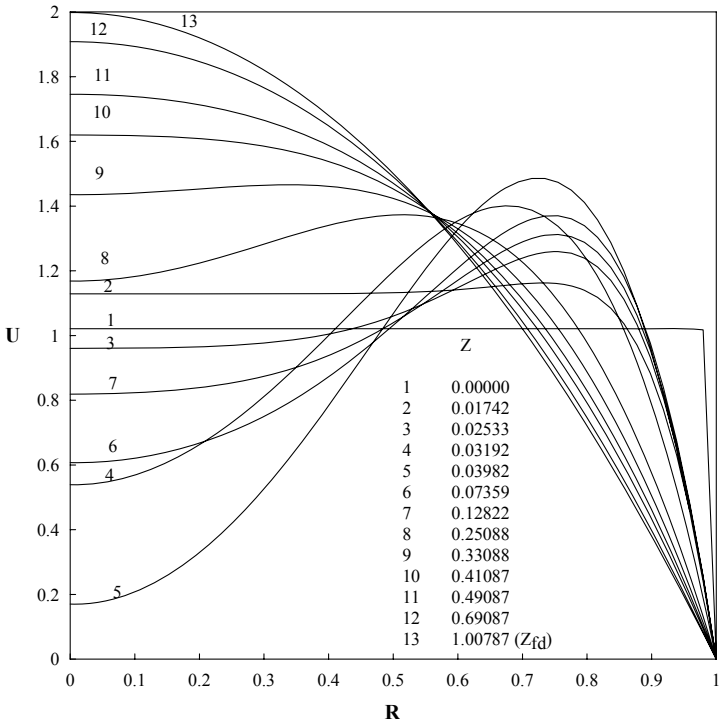

Figure 8.1 Development of axial velocity profile (U) for Gr/Re = 120 at different locations of axial distance (Z) in vertical circular tube

From the fact, that buoyancy effects reduce the negativity of the pressure gradient and increase the pressure build up due to higher heating rates Gr/Re in buoyancy aided flows as can be seen clearly in the Figures 8.2(a & b). With further increase in heating rates Gr/Re >> $(Gr/Re)_{crt}$, the buoyancy effects become more significant near the channel entrance, causes flow instability resulting into numerical instability. Since the present numerical code cannot solve the flow instability problem, so it cannot be trusted for the values of buoyancy parameter greater than 140 and are limited to ranging from -100 to 140. However, locations of fully developed length for the investigated positive values of buoyancy parameter Gr/Re are presented in Table 8.1.

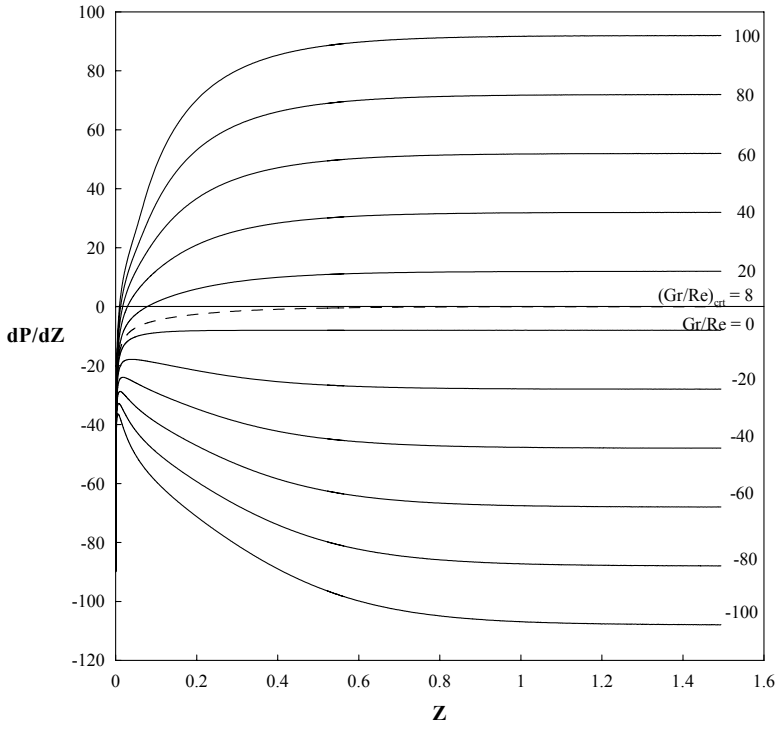

Figure 8.2(a) Variation of pressure gradient along the axial distance for different Gr/Re, for UWT boundary condition in vertical circular tube

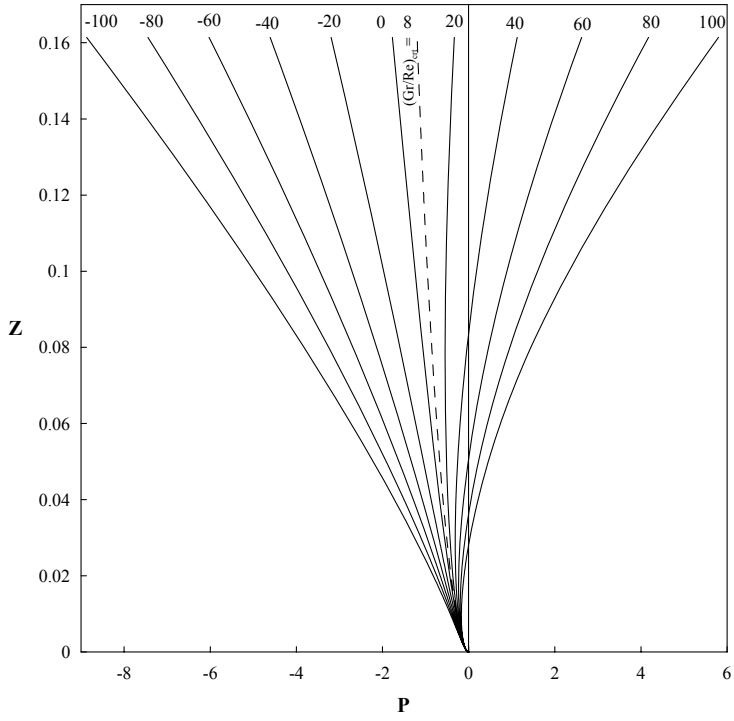

Figure 8.2(b) Pressure variation versus axial distance for different Gr/Re, for UWT boundary condition in vertical circular tube

Table 8.1 Locations of numerical instability (Z_{in}), onset of flow reversal (Z_{fr}) and the hydrodynamic fully development length (Z_{fd}) in circular tube under UWT boundary condition

Gr/Re	**Z_{in}**	**Z_{fr}**	**Z_{fd}**
0		NFR	0.22689
8		NFR	0.63688
12		NFR	0.70887
20		NFR	0.79587
30		NFR	0.85687
40		NFR	0.90087
50		NFR	0.92887
60		NFR	0.95087
70		NFR	0.96787
80		NFR	0.98587
90		NFR	0.98687
100		NFR	0.99387
110		NFR	1.00687
120		NFR	1.00787
130		NFR	1.01887
140		NFR	1.02187

It is worth mentioning that the hydrodynamic development length increases with the buoyancy parameter. This implies that the flow needs more length to overcome the distortion of the velocity profiles introduced by the buoyancy effects. On the other hand, the distance from the entrance at which the pressure gradient cross the zero value become shorter, i.e. this location becomes closer to the entrance with the increase of the buoyancy parameter Gr/Re, which implies again the buoyancy effects.

Moreover the locations at which the pressure gradient (dP/dZ) and pressure starts to become positive or at which the buoyancy forces balance out the viscous forces are presented in Table 8.2. This table will provide qualitative information for the designer to properly size the pumping device. These locations (distance from the channel entrance) represents as a function of buoyancy parameter Gr/Re as shown in Figures 8.3(a & b). These two figures clearly indicate that the locations of Z_I and Z_{II} decreases as the heating rates Gr/Re increases.

Table 8.2 Locations of zero pressure gradient (Z_I) and onset of pressure build up (Z_{II}) in circular tube under UWT boundary condition

Gr/Re	**Z_I**	**Z_{II}**
12	0.18414	0.58376
20	0.07389	0.21826
30	0.03985	0.12016
40	0.02657	0.08194
50	0.01967	0.06192
60	0.01549	0.04966
70	0.01271	0.04139
80	0.01072	0.03545
90	0.00925	0.03097
100	0.00812	0.02748
110	0.00722	0.02468
120	0.00648	0.02239
130	0.00588	0.02048
140	0.00537	0.01887

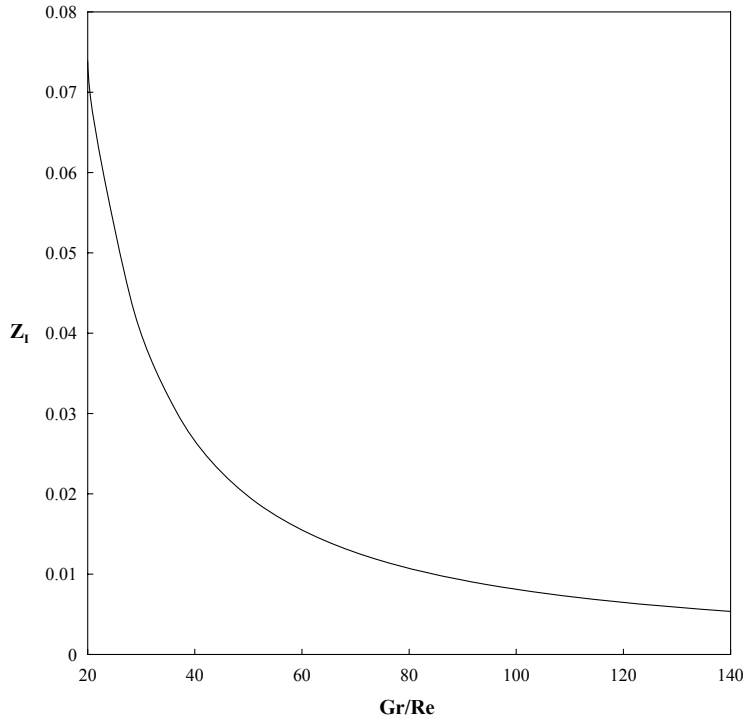

Figure 8.3(a) Graphical representation of location of zero pressure gradient (Z_I) as a function of Gr/Re in vertical circular tube under UWT boundary condition

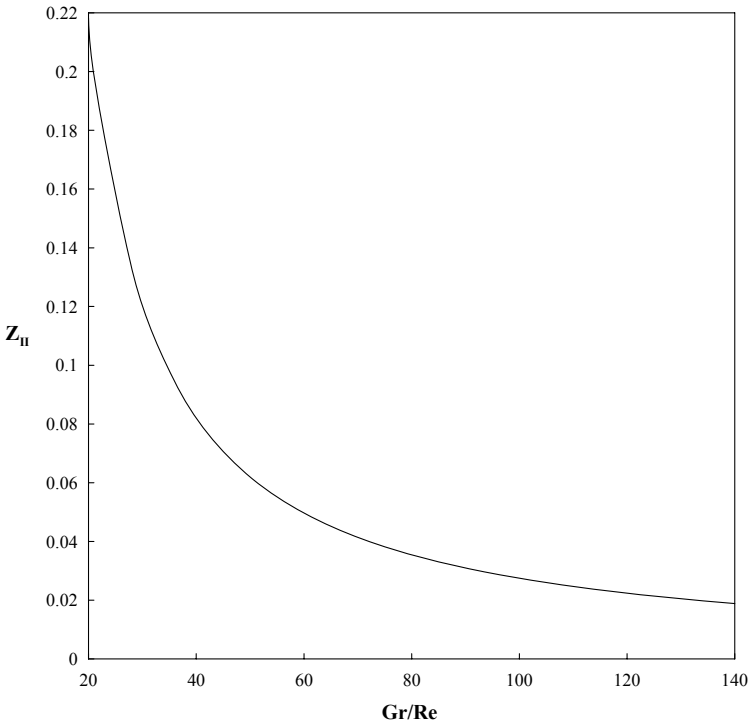

Figure 8.3(b) Graphical representation of location of zero pressure (Z_{II}) as a function of Gr/Re in vertical circular tube under UWT boundary condition

The effects of buoyancy parameter Gr/Re on the thermal fields can be analyzed from Figures 8.4 and 8.5, which show the variation of mean temperature and Nusselt number for different buoyancy parameters Gr/Re along the axial distance. It has been observed in Figure 8.4 that for Gr/Re = 0 (forced convection) and Gr/Re = 8 (critical value), the mean temperature behavior is nearly the same. This means that buoyancy effects are not yet felt. The Nusselt number increases with higher values than that for pure forced convection up to certain axial distance as the heating rates Gr/Re increases and then becomes flat almost constant value equal to the forced convection value. The fully developed Nusselt number as illustrated in Figure 8.5 remains same for all values of heating rates indicating that Nusselt number is independent of buoyancy parameter Gr/Re far downstream of the channel where the thermal and velocity profile becomes invariant.

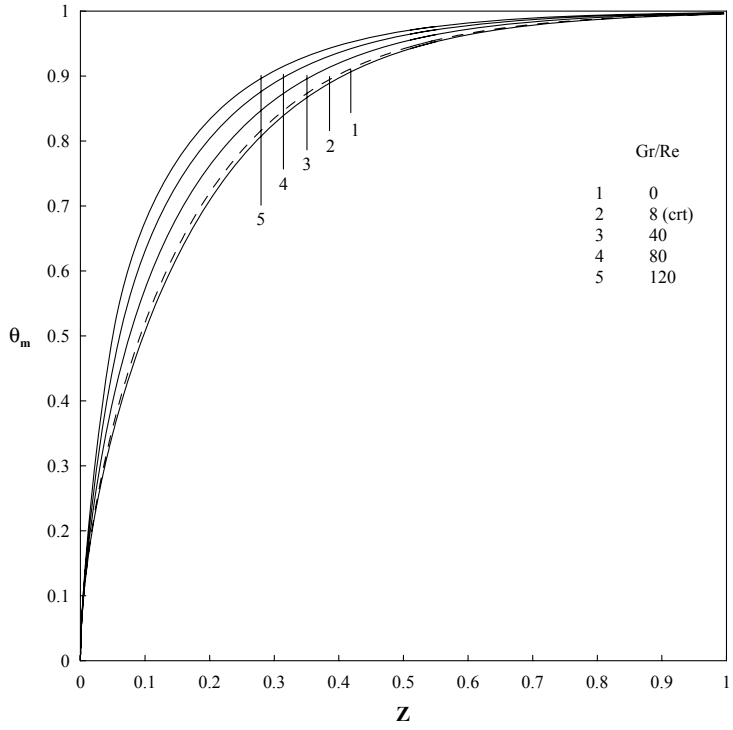

Figure 8.4 Mean or bulk temperature as a function of channel height for different Gr/Re, for UWT boundary condition of circular tube

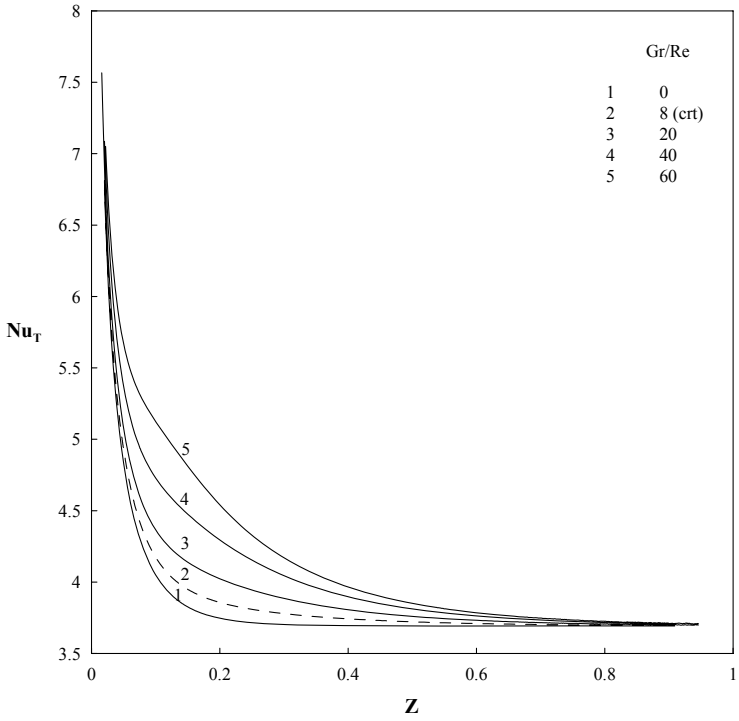

Figure 8.5 Variation of Nusselt number on the heated surface of the tube against axial distance for different Gr/Re, for UWT boundary condition of circular tube

8.3 Results and Discussion for Vertical Concentric Annulus

Results for Case 1.I

The results presented in this section are for the Case 1.I where inner wall is considered as the heat transfer boundary surface.

Figures 8.6(a & b) shows the variation of pressure gradient (dP/dZ) and pressure along the axial distance for positive and negative values of buoyancy parameter Gr/Re for radius ratio N = 0.5. These two figures represent the significance of buoyancy effects on the hydrodynamic behavior in mixed convection inside vertical concentric annulus. It is clearly seen from Fig. 8.6 (b) that for negative values of buoyancy parameter (Gr/Re), the pressure from zero value at the channel entrance increases with negative magnitude and remains negative till the fully developed conditions. Due to this negative increment in

pressure, the corresponding negative pressure gradient shown in Fig. 8.6 (a) will continue increasing and attains a constant value at the fully developed conditions. However, for positive values of buoyancy parameter $Gr/Re > (Gr/Re)_{crt}$ shown in Figures 8.6 (a & b), the pressure build up will take place resulting in positive pressure gradient. This is due to the fact that buoyancy effects become significant and begin to felt above the critical value of buoyancy parameter $(Gr/Re)_{crt}$ obtained in Chapter 4 under first kind thermal boundary. It is clear from the discussion that for buoyancy aided flows, the pressure build up will take place and the Figs. 8.6(a & b) are shown to prove that the pressure build up will never take place for buoyancy opposed flows. Moreover, the buoyancy effects due to higher heating rates $Gr/Re >>> (Gr/Re)_{crt}$ increases the intensity of pressure gradient (dP/dZ) which opposes the fluid particles to move downstream and result in flow reversal near the cold wall of the annulus. The flow reversal become more severe and causes the flow instability and consequently into numerical instability. However for some values of heating rates, the fluid velocity recovers and attains its fully developed profile. The locations at which flow reversal, numerical instability and hydrodynamic fully development length are presented in Table 8.3 for the investigated radius ratio N.

As discussed above, that due to higher heating rates $Gr/Re > (Gr/Re)_{crt}$ the onset of pressure build up take place and there are certain locations at which the transition from negative pressure to positive pressure and from negative pressure gradient (dP/dZ) to positive pressure gradient (dP/dZ) take place. The locations at which this phenomenon takes place are given in Table 8.4 for different radius ratio N. These locations decreases as the heating rates increases which means that buoyancy effects begin to felt very close to the channel entrance as illustrated in Figs. 8.7(a & b).

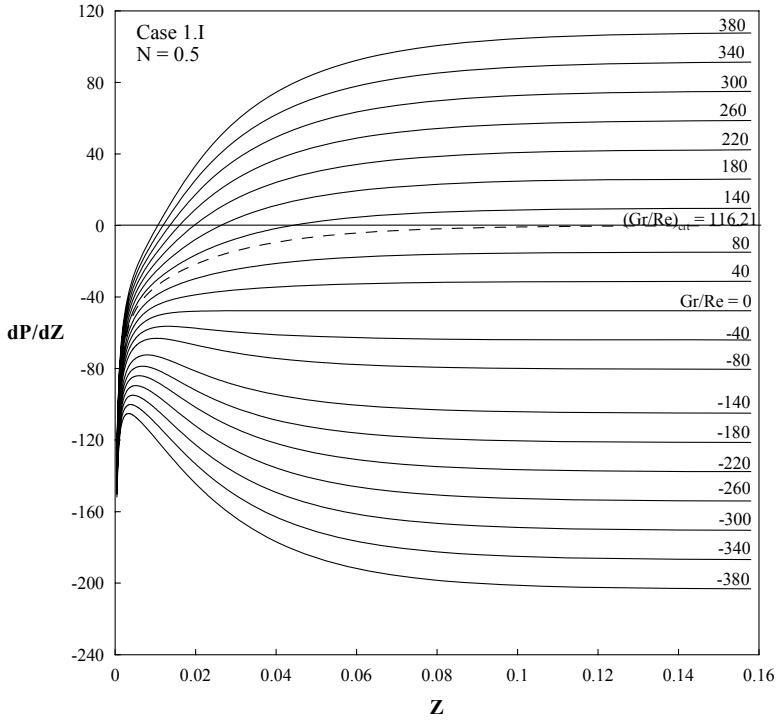

Figure 8.6(a) Variation of pressure gradient along the channel height for positive and negative values of Gr/Re for radius ratio N = 0.5 of vertical concentric annulus, Case 1.I

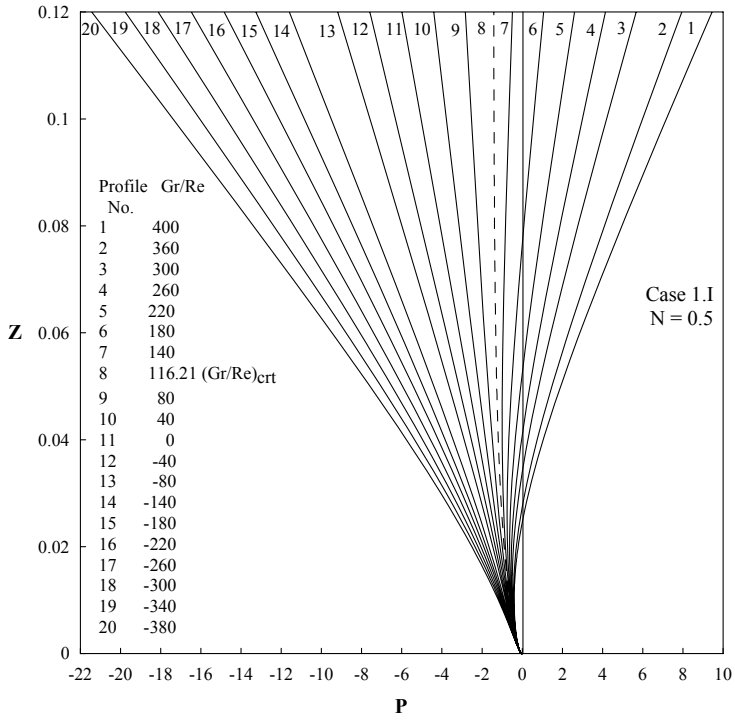

Figure 8.6(b) Pressure variation along the channel height for positive and negative values of Gr/Re for radius ratio N = 0.5 of vertical concentric annulus, Case 1.I

Table 8.3 Locations of numerical instability (Z_{in}), onset of flow reversal (Z_{fr}) and the hydrodynamic fully development length (Z_{fd}) for vertical concentric annuli, Case 1.I

Gr/Re	N = 0.1			N = 0.3			N = 0.5			N = 0.7			N = 0.9		
	Z_{in}	Z_{fr}	Z_{fd}	Z_{in}	Z_{fr}	Z_{fd}	Z_{in}	Z_{fr}	Z_{fd}	Z_{in}	Z_{fr}	Z_{fd}	Z_{in}	Z_{fr}	Z_{fd}
0		NFR	0.0933		NFR	0.0438		NFR	0.0195		NFR	0.0063		NFR	0.0007
20		NFR	0.1412		NFR	0.0787		NFR	0.0387		NFR	0.0134		NFR	0.0015
40		NFR	0.1933		NFR	0.1116		NFR	0.0557		NFR	0.0196		NFR	0.0021
60		NFR	0.2334		NFR	0.1352		NFR	0.0674		NFR	0.0240		NFR	0.0026
80		NFR	0.2658		NFR	0.1546		NFR	0.0772		NFR	0.0273		NFR	0.0030
100		NFR	0.2938		NFR	0.1705		NFR	0.0854		NFR	0.3030		NFR	0.0033
120		NFR	0.3198		NFR	0.1854		NFR	0.0928		NFR	0.0332		NFR	0.0036
140		NFR	0.3418		NFR	0.1990		NFR	0.1000		NFR	0.0356		NFR	0.0039
160		NFR	0.3638		NFR	0.2125		NFR	0.1072		NFR	0.0381		NFR	0.0042
180		NFR	0.3848		NFR	0.2251		NFR	0.1141		NFR	0.0406		NFR	0.0045
200		NFR	0.4048		NFR	0.2382		NFR	0.1215		NFR	0.0436		NFR	0.0048
220		NFR	0.4248		NFR	0.2519		NFR	0.1287		NFR	0.0467		NFR	0.0051
240		NFR	0.4448		NFR	0.2668		NFR	0.1369		NFR	0.0500		NFR	0.0055
260		NFR	0.4648		NFR	0.2818		NFR	0.1474		NFR	0.0543		NFR	0.0060
280		NFR	0.4858		NFR	0.2989		NFR	0.1600		NFR	0.0595		NFR	0.0067
300		NFR	0.5058		NFR	0.3178		NFR	0.1771		NFR	0.0735		NFR	0.0082
320		NFR	0.5298		NFR	0.3418		NFR	0.2048		0.0432	0.0825		0.0027	
340		NFR	0.5518		NFR	0.3768		NFR	0.5298		0.0219	0.1121		0.0019	
360		NFR	0.5768		NFR	0.4258		0.0697			0.0166	0.1443		0.0015	

380		NFR	0.6058		NFR	0.6128		0.0529			0.0138	0.2259		0.0013	
400		NFR	0.6338		0.1698	0.7808		0.0438			0.0119			0.0011	
500		NFR	0.9408		0.0739			0.0260			0.0077			0.0007	
600		0.1982	0.9748		0.0529			0.0198			0.0060			0.0006	
700		0.1399			0.0429		0.0322	0.0165		0.0089	0.0050		0.0011	0.0005	
800		0.1131		0.0973	0.0369		0.0240	0.0144		0.0072	0.0044		0.0008	0.0004	

Table 8.4 Locations of zero pressure gradient (Z_I) and onset of pressure build up (Z_{II}) for different radius ratio N of vertical concentric annuli, Case 1.I

Gr/Re	N = 0.1		N = 0.3		N = 0.5		N = 0.7		N = 0.9	
	Z_I	Z_{II}	Z_I	Z_{II}	Z_I	Z_{II}	Z_I	Z_{II}	Z_I	Z_{II}
120					0.08611	*	0.01852	*	0.00164	*
140			0.16138	*	0.04396	*	0.01223	*	0.00116	0.00358
160			0.09350	*	0.03237	0.10329	0.00946	0.02798	0.00092	0.00260
180			0.07099	*	0.02624	0.07659	0.00783	0.02182	0.00077	0.00208
200	0.21259	*	0.05858	0.17538	0.02234	0.06189	0.00674	0.01809	0.00066	0.00174
220	0.16258	*	0.05050	0.14292	0.01961	0.05245	0.00595	0.01556	0.00059	0.00151
240	0.13538	0.44461	0.04477	0.12185	0.01757	0.04581	0.00534	0.01372	0.00053	0.00134
260	0.11762	0.35870	0.04043	0.10695	0.01597	0.04086	0.00486	0.01232	0.00048	0.00121
280	0.10493	0.30443	0.03702	0.09579	0.01468	0.03701	0.00447	0.01121	0.00044	0.00110
300	0.09533	0.26664	0.03425	0.08709	0.01360	0.03393	0.00413	0.01032	0.00040	0.00101
320	0.08776	0.23862	0.03195	0.08009	0.01269	0.03140	0.00384	0.00957	0.00037	0.00094
340	0.08162	0.21692	0.03000	0.07432	0.01191	0.02928	0.00360	0.00894	0.00035	0.00088
360	0.07652	0.19956	0.02831	0.06949	0.01122	0.02748	0.00338	0.00840	0.00033	0.00083
380	0.07219	0.18531	0.02683	0.06536	0.01061	0.02592	0.00318	0.00793	0.00031	0.00078
400	0.06847	0.17338	0.02553	0.06180	0.01006	0.02456	0.00300	0.00751	0.00029	0.00074
500	0.05546	0.13417	0.02068	0.04932	0.00798	0.01969	0.00233	0.00602	0.00022	0.00059
600	0.04749	0.11204	0.01744	0.04171	0.00656	0.01663	0.00188	0.00506	0.00018	0.00049
700	0.04194	0.09760	0.01506	0.03650	0.00552	0.01449	0.00156	0.00438	0.00015	0.00042
800	0.03779	0.08733	0.01322	0.03266	0.00474	0.01289	0.00133	0.00387	0.00012	0.00037

* For such cases, the pressure defect did not cross the value of zero before the fully developed conditions.

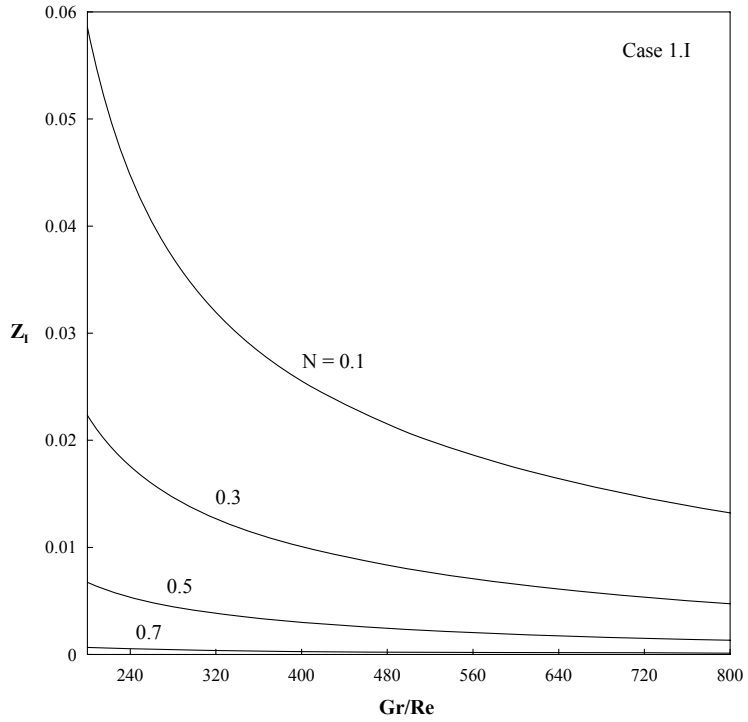

Figure 8.7(a) Graphical representation of location of zero pressure gradient (Z_I) as a function of Gr/Re for different radius ratio N of vertical concentric annuli, Case 1.I

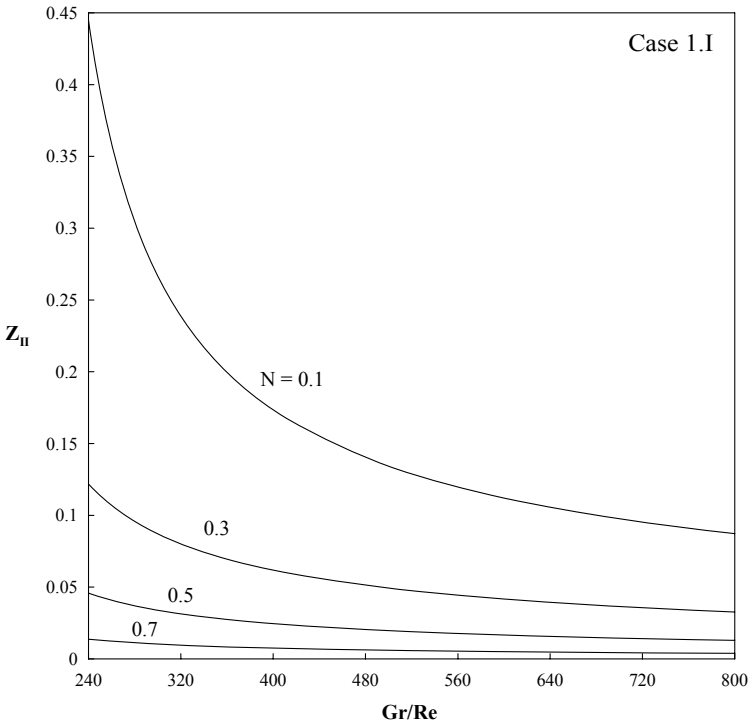

Figure 8.7(b) Graphical representation of location of zero pressure (Z_{II}) as a function of Gr/Re for different radius ratio N of vertical concentric annuli, Case 1.I

The heat transfer characteristics namely mean temperature and Nusselt number are shown in Figures 8.8(a & b). It is evident from Figure 8.8(a), that for a given buoyancy parameter Gr/Re, the mean temperature increases from very small value close to the channel entrance to the fully developed value. This fully developed value is different for different buoyancy parameters Gr/Re and is greater than the forced convection value (Gr/Re = 0). Figure 8.8(b) show the variation of Nusselt number on both heated and cold walls of the annulus as a function of channel length (Z). It is seen that the Nusselt number at the heated side of the annulus falls sharply from high value close to the channel inlet to its fully developed value far downstream of the channel entrance. It is also observed that the difference between the forced convection value and the mixed convection value (Gr/Re > 0) increases as the heating rate increases and vice versa at the cold side of the annulus.

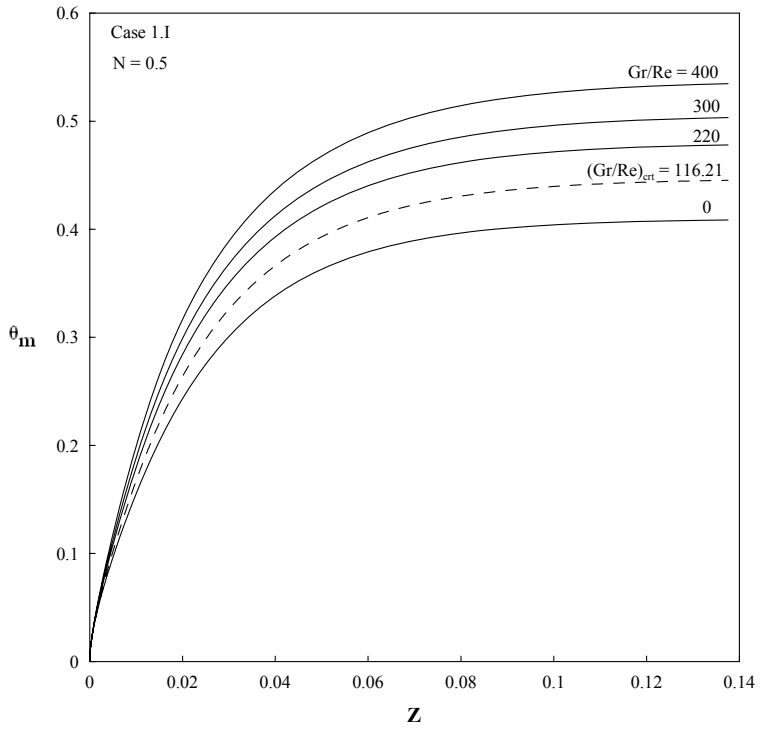

Figure 8.8(a) Mean or bulk temperature variation against channel height for different Gr/Re for radius ratio N = 0.5 of vertical concentric annulus, Case 1.I

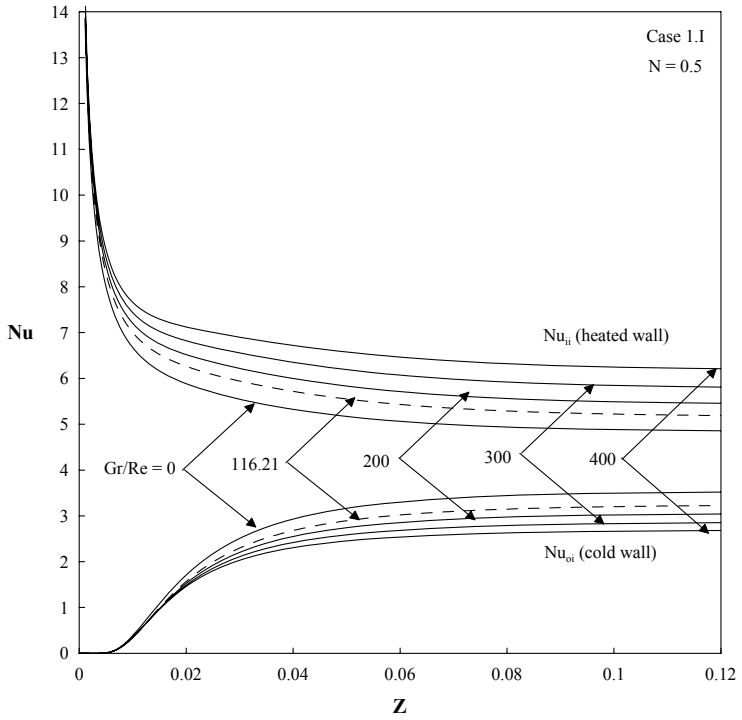

Figure 8.8(b) Variation of Nusselt number along the heated and cold walls of the channel as a function of position (Z) for different Gr/Re for radius ratio N = 0.5 of vertical concentric annulus, Case 1.I

Results for Case 1.O

For this Case 1.O of thermal boundary condition of first kind, the developments of pressure gradient (dP/dZ) and pressure exhibit similar behavior as discussed in Case 1.I for radius ratio N = 0.5. The dotted line shown in Figures 8.9(a & b) show the development of pressure gradient and pressure for the critical value of Gr/Re. For very high heating rates the pressure build up due to the buoyancy-aiding effects flow reversal takes place especially near the cold wall due to back pressure that decelerates the fluid particles in the vertical channel. In such situations, locations of onset of flow reversal at which the velocity gradient at the wall $\partial U / \partial R \leq 0$ are presented for this case in Table 8.5.

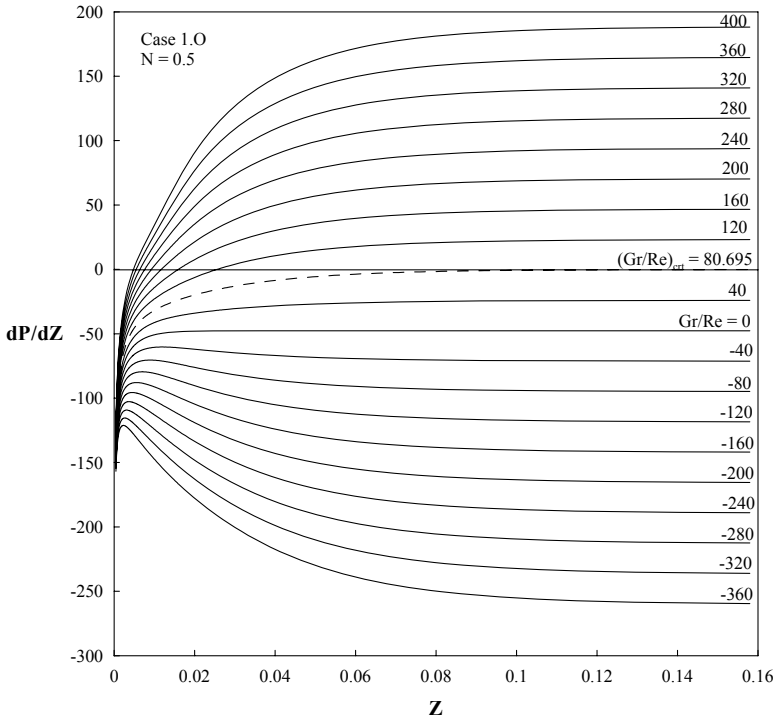

Figure 8.9(a) Variation of pressure gradient along the channel height for positive and negative values of Gr/Re for radius ratio N = 0.5 of vertical concentric annulus, Case 1.O

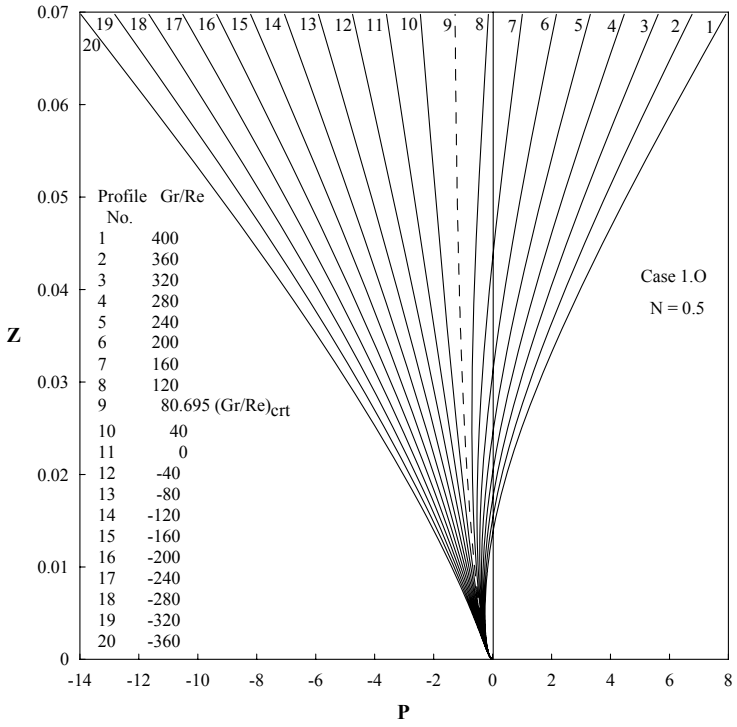

Figure 8.9(b) Pressure variation along the channel height for positive and negative values of Gr/Re for radius ratio N = 0.5 of vertical concentric annulus, Case 1.O

With further increase in heating rates Gr/Re, the flow reversal become severe and results into flow instability, which directly leads to numerical instability and the code fails, since it is not formulated to solve flow instability problem. The locations of numerical instability along with one of the important hydrodynamic parameter called hydrodynamic fully development length are also indicated in Table 8.5. Also the locations at which the pressure starts to build up and the pressure gradient (dP/dZ) starts to become positive are presented in Table 8.6 for the investigated radius ratio N. The variation of these locations (distance from the channel entrance) as a function of buoyancy parameter Gr/Re are shown in Figures 8.10(a & b) which gives similar explanation that the location decreases as heating rates increases for a given radius ratio N.

Table 8.5 Locations of numerical instability (Z_{in}), onset of flow reversal (Z_{fr}) and the hydrodynamic fully development length (Z_{fd}) for vertical concentric annuli, Case 1.O

Gr/Re	N = 0.1			N = 0.3			N = 0.5			N = 0.7			N = 0.9		
	Z_{in}	Z_{fr}	Z_{fd}	Z_{in}	Z_{fr}	Z_{fd}	Z_{in}	Z_{fr}	Z_{fd}	Z_{in}	Z_{fr}	Z_{fd}	Z_{in}	Z_{fr}	Z_{fd}
0		NFR	0.0933		NFR	0.0438		NFR	0.0195		NFR	0.0063		NFR	0.0007
20		NFR	0.1928		NFR	0.0908		NFR	0.0393		NFR	0.0122		NFR	0.0014
40		NFR	0.2528		NFR	0.1199		NFR	0.0540		NFR	0.0176		NFR	0.0021
60		NFR	0.2828		NFR	0.1357		NFR	0.0620		NFR	0.0218		NFR	0.0025
80		NFR	0.3018		NFR	0.1462		NFR	0.0671		NFR	0.0250		NFR	0.0029
100		NFR	0.3148		NFR	0.1533		NFR	0.0740		NFR	0.0280		NFR	0.0032
120		NFR	0.3238		NFR	0.1586		NFR	0.0818		NFR	0.0307		NFR	0.0035
140		NFR	0.3308		NFR	0.1627		NFR	0.0886		NFR	0.0332		NFR	0.0038
160		NFR	0.3358		NFR	0.1676		NFR	0.0955		NFR	0.0359		NFR	0.0041
180		NFR	0.3398		NFR	0.1839		NFR	0.1033		NFR	0.0385		NFR	0.0044
200		NFR	0.3418		NFR	0.1991		NFR	0.1116		NFR	0.0414		NFR	0.0048
220		NFR	0.3438		NFR	0.2178		NFR	0.1215		NFR	0.0448		NFR	0.0052
240		NFR	0.3448		NFR	0.2410		NFR	0.1339		NFR	0.0495		NFR	0.0058
260		NFR	0.3468		NFR	0.2788		NFR	0.1559		NFR	0.0563		NFR	0.0069
280		NFR	0.3468		NFR	0.4098		NFR	0.3088		NFR	0.0870		NFR	0.0243
300		NFR	0.3478		0.1210	0.6208		0.0549			0.0236	0.0968		0.0038	0.1033
320		NFR	0.3488		0.0694			0.0367			0.0153			0.0020	0.2400
340		NFR	0.3498		0.0516			0.0286			0.0118			0.0015	
360		0.0973	0.3548		0.0424			0.0240			0.0099			0.0013	

380		0.0661	0.3718		0.0368			0.0210			0.0085			0.0011	
400		0.0552	0.4168		0.0328			0.0188			0.0076			0.0010	
500		0.0365		0.0367	0.0230		0.0248	0.0131			0.0053			0.0007	
600	0.0349	0.0286		0.0247	0.0186		0.0167	0.0106		0.0072	0.0042		0.0013	0.0005	
700	0.0283	0.0244		0.0199	0.0158		0.0122	0.0090		0.0053	0.0036		0.0009	0.0004	
800	0.0245	0.0215		0.0171	0.0139		0.0102	0.0079		0.0044	0.0032		0.0007	0.0004	

Table 8.6 Locations of zero pressure gradient (Z_I) and onset of pressure build up (Z_{II}) for different radius ratio N of vertical concentric annuli, Case 1.O

Gr/Re	N = 0.1		N = 0.3		N = 0.5		N = 0.7		N = 0.9	
	Z_I	Z_{II}	Z_I	Z_{II}	Z_I	Z_{II}	Z_I	Z_{II}	Z_I	Z_{II}
80	0.11179	*	0.10630	*						
100	0.07108	0.20501	0.05678	*	0.03712	*	0.01704	*	0.00251	*
120	0.05221	0.14514	0.04008	0.11499	0.02488	0.07497	0.01059	*	0.00137	*
140	0.04117	0.11295	0.03120	0.08595	0.01905	0.05358	0.00794	0.02299	0.00100	0.00300
160	0.03390	0.09268	0.02561	0.06915	0.01555	0.04223	0.00643	0.01771	0.00080	0.00225
180	0.02869	0.07870	0.02172	0.05810	0.01319	0.03509	0.00544	0.01454	0.00068	0.00182
200	0.02480	0.06845	0.01882	0.05024	0.01145	0.03016	0.00473	0.01241	0.00059	0.00154
220	0.02178	0.06061	0.01656	0.04435	0.01012	0.02653	0.00419	0.01088	0.00052	0.00135
240	0.01937	0.05441	0.01476	0.03976	0.00905	0.02374	0.00376	0.00971	0.00047	0.00120
260	0.01740	0.04936	0.01327	0.03607	0.00817	0.02152	0.00341	0.00879	0.00043	0.00108
280	0.01578	0.04517	0.01203	0.03303	0.00743	0.01971	0.00311	0.00804	0.00039	0.00099
300	0.01442	0.04163	0.01099	0.03049	0.00680	0.01820	0.00286	0.00743	0.00036	0.00091
320	0.01326	0.03860	0.01010	0.02831	0.00626	0.01692	0.00264	0.00691	0.00033	0.00085
340	0.01227	0.03596	0.00933	0.02643	0.00579	0.01582	0.00245	0.00646	0.00031	0.00079
360	0.01141	0.03365	0.00867	0.02479	0.00538	0.01486	0.00228	0.00607	0.00029	0.00075
380	0.01065	0.03161	0.00809	0.02334	0.00502	0.01401	0.00213	0.00573	0.00027	0.00070
400	0.00999	0.02979	0.00757	0.02204	0.00470	0.01326	0.00200	0.00543	0.00025	0.00067
500	0.00759	0.02302	0.00573	0.01720	0.00355	0.01046	0.00151	0.00432	0.00019	0.00053

* For such cases, the pressure defect did not cross the value of zero before the fully developed conditions.

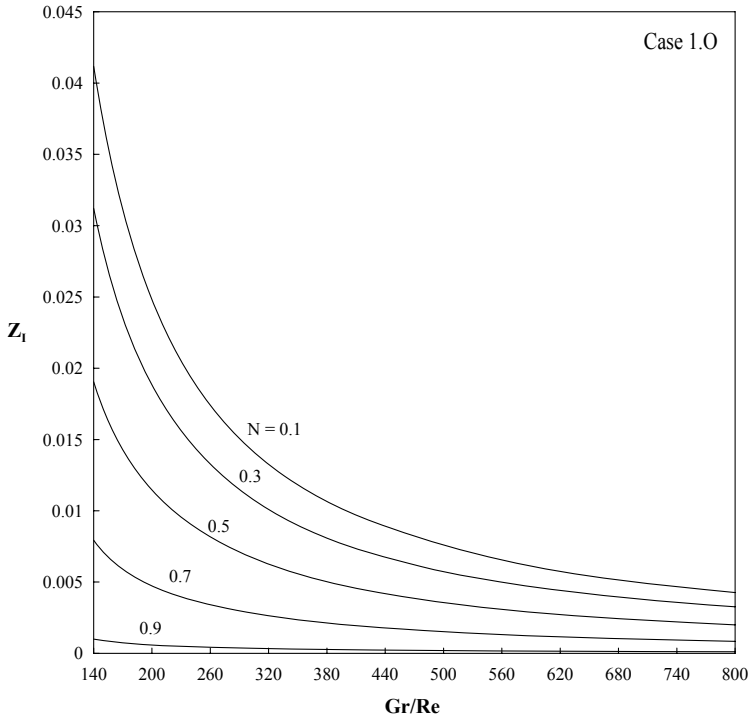

Figure 8.10(a) Graphical representation of location of zero pressure gradient (Z_I) as a function of Gr/Re for different radius ratio N of vertical concentric annuli, Case 1.O

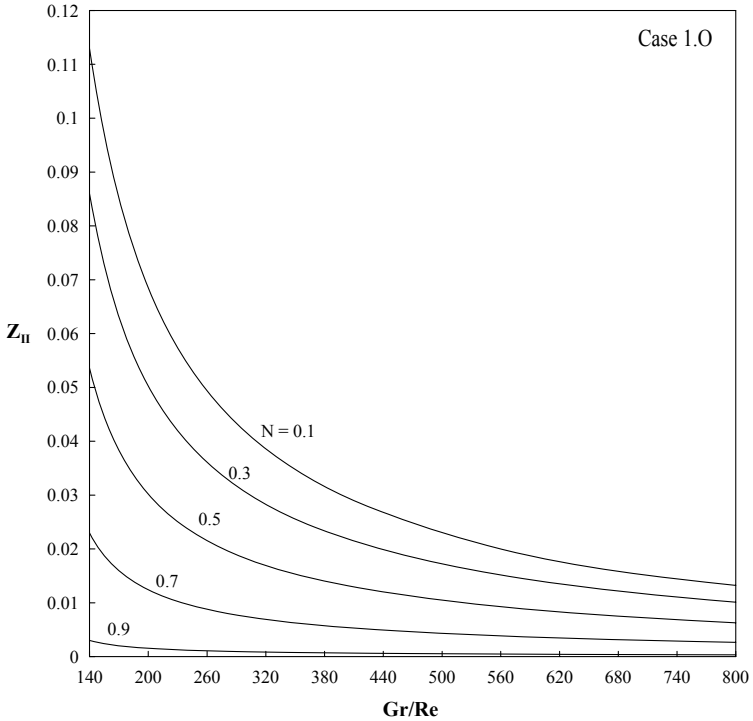

Figure 8.10(b) Graphical representation of location of zero pressure (Z_{II}) as a function of Gr/Re for different radius ratio N of vertical concentric annuli, Case 1.O

Figure 8.11(a) show the variation of mean temperature θ_m against the axial distance. It is clearly seen that the mean temperature develops from zero at the entrance with increasing values that are higher than that of pure forced convection. The difference between mixed convection mean temperature and forced convection mean temperature increases with the increase of Gr/Re at fully developed conditions. In the figure the dotted line represents the curve of mean temperature obtained for critical value of buoyancy parameter Gr/Re.

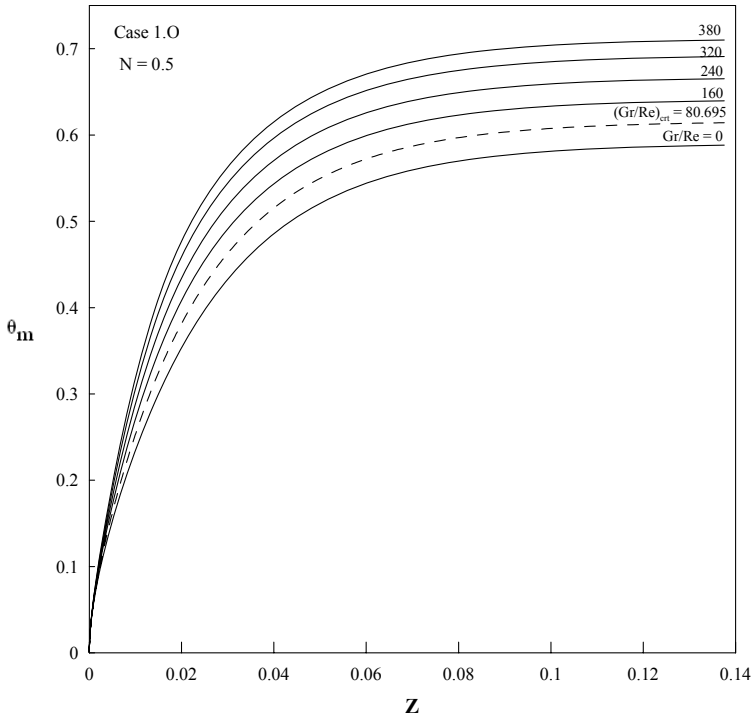

Figure 8.11(a) Mean or bulk temperature variation against channel height for different Gr/Re for radius ratio N = 0.5 of vertical concentric annulus, Case 1.O

Figure 8.11(b) show the variation of Nusselt number along the axial distance for the heated outer wall of the annulus. It is evident from the figure that the Nusselt number increases with higher values than that of pure forced convection. The deviation from forced convection increases as the heating rate Gr/Re increases and vice versa on the cold side of the annulus.

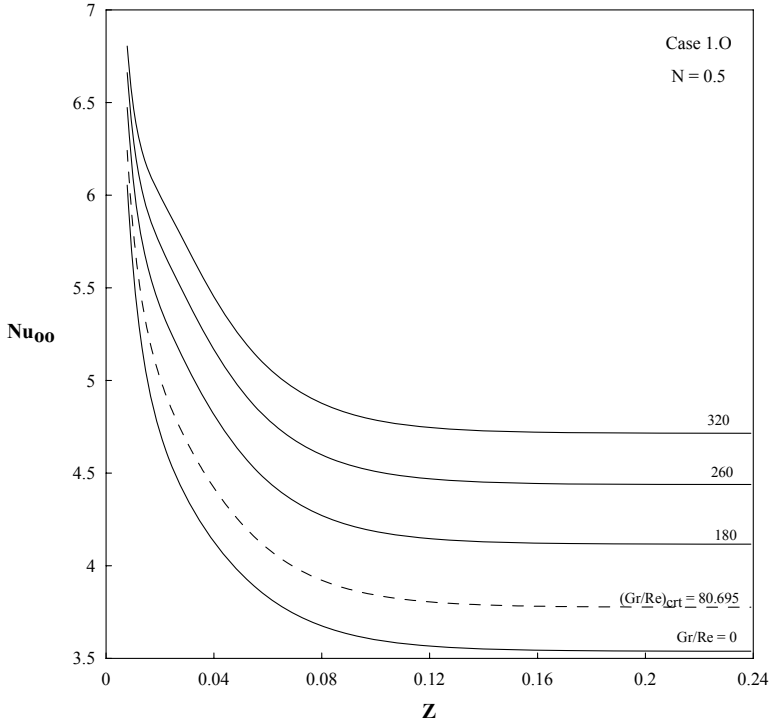

Figure 8.11(b) Variation of Nusselt number on heated wall of the channel as a function of position (Z) for different Gr/Re for radius ratio N = 0.5 of vertical concentric annulus, Case 1.O

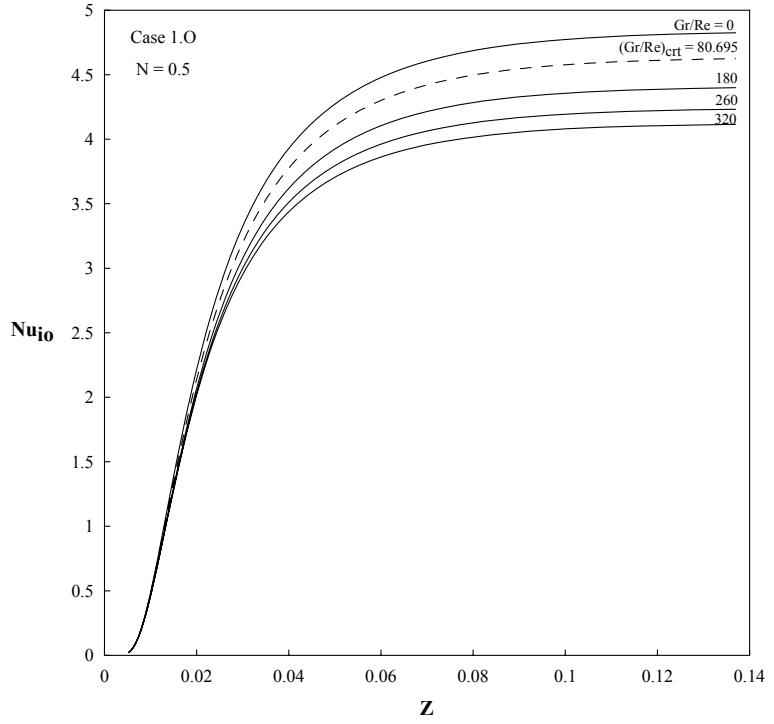

Figure 8.11(c) Variation of Nusselt number on cold wall of the channel as a function of position (Z) for different Gr/Re for radius ratio N = 0.5 of vertical concentric annulus, Case 1.O

Chapter 9

RESULTS AND DISCUSSION FOR LAMINAR MIXED CONVECTION IN VERTICAL ECCENTRIC ANNULUS

9.1 Introduction

This chapter presents the critical values of buoyancy parameter Gr/Re obtained numerically under the thermal boundary condition of first kind. Having the confidence in the mathematical model, numerical scheme and the code, the computer code has been used to generate a huge amount of data for mixed convection under a wide range of the buoyancy parameter Gr/Re in vertical eccentric annuli of radius ratio N = 0.5 with a wide range of eccentricity E = 0.1-0.7. All the results presented in this chapter are obtained for a fluid of Pr = 0.7. Several runs and tuning of the buoyancy parameter (Gr/Re) were conducted for each of the geometric parameters considered till a pressure gradient of zero prevails along the channel. In the present work, positive and negative values of the buoyancy parameter (Gr/Re), representing the buoyancy-aided and buoyancy-opposed flow situations, were considered. However, more emphasize is devoted to the buoyancy-aided flow situations. This was based on the fact that the pressure build-up will only take place downstream a vertical channel under buoyancy-aided flow conditions as reported earlier in [34] and [37]. The buoyancy parameters that lead to zero pressure gradients are nothing but the critical values of the buoyancy parameter $(Gr/Re)_{crt}$. Moreover, parameters of engineering importance are also presented. These parameters include the locations at which the negative pressure gradient becomes zero and then changes its sign

to be positive and the locations at which the pressure defect along the channel also becomes zero and pressure build-up takes place thereafter. Moreover, the fully developed length for different values of the buoyancy parameter Gr/Re is also reported for all cases under investigation.

Due to the mathematical difficulties, the analytical solution for the fully developed governing equations in order to calculate the critical values of Gr/Re is not amenable and is beyond the scope of the present study. Thus, these critical values are obtained numerically by solving the developing region governing equations. Several numerical tests and tuning of different values of Gr/Re are conducted until $(dP/dZ)_{fd,\ mxd}$, = 0. Moreover, the relation between the critical values of buoyancy parameter Gr/Re and the dimensionless eccentricity E is obtained and presented for a given radius ratio N = 0.5. The mathematical model and the numerical code validated and tested for mesh independence earlier by Mokheimer [35] is used to obtain the critical values of buoyancy parameter Gr/Re at which the pressure gradient becomes zero and beyond which the pressure build up will takes place.

9.2 Results and Discussion

Table 9.1 show the critical values of $(Gr/Re)_{crt}$ obtained numerically for the thermal boundary condition of first kind for Case 1.I and Case 1.O for radius ratio N = 0.5 as a sample of results obtained. It is seen from the table that for small eccentricity E = 0.1 and for a given radius ratio (N = 0.5), the critical value of buoyancy parameter $(Gr/Re)_{crt}$ is high and decreases as the eccentricity E increases. This can also be predicted from the Figure 9.1 which shows that the critical value of buoyancy parameter $(Gr/Re)_{crt}$ as a function of dimensionless eccentricity E. Also the critical value of buoyancy parameter

Gr/Re for Case 1.I is higher than the critical value of buoyancy parameter $(Gr/Re)_{crt}$ for Case 1.O. This can physically be attributed to the fact that the buoyancy effects are to be more effective overcoming the viscous forces right after the channel entrance. This speeds up the development of the pressure gradient to become positive leading to an earlier incipient of positive pressure build under thermal boundary condition (O) than that under thermal boundary condition (I) due to the larger heated surface area associated with former boundary condition than that with the latter. It is worth noticing here that same trend was reported for the concentric annulus.

Due to its practical importance, the relation between the critical values of the buoyancy parameters $(Gr/Re)_{crt}$ and the geometric parameters of an eccentric annulus has been put in a correlation form for the two thermal boundary conditions under consideration. The correlation between the critical value of buoyancy parameter $(Gr/Re)_{crt}$ and dimensionless eccentricity E for both Case 1.I and Case 1.O for radius ratio N = 0.5 are of high coefficient of multiple determination ($R^2 \approx 0.998$) and are given as:

$$(Gr/Re)_{crt} = 121.05625 - 36.75 \times E - 35.625 \times E^2 \quad \text{(for Case 1.I)} \quad (9.1)$$

$$(Gr/Re)_{crt} = 85.4825 - 42.3 \times E - 21.25 \times E^2 \quad \text{(for Case 1.O)} \quad (9.2)$$

Table 9.1 Critical values of $(Gr/Re)_{crt}$ for different eccentricity E under the thermal boundary condition of first kind (Case 1.I & Case 1.O), for N = 0.5

$(Gr/Re)_{crt}$		
E	**Case 1.I**	**Case 1.O**
0.1	116.8	80.8
0.3	107.5	71.6
0.5	93.1	58.3
0.7	78.1	45.7

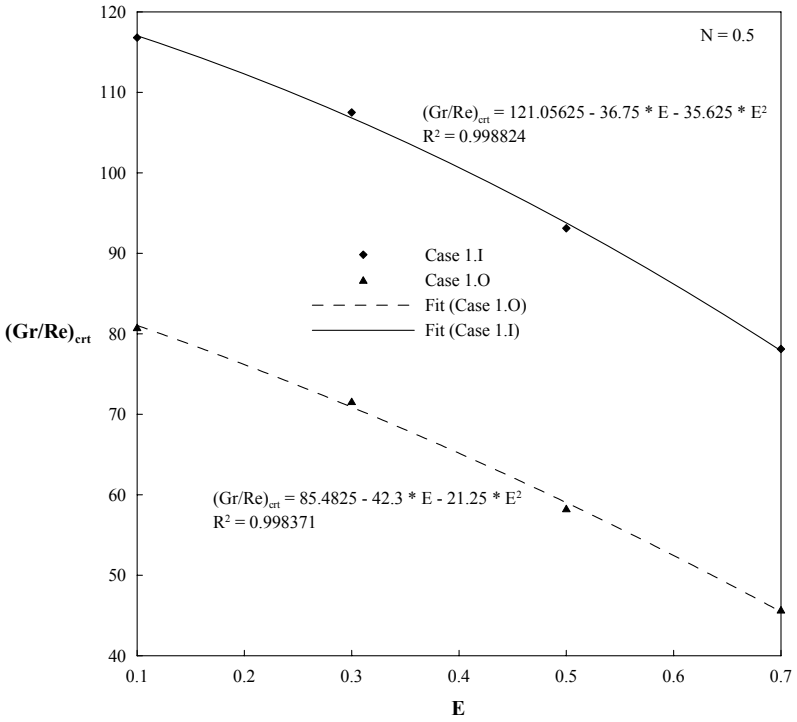

Figure 9.1 Critical values of Gr/Re as a function of eccentricity E in vertical eccentric annulus

Figures 9.2(a & b) show the development of the dimensionless pressure gradient and the dimensionless pressure defect downstream the channel for thermal boundary condition (1.I) for radius ratio, N = 0.5, and eccentricity, E = 0.5. These two figures show how the values of buoyancy parameter Gr/Re affect the development of the pressure gradient as well as the pressure defect downstream the channel. Negative values of the buoyancy parameter Gr/Re represent the buoyancy-opposed flow situations. In such cases, the increase of the opposing buoyancy increases the negativity of the pressure gradient resulting in an increase in the pressure drop (i.e. increases the negative values of the pressure defect) downstream the entrance and along the whole channel. On the other hand, positive values of buoyancy parameter, Gr/Re, decrease the negativity of the pressure gradient and there is certain value of buoyancy parameter, $Gr/Re = (Gr/Re)_{crt}$ at which the negativity of pressure gradient vanishes with possible onset of pressure build-

up. This means that for these particular values of the buoyancy parameter, $(Gr/Re)_{crt}$, the buoyancy effects are balancing the viscous effects at this value which is presented in Table 9.1 for the different eccentricities E for radius ratio N = 0.5. At large values of buoyancy parameter, $Gr/Re >> (Gr/Re)_{crt}$, the pressure gradient become positive and pressure builds up. More increase in heating rates, $Gr/Re >> (Gr/Re)_{crt}$, the pressure build-up takes place close to the channel entrance and might result in back pressure that prevent fluid particles penetrating downstream near the cold walls resulting in flow reversal. Such condition is presented in the Table 9.2(a) which show that for N = 0.5, the distance at which the flow reversal onsets, Z_{fr}, decreases as the heating rates Gr/Re increases for the investigated eccentricities E. Onset of flow reversal close to the channel entrance near the cold region of the annulus due to higher pressure gradient might cause the flow instability and consequently numerical instability because boundary layer separation may occur and the boundary layer assumptions might not further be applicable. However, for some values of the relatively high buoyancy parameter, Gr/Re, the flow might overcome this disturbance of mild flow reversal and attain its asymptotic fully developed profile at a distance far downstream of the channel where the velocity becomes invariant. The locations (distance from the channel entrance) at which any of the three phenomenon takes place are presented in Table 9.2(a) for a wide range of the buoyancy parameter (Gr/Re).

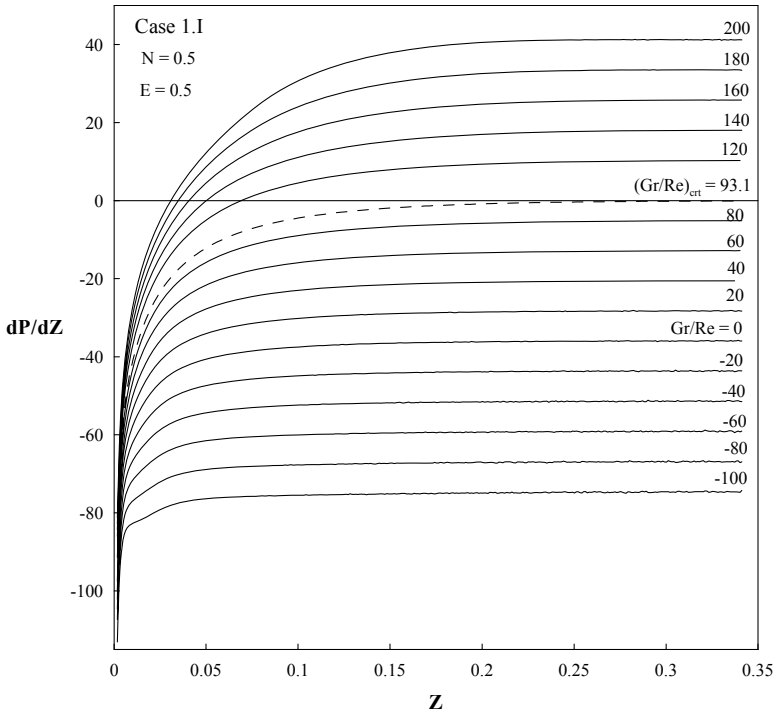

Figure 9.2(a) Variation of pressure gradient along the axial distance for N = 0.5 and E = 0.5 of vertical eccentric annuli, Case 1.I

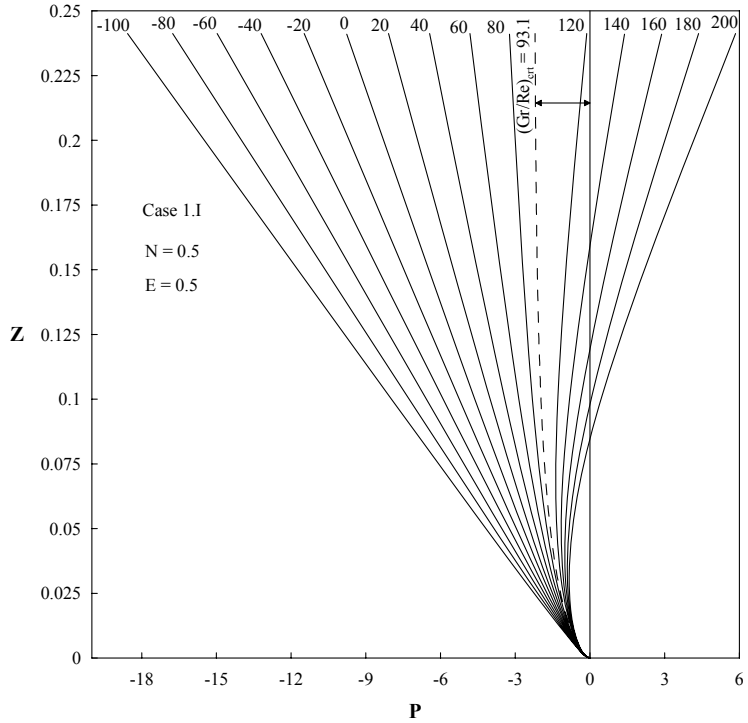

Figure 9.2(b) Pressure variation along the axial distance for N = 0.5 & E = 0.5 of vertical eccentric annuli, Case 1.I

Table 9.2(a) Locations of numerical instability (Z_{in}), onset of flow reversal (Z_{fr}) and the hydrodynamic fully development length (Z_{fd}) for mixed convection in a vertical eccentric annulus of radius ratio N = 0.5, Case 1.I

Gr/Re	**E = 0.1**			**E = 0.3**			**E = 0.5**			**E = 0.7**		
	Z_{in}	Z_{fr}	Z_{fd}	Z_{in}	Z_{fr}	Z_{fd}	Z_{in}	Z_{fr}	Z_{fd}	Z_{in}	Z_{fr}	Z_{fd}
0		NFR	0.0572		NFR	0.1492		NFR	0.1852		NFR	0.2332
40		NFR	0.1202		NFR	0.1822		NFR	0.2532		NFR	0.3642
60		NFR	0.1372		NFR	0.2012		NFR	0.3122		NFR	0.4772
80		NFR	0.1632		NFR	0.2242		NFR	0.3972		NFR	0.5122
100		NFR	0.1941		NFR	0.2902		NFR	0.4502		1.3182	0.6152
120		NFR	0.2532		NFR	0.3052		NFR	0.4592		0.6792	0.6622
140		NFR	0.2822		NFR	0.4192		NFR	0.4732		0.4942	0.6982
160		NFR	0.2932		NFR	0.4332		NFR	0.5302		0.3522	0.7242
180		NFR	0.3012		NFR	0.5022		1.6532	0.6242		0.2932	0.7852
200		NFR	0.3302		NFR	0.5892		0.9252	0.6746		0.2672	0.8182
400	0.0342	0.0292		0.0342	0.0282		0.0392	0.0312		0.0412	0.0352	
600	0.0252	0.0212		0.0272	0.0212		0.0302	0.0242		0.0322	0.0272	
800	0.0212	0.0182		0.0232	0.0182		0.0242	0.0202		0.0272	0.0232	

Table 9.2(b) summarizes the locations at which the pressure gradient vanishes, Z_I, and changing its sign to be positive for different values of the Gr/Re >> $(Gr/Re)_{crt}$. This positive pressure gradients leads to a pressure build-up along the channel. Thus the dimensionless pressure defect that is developing from a zero value at the entrance into a negative value due to the viscous effects will develop more but with a decreasing negativity under this conditions, Gr/Re >> $(Gr/Re)_{crt}$. Eventually, the pressure defect will attain a value of zero at a distance Z_{II} from the channel entrance after the flow achieves its zero pressure gradient and starts having its positive value at distance Z_I from the channel entrance. After the distance Z_{II}, the pressure defect will attain positive values.

This means that the pressure is building up along the channel just after this location. This implies that if a vertical channel has a height greater than Z_{II} and a buoyancy parameter $Gr/Re >> (Gr/Re)_{crt}$, such a channel might work as a thermal diffuser. The values of Z_{II} are given in Table 9.2(b).

Table 9.2(b) Locations of zero pressure gradient (Z_I) and onset of pressure build up (Z_{II}) in an eccentric annulus of radius ratio N = 0.5, Case 1.I

	E = 0.1		**E = 0.3**		**E = 0.5**		**E = 0.7**	
Gr/Re	**Z_I**	**Z_{II}**	**Z_I**	**Z_{II}**	**Z_I**	**Z_{II}**	**Z_I**	**Z_{II}**
80							0.26514	*
100					0.13429	0.88080	0.09212	0.35310
120	0.10382	1.30682	0.08334	0.41376	0.06905	0.25437	0.06249	0.20388
140	0.04940	0.19963	0.05123	0.17846	0.05019	0.15937	0.04930	0.14884
160	0.03676	0.11936	0.03892	0.12061	0.04072	0.11974	0.04168	0.12042
180	0.03037	0.08883	0.03228	0.09351	0.03486	0.09810	0.03663	0.10342
200	0.02642	0.07245	0.02807	0.07782	0.03083	0.08474	0.03299	0.09237

* For this case, the pressure defect did not cross the value of zero before the fully developed conditions.

The development of the dimensionless pressure gradient and the dimensionless pressure defect for case 1.O are shown in Figures 9.3(a & b) for E = 0.5. Similar trend is found for this boundary condition as that obtained for thermal boundary condition (1.I). The dotted line shown in Figures 9.3(a & b) represents the development of pressure gradient and pressure for the critical value of buoyancy parameter $(Gr/Re)_{crt.}$ The locations of possibility of onset of flow reversal resulting in flow instability, numerical instability and the location of hydrodynamic fully development lengths are presented in Table 9.3(a). It

is clear from this table that Z_{fd} increases with the increase of the heating rates, Gr/Re. The data also show that the value of the fully developed length Z_{fd} is larger for case 1.O than that for case 1.I. This implies that it takes the flow more distance to achieve its fully developed condition in the case of mixed convection compared to that of pure forced convection as it is clear from Tables 9. 2(a) and 9. 3(a) for both cases 1.I and 1.O. This is attributed to the fact that the buoyancy effects distort the flow velocity profile of the pure forced convection. This distortion increase with the increase of the buoyancy forces represented by the buoyancy parameter Gr/Re. thus the length required by the flow to reach full development increases with Gr/Re for both cases 1.I and 1.O.

Moreover, the buoyancy effects and consequently the distortion of the velocity profiles increases with the increase of the heating rates provided through larger surface area for case 1.O compared with that for case 1.I. Thus, the fully developed length Z_{fd} for case 1.O is larger than that for case 1.I. On the other hand, the distance at which the flow reversal takes place, Z_{fr} decreases as the heating rates Gr/Re increases. Also for same value of Gr/Re, Z_{fr} is smaller for case 1.O than the one for case 1.I. This is again is attributed to the increase of the buoyancy effects which severely distorts the velocity profiles that increases with the increase of GR/Re. This distortion is more effective for the larger heated surface associated with the thermal boundary condition of case 1.O. In other words, the increase of Gr/Re and the increase of the heating surface area, case 1.O, speeds up the velocity profiles distortions to the limits of the flow reversal. This explains why Z_{fr} decreases with Gr/Re and why it is less for case 1.O compared to that for case 1.I. The locations of zero pressure gradient, Z_I and the locations of pressure build-up onset, Z_{II} for case 1.O are given in Table 9.3(b).

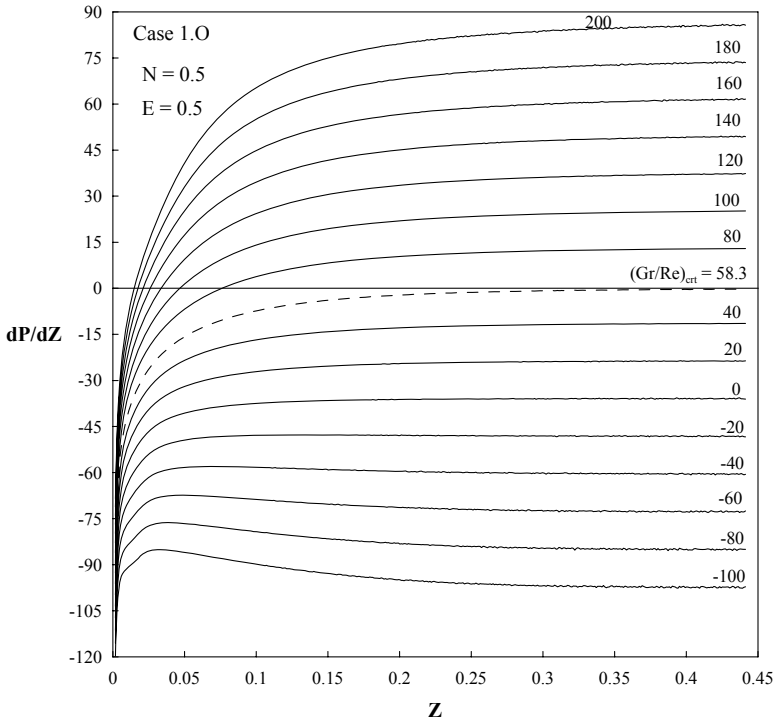

Figure 9.3(a) Variation of pressure gradient along the axial distance for N = 0.5 and E = 0.5 of vertical eccentric annuli, Case 1.O

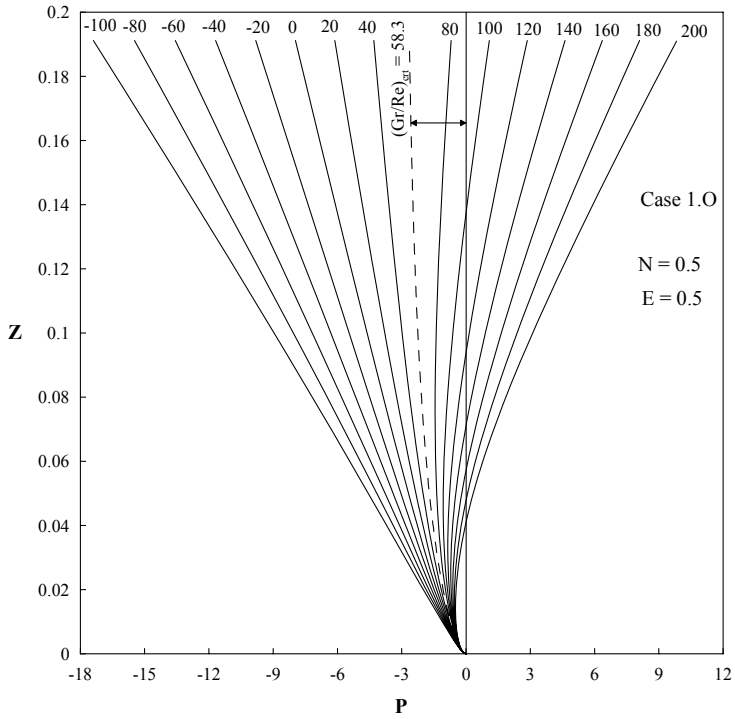

Figure 9.3(b) Pressure variation along the axial distance for N = 0.5 & E = 0.5 of vertical eccentric annuli, Case 1.O

Table 9.3(a) Locations of numerical instability (Z_{in}), onset of flow reversal (Z_{fr}) and the hydrodynamic fully development length (Z_{fd}) for mixed convection in a vertical eccentric annulus of radius ratio N = 0.5, Case 1.O

Gr/Re	**E = 0.1**			**E = 0.3**			**E = 0.5**			**E = 0.7**		
	Z_{in}	Z_{fr}	Z_{fd}	Z_{in}	Z_{fr}	Z_{fd}	Z_{in}	Z_{fr}	Z_{fd}	Z_{in}	Z_{fr}	Z_{fd}
0		NFR	0.1122		NFR	0.3022		NFR	0.3542		NFR	0.4962
40		NFR	0.1612		NFR	0.3372		NFR	0.4322		NFR	0.6002
60		NFR	0.2222		NFR	0.4432		NFR	0.6532		NFR	0.6462
80		NFR	0.3712		NFR	0.5462		NFR	0.8142		0.5782	0.7462
100		NFR	0.3822		NFR	0.5962		NFR	0.8422		0.3652	0.7702
120		NFR	0.3992		NFR	0.6032		NFR	0.8552		0.2342	0.8242
140		NFR	0.4122		NFR	0.6622		NFR	0.9392		0.1802	0.8662
160		NFR	0.4252		NFR	0.7272		0.3422	1.0552		0.0842	0.9582
180		NFR	0.4392		NFR	0.8122		0.0882	1.1032		0.0612	1.0402
200		NFR	0.4462		NFR	0.8602		0.0552	1.1622		0.0520	1.1332
400		0.0222	0.5542		0.0202	0.9992	0.0335	0.0212		0.0352	0.0222	
600	0.0282	0.0152		0.0252	0.0152		0.0242	0.0152		0.0252	0.0152	
800	0.0222	0.0122		0.0212	0.0122		0.0212	0.0122		0.0222	0.0122	

Table 9.3(b) Locations of zero pressure gradient (Z_I) and onset of pressure build up (Z_{II}) in an eccentric annulus of radius ratio N = 0.5, Case 1.O

Gr/Re	**E = 0.1**		**E = 0.3**		**E = 0.5**		**E = 0.7**	
	$\mathbf{Z_I}$	$\mathbf{Z_{II}}$	$\mathbf{Z_I}$	$\mathbf{Z_{II}}$	$\mathbf{Z_I}$	$\mathbf{Z_{II}}$	$\mathbf{Z_I}$	$\mathbf{Z_{II}}$
60							0.1042	0.3795
80			0.1079	0.4899	0.0750	0.2546	0.0560	0.1719
100	0.0416	0.1537	0.0467	0.1534	0.0469	0.1374	0.0386	0.1126
120	0.0279	0.0828	0.0305	0.0907	0.0338	0.0939	0.0295	0.0843
140	0.0216	0.0589	0.0231	0.0645	0.0261	0.0711	0.0238	0.0677
160	0.0180	0.0466	0.0188	0.0505	0.0211	0.0572	0.0199	0.0569
180	0.0155	0.0391	0.0159	0.0419	0.0175	0.0478	0.0171	0.0492
200	0.0137	0.0339	0.0138	0.0360	0.0149	0.0410	0.0149	0.0434

The information presented in Figs. 9.2(a & b) and 9.3(a & b) are of real technical importance. Figures 9.2 and 9.3 show clearly how the development of the pressure gradient and the pressure defect for mixed convection flows are deviated from those of pure forced convection flows. These figures demonstrate the fact of existing a critical value of the buoyancy parameter $(Gr/Re)_{crt}$, only for buoyancy-aided flows, at which the pressure gradient develops from a high negative value at the entrance due to the presence of the two walls with a decreasing negative rate till it vanishes asymptotically to exactly zero in the fully developed region. These figures show also that the positive pressure gradient and the possibility of having pressure build-up downstream the channel entrance is achievable only for buoyancy-aided flow situations with buoyancy parameter $Gr/Re >> (Gr/Re)_{crt}$.

The data summarized in Tables 9.2(a & b) and 9.3(a & b) are also of technical relevance. For example, Tables 9.2(a) and 9.3(a) give the fully developed length, Z_{fd}, of vertical channels of different eccentricities under different heating rates, Gr/Re. This fully developed length is very important to be known by the designers to not assume that the fully developed conditions prevails directly from the channel entrance for a channel of a length (height) less than its fully developed length. The assumptions of fully developed conditions for short channels would result in considerable errors in calculating the pressure drop as well as the heat transfer rates in this developing entry region. However, if the channel is sufficiently high with respect to its fully developed length, this error might be small. These tables also give the values of the channel heights that would result in flow reversal, Z_{fr}, and consequently flow instability. Knowing these values, the designers would have channels with heights less than Z_{fr} and Z_{in} to avoid the flow

reversal and the flow instability. On the other hand, Tables 9.2(b) and 9.3(b) give the locations at which the pressure gradient vanishes, Z_I, and the locations at which the pressure defect starts to become zero, Z_{II}, for channels of different eccentricities under different heating rates, Gr/Re. It is worth noting here that due to pressure build-up downstream the channel height of Z_{II}, the channel starts working as a thermal diffuser thereafter. Thus, the locations of pressure build-up onset, Z_{II} is of technical importance to the designers who would decide the real size of the pumping device needed to pump a fluid in a vertical eccentric channel under mixed convection operating conditions. For example, for a vertical channel that works under buoyancy-aided flow conditions with $Gr/Re >> (Gr/Re)_{crt}$ (i.e., for buoyancy-aided flow situations) and is of a height greater than Z_{II}, the pressure build-up is expected and the pumping device in such a case might work as a flow regulator, Han [20].

Chapter 10

CONCLUSIONS AND RECOMMENDATIONS

The present work aimed at obtaining critical values of buoyancy parameter Gr/Re for laminar mixed convection in different vertical channels investigated under different isothermal boundary conditions for fully developed governing equations. Emphasis was devoted to investigate the hydrodynamics for buoyancy aided flow situations. Numerical analysis is performed in the developing entry region of laminar mixed convection in the investigated vertical channels namely parallel plates, circular tube, concentric annulus and eccentric annulus. Effects of buoyancy forces on hydrodynamic and thermal parameters are extensively studied in the present work.

10.1 Conclusions

The following conclusions can be deduced from the present work:

1. The presence of critical values of buoyancy parameter Gr/Re at which negativity of pressure gradient vanishes and incipient of pressure build up takes place was demonstrated from fully developed laminar mixed convection in different vertical channels under different isothermal boundary conditions in buoyancy aided flow situations.
2. Above these critical values of buoyancy parameter (Gr/Re), pressure will build up downstream and the vertical channel can act as a diffuser with possible incipient of flow reversal.

3. Locations at which buoyancy forces balance out viscous forces (i.e. Z_I and Z_{II}) are calculated for all investigated cases.
4. Locations of onset of flow reversal at which buoyancy aided flow is converted to opposed flow due to higher buoyancy effects (higher heating rates) are calculated and presented for all investigated cases. These locations become closer to the entrance with increase of Gr/Re.
5. Locations of numerical instability due to flow reversal are calculated.
6. Numerical values of the hydrodynamic development length which increases due to higher heating rates or due to higher values of Gr/Re are presented.
7. Finally, this qualitative and quantitative information will help the designer to properly size the pumping device such that it satisfies the required conditions.

10.2 Recommendations

Due to the wide scope of the present work from application point of view, the following recommendations are suggested for the future work:

1. Experimental validation of the reported results needs to be conducted.
2. Radiation effects which become more significant under large temperature difference can be considered to calculate critical values of buoyancy parameter Gr/Re for laminar fully developed mixed convection in different vertical channels.
3. Computational approach can be suggested to study the turbulent mixed convection in vertical channels.

REFERENCES

[1] W. Aung, Mixed convection in internal flow, Hand Book of Single-Phase Convective Heat Transfer (chapter 15), Edited by S. Kakaç, R. K. Shah and W. Aung, John Wiley & Sons, 1987.

[2] T. Inagaki and K. Komori, "Numerical modeling on turbulent transport with combined forced and natural convection between two vertical parallel plates", *Numerical Heat Transfer, Part A*. 27(4), (1995), pp. 417-431.

[3] T. Cebeci, A.A. Khattab, and R. LaMont, "Combined Natural and Forced Convection in Vertical Ducts", *Heat Transfer,* Vol. 2, (1982), pp. 419-424.

[4] W. Aung and G. Worku, "Theory of Fully Developed Combined Convection Including Flow Reversal", *Journal of Heat Transfer,* Vol. 108, (1986), pp. 485-488.

[5] K. Boulama and N. Galanis, "Analytical solution for fully developed mixed convection between parallel vertical plates with heat and mass transfer", *ASME Transactions, Journal of Heat transfer,* Vol. 126, (2004), pp. 381-388.

[6] T.T. Hamadah and R.A. Wirtz, "Analysis of laminar fully developed mixed convection in a vertical channel with opposing buoyancy", *Transactions of ASME, Journal of Heat Transfer,* Vol. 113, (1991), pp. 507-510.

[7] L.S. Yao, "Free and Forced Convection in the Entry Region of a Heated Vertical Channel", *Int. J. Heat Mass Transfer,* Vol. 26(1), (1983), pp. 65-72.

[8] W. Aung and G. Worku, "Developing flow and flow reversal in a vertical channel with asymmetric wall temperatures", *Transactions of the ASME, Journal of Heat Transfer*, Vol. 108, (1986), pp. 299-307.

[9] R.A. Wirtz and P. McKinley, "Buoyancy effects on downward laminar convection between parallel plates", *Fundamentals of Forced & Mixed Convection, ASME Publication, HTD* Vol. 42, (1985), pp. 105-112.

[10] D. B. Ingham, D. J. Keen and P. J. Heggs, "Flows in vertical channels with asymmetric wall temperatures and including situations where reverse flows occur", *ASME Transactions, Journal of Heat Transfer,* Vol. 110, (1988), pp. 910-917.

[11] Zouhair Ait Hammou, Brahim Benhamou, N. Galanis and Jamel Orfi, "Laminar mixed convection of humid air in a vertical channel with evaporation or condensation at the wall", *Int. J. of thermal sciences,* Vol. 43, (2004), pp. 531-539.

[12] A. Barletta, S. Lazzari and E. Zanchini, "Non-axisymmetric forced and free flow in a vertical circular duct", *International Journal of Heat and Mass Transfer,* Vol. 46, (2003), pp. 4499-4512.

[13] A. Behazadmher, N. Galanis and A. Laneville, "Low Reynolds number mixed convection in vertical tubes with uniform wall heat flux", *International Journal of Heat and Mass Transfer,* Vol. 46, (2003), pp. 4823-4833.

[14] B. Metais and E. R. G. Eckert, "Forced, mixed, and free convection regimes", *Journal of Heat Transfer, Transactions of the ASME,* Vol. 86, (1964), pp. 295-296.

[15] T. M. Hallman, "Experimental study of combined forced and free laminar convection in a vertical tube", *NASA TN D-1104,* (1961).

[16] H. Brauer, M. Dylag and J. Kasz, "Heat transfer by combined free and forced convection in vertical tubes", *Waerme-und Stoffuebertragung/Thermo- and Fluid Dynamics,* Vol. 23(2), (1988), pp. 61-68.

[17] A. Barletta and E. R. di Schio, “Effect of viscous dissipation on mixed convection heat transfer in a vertical tube with uniform wall heat flux”, *Heat and Mass Transfer,* Vol. 38, (2001), pp. 129-140.

[18] D. D. Joye, “Pressure drop correlation for laminar, mixed convection, aiding flow heat transfer in a vertical tube”, *International Journal of Heat and Fluid Flow,* Vol. 24, (2003), pp. 260-266.

[19] P. E. Saylor and D. D. Joye, “Hydrostatic correction and pressure drop measurement in mixed convection heat transfer in a vertical tube”, *Industrial Engineering Chemistry Research,* Vol. 30, (1991), pp. 784-788.

[20] J. C. Han, “Hydraulic characteristics of mixed convection in a heated vertical pipe”, *Transactions of the ASME, J. of Fluid Engineering,* Vol. 115, (1993), pp. 41-47.

[21] E. M. A. Mokheimer and M. A. I. El-Shaarawi, “Critical values of Gr/Re for mixed convection in vertical eccentric annuli with isothermal/adiabatic walls”, *Transactions of the ASME, Journal of Heat Transfer,* (2004), pp. 479-482.

[22] H. Nesreddine, N. Galanis and C. T. Nguyn, “Variable-property effects in laminar aiding and opposing mixed convection of air in vertical tubes”, *Numerical Heat Transfer, Part A,* Vol. 31, (1997), pp. 53-69.

[23] J. K. Kim, “Analysis of laminar mixed convection in vertical tube annulus with upward flow”, *Fundamentals of forced and nixed convection, ASME, HTD*. 142 (1985), pp. 91-98.

[24] G. M. Zaki, M. S. El-Genk and T. E. Williams, “Experimental heat transfer studies for water in annulus at low Reynolds number”, *ASME, HTD* 42 (1985), pp. 113-120.

[25] A. Barletta, "Combined forced and free flow of power-law fluid in a vertical annular duct", *Int. Journal of Heat and Mass Transfer,* Vol. 43, (2000), pp. 3673-3686.

[26] M. S. El-Genk and D. V. Rao, "Heat transfer experiments and correlations for low-Reynolds-number flows of water in vertical annuli", *Heat Transfer Engineering,* Vol. 10(2), (1989), pp. 44-57.

[27] M. A. I. El-Shaarawi and A. Sarhan, "Combined forced-free laminar convection in the entry region of a vertical annulus with a rotating inner cylinder", *International Journal of Heat and Mass Transfer,* Vol. 25(2), (1982), pp. 175-186.

[28] M. A. Hessami, G. D. E Vahl Davis, E. Leonardi and J. A. Reizes, "Mixed convection in vertical cylindrical annuli", *International Journal of Heat and Mass Transfer,* Vol. 30(1), (1987), pp. 151-164.

[29] C. J. Ho and F. J. Tu, "Laminar mixed convection of cold water in a vertical annulus with a heated rotating inner cylinder", *Transactions of the ASME, Journal of Heat Transfer,* Vol. 114, (1987), pp. 418-424.

[30] P. Sathymurthy, K. C. Karki and S. V. Patankar, "Laminar Fully Developed Mixed Convection in a Vertical Eccentric Annulus", *Numerical Heat Transfer, Part (A)* Vol. 22, (1992), pp. 71-85.

[31] N. Patel and D. B. Ingham, "Mixed Convection Flow of a Bingham Plastic in an Eccentric Annulus", *Int. J. Heat and Fluid Flow,* Vol. 15(2), (1994), pp. 132-141.

[32] D. B. Ingham and N. Patel, "Developing Combined Convection in an Eccentric Annulus", *Numerical Heat transfer, Part A,* Vol. 29, (1996), pp. 707-724.

[33] D. B. Ingham and N. Patel, "Developing Combined Convection of Non-Newtonian Fluids in an Eccentric Annulus", *ACTA Mechanica,* Vol. 121, (1997), pp. 35-49.

[34] E. M. A. Mokheimer and M. A. I. El-Shaarawi, "Developing Mixed Convection in Vertical Eccentric Annuli", *Heat and Mass Transfer,* Vol. 41(2), (2005), pp. 176-187.

[35] E. M. A. Mokheimer, "Heat Transfer in Eccentric Annuli", PhD, Thesis, King Fahd University of Petroleum & Minerals, (1995).

[36] R. K. Shah and A. L. London, "Advances in Heat Transfer" Supplement 1 Laminar Flow Forced Convection in Ducts, (1978).

[37] M. A. I. El-Shaarawi and A. Sarhan, "Free convection effects on the developing laminar flow in Vertical Concentric Annuli", *Journal of Heat Transfer,* Vol. 102 (1980), pp. 617-622.

[38] B. Carnahan, H. A. Luther and J. D. Wilkes, "Applied Numerical methods", Wiley, (1969), pp. 298-301, 450.

Appendix

Selection of dimensionless parameters

Parallel Plates

$$U = \frac{u}{u_o},\ V = \frac{v}{u_o},\ P = \frac{p - p_o}{\rho u_o^{\,2}},\ \theta = \frac{T - T_o}{T_w - T_o},\ Z = \frac{z}{D_h \,\mathrm{Re}},\ D_h = b \tag{A.1}$$

Concentric Annulus

$$U = \frac{u}{u_o},\ V = \frac{v r_o}{\nu}, P = \frac{p - p_o}{\rho u_o^{\,2}},\ \theta = \frac{T - T_o}{T_{jw} - T_o} \quad j = i - inner\ wall,\ o - outer\ wall$$

$$R = \frac{r}{r_o},\ Z = \frac{2(1 - N)z}{D_n \,\mathrm{Re}},\ D_h = r_o \tag{A.2}$$

Circular Tube

$$U = \frac{u}{u_o},\ V = \frac{\mathrm{Re}\, v}{u_o},\ P = \frac{p - p_o}{\rho u_o^{\,2}},\ R = \frac{r}{D_n},\ Z = \frac{z}{D_h \,\mathrm{Re}},\ \theta = \frac{T - T_o}{T_w - T_o},\ D_h = r_o \tag{A.3}$$

VITAE

SHAIK SAMIVULLAH

- Completed B. Tech in Mechanical Engineering from J. N. T. University, India in June, 2000.
- Awarded with Research Assistantship at King Fahd University of Petroleum & Minerals, Saudi Arabia.
- Completed Master of Science in Mechanical Engineering (Thermo Fluids) from King Fahd University of Petroleum & Minerals, Saudi Arabia in May, 2005.